

EXPLORING THE ROLE OF TET1 IN GENOMIC IMPRINTING

Jennifer Myers SanMiguel

A DISSERTATION

in

Cell and Molecular Biology

Presented to the Faculties of the University of Pennsylvania

in

Partial Fulfillment of the Requirements for the

Degree of Doctor of Philosophy

2018

Supervisor of Dissertation

Marisa S. Bartolomei, Ph.D., Professor of Cell and Developmental Biology

Graduate Group Chairperson

Daniel S. Kessler, Ph.D., Associate Professor of Cell and Developmental Biology

Dissertation Committee

Rahul Kohli, M.D., Ph.D., Assistant Professor of Medicine and Biochemistry &

Biophysics

Klaus Kaestner, Ph.D., M.S., Thomas and Evelyn Suor Butterworth Professor in Genetics

Jennifer E. Phillips-Cremins, Ph.D., Assistant Professor of Bioengineering

Zhaolan Zhou, Ph.D., Associate Professor of Genetics

EXPLORING THE ROLE OF TET1 IN GENOMIC IMPRINTING

COPYRIGHT

2018

Jennifer Myers SanMiguel

This work is licensed under the
Creative Commons Attribution-
NonCommercial-ShareAlike 3.0
License

To view a copy of this license, visit

<https://creativecommons.org/licenses/by-nc-sa/3.0/us/>

In loving memory of my grandfather, Alan Erickson.

*Thank you for nurturing my love of science and delighting in my discoveries, no matter
how small.*

Acknowledgements

First and foremost, I want to thank my advisor, Dr. Marisa Bartolomei. I am so grateful for her tireless mentorship: reading thousands of drafts and late-night emails, sitting through countless practice talks, pushing me to the finish line, and reminding me of the big picture when I could only see details and missing pieces. Her love of science and advocacy for women in this field are attributes I will strive to emulate in my own career.

Secondly, I want to deeply thank my thesis committee: Dr. Rahul Kohli, Dr. Klaus Kaestner, Dr. Jennifer Phillips-Cremins, and Dr. Zhaolan Zhou. I consider myself very lucky to have chosen such bright, thoughtful, and supportive people to work with me through my time at Penn. They have all been so happy to help when I needed it and I thank them for their mentorship and guidance.

I also want to thank Dr. Rahul Kohli and Emily Schutsky for allowing us to work together to adapt their method of 5hmC profiling to pyrosequencing and thus giving me the opportunity to learn and use the technique as well. It has been a pleasure working with you both.

I want to show my gratitude to my funding sources, the Genetics T32 and the NIH F31. Relatedly, I want to particularly acknowledge Dr. Meera Sundaram and Dr. Doug Epstein for their mentorship through the Genetics T32 as well as through GGR and their teaching in CAMB 550 and CAMB 608, respectively. Lastly, I want to thank Meagan Schofer for all her assistance administratively during my tenure in this program.

I would like to acknowledge the wonderful training and support in all things during my Ph.D. from Dr. Joanne Thorvaldsen and Chris Krapp. Joanne was always willing to help teach or work alongside with me starting from day one in the Bartolomei lab. Her depth of knowledge, her thoughtful questions in lab meeting or on manuscript

edits, and curiosity about my work always made me feel supported and challenged, in the best way possible. Chris similarly never hesitated to offer and assist with mouse work, ordering reagents, or helping in any way, science or otherwise. His sarcasm and humor were invaluable in keeping the lab lighthearted and fun. I sincerely appreciate everything these two individuals have given me over the past six years.

My former labmates were particularly influential to my success as a student in the Bartolomei lab. I particularly want to acknowledge Dr. Lara Abramowitz for initiating the *Tet1* project and continuing to support me and the project even after she started her postdoc. Dr. Rob Plasschaert is one of the smartest and most hilarious people I have ever met. I'm so happy we were baymates. I learned very valuable advice from Rob about not taking everything so seriously and learned so much from watching him think critically about science from every angle possible. Thank you both for being wonderful humans and great examples of graduate students. Dr. Martha Susiarjo was another lighthearted and warm member of the Bartolomei lab who taught me how to collect mouse oocytes. I deeply appreciate how welcome she made me when I first came to lab and the friendship and mentorship she provided while we overlapped. Lastly, I want to thank Dr. Jennifer Kalish and Dr. Sébastien Vigneau for their help and support. Jenn was also particularly helpful in sharing her new lab space for bisulfite experiments, which was instrumental in making forward progress on the *Tet1* story.

I shudder to think what my lab life would be like without my current labmates. Drs. Lisa Vrooman and Laren Riesche are people I could always turn to for encouragement, commiseration, a laugh, or a run to Starbucks to refuel. Thank you both for always being there to listen. My fellow graduate students, Aimee Juan and Suhee Chang are amazing, smart, talented individuals who have given me more than I can possibly put into words. Laughs, tears, drinks, and love are the four best words to

describe my relationship with these wonderful people. I was lucky enough to have Blake Alexander Caldwell first, as my rotation student, and then my friend. I truly value our conversations, whether they be about TETs, Flight of the Concorde, Harry Potter houses, or the Turing test. I have learned so much from him and hope I have given back even a fraction of what he has given me. Frances Xin is a brilliant scientist, rigorous, hard-working and deeply thoughtful. In addition, she is a compassionate friend and one of the best people I could have possibly been able to be side by side with during my entire Ph.D. Words cannot describe how much her love, sharp thinking, and humor have carried me through my time at Penn.

I am additionally grateful to my amazing support network outside of lab. Dr. Suzi Shapira and I have been friends since we interviewed together at Penn. She is one of the most incredible people. Her intellect, resilience, and love are things I cherish and I will never stop admiring her. Dr. Katie Wetzel, Chris Wetzel, Dr. Jeffrey Rosa, Steve Goldstein, and Jackie Solomont have been constant sources of love and fun. I truly appreciate how well they took care of me, especially after my husband moved for his job and I am forever grateful for their friendship.

I was additionally extremely lucky to share my entire graduate school journey with my husband, Dr. Adam SanMiguel. Being able to discuss both my frustrations and my triumphs, in painstaking scientific detail, and at long length no less, has been a gift. He never stopped believing in me and this gave me the confidence and strength to move forward when I did not think it was possible.

Last but certainly not least, I also want to sincerely thank my parents, brother, extended family, and in-laws for always being so supportive and loving. I never could have made it through without their kind words and faith in my abilities.

ABSTRACT

EXPLORING THE ROLE OF TET1 IN GENOMIC IMPRINTING

Jennifer Myers SanMiguel

Marisa S. Bartolomei

DNA methylation is an essential epigenetic mark crucial for normal mammalian development. This modification controls the expression of a unique class of genes, designated as imprinted, which are expressed monoallelically and in a parent-of-origin-specific manner. Proper parental allele-specific DNA methylation at imprinting control regions (ICRs) is necessary for appropriate imprinting. Processes that deregulate DNA methylation of imprinted loci cause disease in humans. DNA methylation patterns dramatically change during mammalian development: first, the majority of the genome, with the exception of ICRs, is demethylated after fertilization, and subsequently undergoes genome-wide de novo DNA methylation. Secondly, after primordial germ cells are specified in the embryo, another wave of demethylation occurs, with ICR demethylation occurring late in the process. Lastly, ICRs reacquire DNA methylation imprints in developing germ cells. Although much is known about DNA methylation establishment, DNA demethylation is less well understood. Recently, the Ten-Eleven Translocation proteins (TET1-3) have been shown to initiate DNA demethylation, with *Tet1*^{-/-} mice exhibiting aberrant levels of imprinted gene expression and ICR methylation. Nevertheless, TET1's role in demethylating ICRs in the female germline and controlling allele-specific expression remains to be determined. Here, we examined ICR-specific DNA methylation in *Tet1*^{-/-} germ cells and ascertained whether abnormal ICR methylation impacted imprinted gene expression in F1 hybrid somatic tissues derived from *Tet1*^{-/-} eggs or sperm. We show that *Tet1* deficiency is associated with hypermethylation of a subset of ICRs in germ cells. Moreover, ICRs with defective germline reprogramming exhibit aberrant DNA methylation and biallelic expression of linked imprinted genes in somatic tissues. Thus, we define a discrete set of genomic

regions that require TET1 for germline reprogramming and discuss mechanisms for stochastic imprinting defects.

TABLE OF CONTENTS

ABSTRACT	vii
TABLE OF CONTENTS.....	ix
LIST OF TABLES	xiii
LIST OF FIGURES	xiv
CHAPTER 1: INTRODUCTION.....	1
1.1 DNA METHYLTRANSFERASES ADD AND MAINTAIN DNA METHYLATION.....	1
1.2 GENOMIC IMPRINTING.....	3
1.2.1 Definition.....	3
1.2.2 Historical Perspective.....	4
1.2.3 Mechanisms of ICR Functions.....	5
1.2.5. Secondary DMRs	7
1.2.6. Histone modifications at ICRs.....	8
1.2.7 Imprinted genes in health and disease.....	10
1.2.5 ICR methylation dynamics overview.....	11
1.3 EPIGENETIC REPROGRAMMING	11
1.3.1 Evidence for active DNA demethylation.....	13
1.3.3 Oxidative Demethylation by TET1, TET2, and TET3	13
1.3.4 TETs: Gene and Protein Structure and Function	14
1.3.5 TDG and base excision repair	16
1.4 PREIMPLANTATION DNA METHYLATION REPROGRAMMING	16
1.4.1 Genome-Wide DNA Demethylation	16

1.4.2 Imprinted Regions Escape Preimplantation DNA Methylation Reprogramming	18
1.5 PERI-IMPLANTATION DE NOVO METHYLATION OF THE GENOME	20
1.6 PGC DNA METHYLATION REPROGRAMMING	20
1.6.1 Bulk genome-wide demethylation in PGCs: The early wave.....	21
1.6.2 Chromatin Landscape Dynamics during DNA Demethylation in PGCs.....	23
1.6.3 ICR demethylation in PGCs	24
1.6.4 Repetitive Elements.....	25
1.6.5 TET-mediated demethylation of ICRs in the second wave of PGC demethylation	25
1.7 REACQUISITION OF DNA METHYLATION AT ICRS.....	26
1.8 BEYOND EPIGENETIC REPROGRAMMING: OTHER ROLES OF 5HMC	27
1.9 SUMMARY	28
1.10 CONTRIBUTIONS	29

CHAPTER 2: IMPRINTED GENE DYSREGULATION IN A <i>TET1</i> NULL MOUSE MODEL IS STOCHASTIC AND VARIABLE IN THE GERMLINE AND OFFSPRING	35
2.1 INTRODUCTION.....	35
2.2 RESULTS.....	37
2.2.1 Loss of <i>Tet1</i> leads to stochastic and variable DNA hypermethylation at ICRs in oocytes.....	37
2.2.2 Loss of <i>Tet1</i> leads to biallelic expression and changes in DNA methylation of imprinted genes in the offspring of female KO mice.	38
2.2.3 Loss of <i>Tet1</i> leads to stochastic DNA hypermethylation at ICRs in sperm.	41

2.2.4 Loss of <i>Tet1</i> leads to biallelic expression and changes in DNA methylation of imprinted genes in the offspring of male KO mice.....	41
2.3 DISCUSSION.....	43
2.4 CONTRIBUTIONS.....	51
CHAPTER 3: FUTURE DIRECTIONS	71
3.1 PARSE THE REQUIREMENTS OF INDIVIDUAL TET PROTEINS FOR ICR DEMETHYLATION DURING PGC REPROGRAMMING IN MICE.	71
3.2 DETERMINE IF EPIGENETIC FACTORS CONTROL TET1 BINDING AT SPECIFIC ICRS DURING DEMETHYLATION.	74
4.3 TET1 AND HUMAN IMPRINTING DISORDERS	80
3.4 TET1 KNOCKOUT BY TET1 KNOCKOUT BREEDING.....	85
3.5 CONCLUSION	86
CHAPTER 4: MATERIALS AND METHODS.....	97
4.1 ANIMALS.....	97
4.2 GERM CELL COLLECTION	97
4.2.1 Oocytes	97
4.2.2 Sperm	98
4.2.3 PGCs	98
4.3 TISSUE HOMOGENIZATION.....	99
4.4 RNA AND CDNA CONVERSION	99
4.5 QPCR ANALYSIS	99
4.6 ALLELE-SPECIFIC EXPRESSION ANALYSIS.....	100
4.7 DNA EXTRACTION	101
4.8 BISULFITE TREATMENT.....	101

4.9 PYROSEQUENCING..... 101

4.10 BISULFITE, CLONE, AND SEQUENCING ANALYSIS.....102

4.11 STATISTICS102

BIBLIOGRAPHY.....107

LIST OF TABLES

Table 1.1. Genetic models of imprinted expression and DNA methylation regulators at the <i>H19</i> locus in mice	32-33
Table 1.2. Genetic models of imprinted expression and DNA methylation regulators at the <i>Igf2r</i> locus in mice	34
Table S2.1. % DNA methylation at ICRs in <i>Tet1</i> oocytes with inclusion data.	64
Table S2.2. Litter (denoted with unique letters), sex (M= male, F = female), allele-specific expression, and DNA methylation data for all E10.5 mCON and mKO embryo and placentas.	65
Table S2.3. Sex ratio information for both maternal and paternal <i>Tet1</i> offspring.	66
Table S2.4. Litter (denoted with unique letters), sex (M= male, F = female), allele-specific expression, and DNA methylation data for all Po mCON and mKO brain, liver, and tongue.	67
Table S2.5. % DNA methylation at ICRs in <i>Tet1</i> Sperm	68
Table S2.6. Litter (denoted with unique letters), sex (M= male, F = female), allele-specific expression, and DNA methylation data for all E12.5 pCON and pKO embryo and placentas.	69
Table S2.7. Litter (denoted with unique letters), sex (M= male, F = female), allele-specific expression and DNA methylation data for all Po pCON and pKO brain, liver, and tongue.	70
Table 3.1. Potentially deleterious splice site, indel, and nonsense mutations reported for the human <i>TET1</i> gene	92-94
Table 3.2. Summary of litter size and sex from KO x KO and KO x Het control crosses	95
Table 4.1. List of primers used for each assay in this study.	104
Table 4.2. List of PCR cycling conditions for each PCR used in this study.	105
Table 4.3. Complete PCR protocols with linear range information for imprinted genes	106

LIST OF FIGURES

Figure 1.1. Schematic of the <i>H19</i> imprinted locus in mice.	30
Figure 1.2. The life cycle of a DNA methylation imprint.	31
Figure 2.1. Hypermethylation occurs stochastically in <i>Tet1</i> ^{-/-} oocytes at the <i>H19/Igf2</i> ICR and the <i>IG-DMR</i> .	52
Figure 2.2. Abnormal allele-specific expression and methylation of <i>Igf2</i> in E10.5 mKO offspring.	53
Figure 2.3. Abnormal methylation and total expression at the <i>IG-DMR</i> in E10.5 mKO offspring.	54
Figure 2.4. Allelic expression of <i>Igf2</i> and methylation at the <i>H19/Igf2</i> ICR is consistent across different tissues in P0 newborn mKO offspring.	55
Figure 2.5. Hypermethylation occurs at a subset of ICRs in <i>Tet1</i> ^{-/-} sperm.	56
Figure 2.6. Biallelic expression of <i>Cdkn1c</i> is prevalent in E12.5 pKO offspring.	57
Figure 2.7. P0 pKO pups show biallelic <i>Cdkn1c</i> expression and methylation defects across tissues.	58
Supplemental Figure 2.1. Further characterization of oocyte DNA methylation.	59
Supplemental Figure 2.2. F1 hybrid breeding schemes for analyzing allele-specific expression.	60
Supplemental Figure 2.3. Bisulfite sequencing validation of <i>Tet1</i> sperm DNA methylation.	61
Supplemental Figure 2.4. Hypermethylation at the <i>KvDMR</i> and <i>Peg3</i> ICRs is mutually exclusive in E12.5 pKO embryos and P0 newborns.	62
Supplemental Figure 2.5. Abnormal biallelic expression and DNA hypermethylation are consistent in the E12.5 placental tissues.	63
Figure 3.1. <i>Tet1</i> ; <i>Oct4-eGFP</i> mouse crossing strategy.	88
Figure 3.2. E13.5 PGC sorting using the EGFP reporter.	89
Figure 3.3. TET1 is not localized to ICRs but is localized at secondary DMRs in mouse ESCs.	90
Figure 3.4. Models of how H3K9me2/3 might repress TET1.	91
Figure 3.5. Preliminary data regarding differences in (A) litter size or (B) weight (g) of KO x KO pups	96

CHAPTER 1: INTRODUCTION

All cells within an organism contain the same genetic information, yet the phenotypes of these cells vary drastically across tissues and stages of development. Epigenetic control of gene expression allows for the distinct usage and expression of genes, ultimately giving rise to the diverse set of cells and functions within the body. Epigenetics broadly encompasses heritable mechanisms that lead to changes in gene expression without altering the underlying DNA sequence, such as nucleosome positioning and composition, histone post-translational modifications, non-coding RNAs, and DNA methylation. DNA methylation, the best studied epigenetic modification, involves the covalent addition of a methyl group to the carbon 5 position on cytosine (5mC), typically within the context of a cytosine guanine dinucleotide, connected by a phosphodiester bond (CpG). This epigenetic mark is involved in a variety of functions in the mammalian genome, including X chromosome inactivation, gene silencing, genomic stability, cellular identity, and genomic imprinting.

1.1 DNA methyltransferases add and maintain DNA methylation

DNA methylation is a catalytic reaction carried out through the use of the methyl donor, S-adenosylmethionine (SAM). This covalent modification of cytosine residues typically occurs in a CpG context, although non-CpG methylation has been observed, particularly in the brain and in oocytes (Guo et al., 2014a; Smith et al., 2012). Collectively, the DNA methyltransferase enzymes (DNMTs) add and maintain levels of DNA methylation throughout the genome (Lyko, 2018).

The first identified family member of DNMTs was DNMT1. *Dnmt1* homozygous null animals die during midgestation, indicating the importance of DNA methylation during development (Li et al., 1992). DNMT1 maintains DNA methylation by copying

existing methylation patterns onto newly replicated DNA strands. Evidence suggests that DNMT1 can methylate cytosines in a de novo fashion (Vertino et al., 1996), although the enzyme's preferred substrate is hemimethylated DNA (Fatemi et al., 2001). The maintenance function of DNMT1 is accomplished by binding to ubiquitin-like with PHD and ring finger domains 1 (UHRF1, also known as nuclear protein, 95 kDa (NP95))(Bostick et al., 2007). UHRF1 binds to proliferating cell nuclear antigen (PCNA), the sliding clamp of the DNA replication fork (Uemura et al., 2000). UHRF1 additionally is recruited to the replication fork by DNA ligase 1 (LIG1) (Ferry et al., 2017). Thus, DNMT1 is targeted to the replication machinery, which explains the mechanism behind its maintenance function.

Evidence for additional DNA methyltransferase enzymes became apparent when residual DNA methylation was observed in *Dnmt1* null embryonic stem cells (ESCs) and mice (Li et al., 1993a). Through homology searches, two additional methyltransferases were discovered, called DNMT3A and DNMT3B (Okano et al., 1998). They were designated the *de novo* methyltransferases because they can add DNA methylation with equal affinity for non-methylated and hemimethylated DNA substrates, but they have also been shown to have some maintenance functions as well (Okano et al., 1998; Rhee et al., 2000). *Dnmt3a* null mice die approximately four weeks after birth, whereas *Dnmt3b* homozygous knockout animals die after E9.5 (Okano et al., 1998; Okano et al., 1999).

The DNMT3L protein lacks a catalytic domain but binds to both of the *de novo* methyltransferases and acts as a stimulatory cofactor. DNMT3L contains a plant homeodomain-like domain (PHD) that recognizes unmethylated histone 3 lysine 4 (H3K4) residues and therefore is important for targeting DNMT3A and DNMT3B to chromatin. *Dnmt3l* homozygous knockout animals also die around E9.5 (reviewed in (Dan and Chen, 2016; Jurkowska and Jeltsch, 2016)). Interestingly, mouse ESCs can

tolerate the combined deletion of DNMT1, DNMT3A, and DNMT3B despite the near complete abolishment of DNA methylation. However, these cells have compromised differentiation, emphasizing the critical role of DNA methylation in development (Tsumura et al., 2006).

Lastly, a rodent-specific DNA methyltransferase gene, *Dnmt3c*, was recently discovered (Barau et al., 2016). This gene resulted from a duplication of *Dnmt3b*. DNMT3C is responsible for adding DNA methylation to promoters of young retrotransposons in the male germline. *Dnmt3c* homozygous mutant mice develop normally but are sterile, due to azoospermia caused by disruptions of chromosome synapsis during meiotic prophase I. Thus, this gene is important for normal male fertility in mice (Barau et al., 2016).

1.2 Genomic Imprinting

1.2.1 Definition

Genomic imprinting is a phenomenon where a subset of genes in the mammalian genome is expressed from a single parental allele. We contrast this definition of imprinted genes with genes that show allelically-biased expression, as the mechanism governing biased expression is unclear. Currently, approximately 150 imprinted genes in mice and about 100 in humans have been identified, many of which are imprinted in both species. Imprinted genes tend to be found in clusters, and this allows for their coordinated regulation by a *cis*-acting regulatory element called an imprinting control region (ICR). ICRs are characterized by parental-allele-specific DNA methylation, which regulates their unique expression pattern (Barlow and Bartolomei, 2014). I describe the identification and characterization of ICRs below.

1.2.2 Historical Perspective

The inequivalence of the paternal and maternal genomes was known well before the identification of imprinted genes. Nuclear transfer experiments in mouse demonstrated that both maternal and paternal contributions were necessary for viable pups, whereas uniparental embryos failed to develop to term (McGrath and Solter, 1984; Surani et al., 1986). Additionally, it was shown that uniparental disomies in specific genomic regions were detrimental or gave rise to phenotypes dependent upon the parent-of-origin, in both mouse and humans (Cattanach and Kirk, 1985; Searle and Beechey, 1978). Lastly, a subset transgenic mouse lines exhibited parent-of-origin specific expression of the transgene (Swain et al., 1987), suggesting that some genomic sequences could be differentially modified in the germline (Barlow and Bartolomei, 2014).

The first three imprinted genes were described in the early 1990s: insulin-like growth factor receptor 2 (*Igf2r*) (Barlow et al., 1991), *H19* (Bartolomei et al., 1991), and insulin-like growth factor 2 (*Igf2*) (DeChiara et al., 1991). Two of these genes (*H19* and *Igf2*) are linked (Figure 1) (Zemel et al., 1992), which prompted the original suggestion that imprinted genes are clustered. Once imprinted genes were identified, the question of how this unique expression pattern is conferred was pursued. It was hypothesized that a specific sequence could be marked epigenetically, or that a sequence could be recognized by a trans-acting epigenetic regulatory protein. Given the suggestion that imprints must be set in the germline, maintained through fertilization, and erased in embryonic germ cells, it was speculated that DNA methylation may be the epigenetic mark that fit these criteria (DeChiara et al., 1991). Definitive evidence that DNA methylation regulates imprinted gene expression came from a mouse knockout model of the DNA methyltransferase 1 (*Dnmt1*) gene, which resulted in DNA hypomethylation and loss of

imprinted gene expression (Tables 1.1 and 1.2) (Li et al., 1993b). Consequently, for each imprinted loci, rigorous searches for the specific sequence that was differentially DNA methylated and met the criteria of imprints were undertaken. For example, at the *H19* locus, a region of paternal-specific methylation was found in a 7-9 kilobase region encompassing part of the *H19* gene itself, as well as a 5' region (Bartolomei et al., 1993). This region was further refined to a 2 kilobase region 5' of *H19* that was found to be DNA methylated in sperm but not oocytes, and this differential methylation was maintained during development (Tremblay et al., 1995; Tremblay et al., 1997). More recently, genome-wide analyses using F1 hybrid animals have confirmed existing regions as well as uncovered new differentially methylated regions (DMRs) in mice (Xie et al., 2012).

1.2.3 Mechanisms of ICR Functions

Ultimately, the test of whether a DMR is an ICR and conferred imprinted expression of one or multiple genes was undertaken using genetic deletion and mutations in mice. Loss of imprinted gene expression upon deletion of a DMR provided evidence that the sequence was causal in conferring imprinted gene expression—these regions are designated as ICRs. How these ICRs control monoallelic expression is still not fully understood, but mechanisms at two or more imprinted loci have been carefully dissected and thus two predominant models of imprinting have been described: the enhancer blocking model at the *H19/Igf2* locus and the long noncoding RNA model at the *Igf2r* locus (Barlow and Bartolomei, 2014). These models are by no means exhaustive and thus the mechanisms across other imprinted loci remain to be determined. I describe the two imprinting models below.

The *H19* ICR is DNA methylated exclusively on the paternal allele (Tremblay et al., 1997). CCCTC binding factor (CTCF), a multifunctional, methylation-sensitive architectural protein, binds to the unmethylated maternal ICR and forms a functional

insulator blocking the access of downstream enhancers from interacting with the upstream *Igf2* promoter (reviewed by Singh et al., 2012). On the paternal allele, DNA methylation at the ICR prevents CTCF binding, allowing the downstream enhancers to interact with the *Igf2* promoter and promote transcription. The DNA methylation from the ICR spreads into the *H19* promoter, silencing *H19* expression (Davis et al., 2000) (Fig 1.1). A paternally inherited 1.6 kb deletion of the *H19* DMR in mice caused activation of paternal *H19* expression and concurrent repression of paternal *Igf2* expression whereas the maternal inheritance of the same deletion caused the opposite effect: *H19* expression was repressed, whereas *Igf2* expression was activated on the maternal allele (Thorvaldsen et al., 1998). This study highlights the crucial function of the *H19* ICR for regulating monoallelic expression of both *H19* and *Igf2*.

In an alternative model, certain other ICRs overlap with promoters for noncoding RNAs. For example, the paternally unmethylated *Igf2r* ICR overlaps the promoter for the paternally-expressed *Airn*, the *KvDMR* shares sequence with the promoter for the paternally-expressed *Kcnq1ot1*, and the *Snrpn* ICR overlaps with the promoter for *Ubez1a-ats*, (Barlow and Bartolomei, 2014). At the aforementioned *Igf2r* locus, the ICR is in an intron of the *Igf2r* gene (Stöger et al., 1993). The ICR is methylated on the maternal allele, silencing the expression of the long noncoding RNA, *Airn*. On the paternal allele, the ICR is unmethylated, allowing transcription of *Airn*, which interferes with the transcription of *Igf2r* in *cis* by transcriptional interference at the *Igf2r* promoter (Latos et al., 2012). This model has also suggested to be partially how the *KvDMR* functions but is not sufficient to explain imprinting across the entire locus in certain tissues, such as the heart (Barlow and Bartolomei, 2014; Korostowski et al., 2012).

1.2.5. Secondary DMRs

In contrast to an ICR that gains DNA methylation in the germline and controls the monoallelic expression of imprinted genes in the locus, certain imprinted loci contain additional DMRs that gain methylation later in development or gain methylation in the germline, lose methylation during preimplantation, and are remethylated post-implantation. These are known as secondary or somatic DMRs. For example, at the *Igf2r* locus, two DMRs were identified using southern blots. DMR2 serves as the primary ICR that gains methylation in the germline on the maternal allele. In contrast, DMR1 is localized to the promoter of *Igf2r* and the paternal allele that carries DNA methylation is silent (Stöger et al., 1993). This DMR is unmethylated in sperm and ESCs, but gains methylation postimplantation and this methylation is maintained in the adult (Stöger et al., 1993). To understand the role DMR1 plays in imprinted gene expression, a mouse model was created that replaced the endogenous *Igf2r* promoter with the thymidine kinase promoter or deleted the promoter entirely. In both cases, imprinted expression of *Airn*, *Slc22a2* and *Slc22a3* remained intact, arguing against a role of DMR1 in maintaining imprinted expression. However, the alleles lacking the endogenous promoter aberrantly gained methylation on the maternal allele, indicating the sequences contained in this promoter normally repress methylation on the maternal allele in the wild-type situation (Sleutels et al., 2003).

The *KvDMR* locus in mice expresses a long noncoding RNA, *Kcnq1ot1*, from the paternal allele. The promoter of *Kcnq1ot1* is unmethylated on the paternal allele and is associated with *Kcnq1ot1* expression (Smilinich et al., 1999). DNA methylation at the promoter of *Kcnq1ot1* on the maternal allele suppresses its expression and lack of transcription allows an antisense gene, *Kcnq1* to be expressed (Mancini-DiNardo et al., 2006). *Cdkn1c* is also expressed maternally. Interestingly, almost the entire gene body of

Cdkn1c is located within a CpG island (CGI), known as the *Cdkn1c* DMR, methylated on the paternal allele. This DMR, like the *Igf2r* DMR1, gains methylation not in sperm, but later in somatic tissue. Using polymorphisms in F1 hybrid tissue, Bhogal and colleagues determined the parental specific methylation of the *Cdkn1c* DMR begins 650 bp 5' to the start of the gene and ends 3' of exon 2, coinciding with the 3' end of the CGI (Bhogal et al., 2004). In a mouse model where the *KvDMR* had been deleted and inherited on the paternal allele, the *Cdkn1c* DMR lost DNA methylation on the paternal allele and *Cdkn1c* itself was aberrantly biallelically expressed (Bhogal et al., 2004). To test the hypothesis that methylation at the *Cdkn1c* DMR controls allele specific expression of *Cdkn1c*, the authors examined allele-specific expression in early embryos, before the acquisition of the somatic DNA methylation at the DMR. However, *Cdkn1c* was still monoallelically expressed despite the lack of DMR methylation. This supports the idea that the *Cdkn1c* DMR is not responsible for initiating monoallelic expression of *Cdkn1c*. Lastly, in E9.5 *Dnmt1* null embryos, *Cdkn1c* was also biallelically expressed, suggesting that DNA methylation at the *Cdkn1c* DMR is required to maintain imprinted expression (Bhogal et al., 2004; Caspary et al., 1998). Thus, somatic DMRs may influence imprinted expression depending on the locus.

1.2.6. Histone modifications at ICRs

While DNA methylation is perhaps the most well understood mark at ICRs, it is not the only epigenetic modification at these loci. Allele-specific histone modifications are often associated with either the DNA methylated or unmethylated allele depending on the modification. For example, at the *Snrpn* locus, activating histone 3 (H3) lysine 4 (K4) methylation (me) as well as H3K9 and K14 acetylation (ac) are enriched on the paternal, non-DNA methylated ICR in brain tissue, where *Snrpn* is highly expressed (Fournier et al., 2002). Conversely, the DNA methylated maternal allele is enriched in

H3K9 dimethylation (me₂) (Fournier et al., 2002). This association with active, open chromatin acetylation marks is generally true across not only the paternal allele of the *Snrpn* ICR, but across the paternal alleles of many other maternally DNA methylated ICRs, including *Peg1*, *Zac1*, *Gnas1a*, *Peg3*, *Snrpn*, *KvDMR1*, *Igf2r*, and *U2af1* in mouse embryonic fibroblasts (MEFs) (Singh et al., 2010).

Histone modification status has also been investigated at the three known paternally methylated ICRs, *H19*, *IG-DMR*, and the *Rasgrf* ICR in F1 hybrid embryonic stem cells (ESCs). In all three cases, the unmethylated paternal allele was enriched in H3K4me₂ and H3ac. *H19* showed strong enrichment for H4K20me₃ (a repressive modification typical of pericentric chromatin) as well as H3K9me₃. However, no H3K27me₃ was found at either allele of the ICR (Delaval et al., 2007). These patterns of histone modifications were the same at the *IG-DMR* and the *Rasgrf* ICR, with the exception that H3K27me₃ was found on the unmethylated allele at the *Rasgrf* locus (Delaval et al., 2007). H3K9me₃ was also strongly enriched on the DNA methylated paternal allele at the *H19* ICR in MEFs, whereas neither H3K27me₃ nor symmetrically demethylated (me₂s) H4 arginine 3 (R3) showed evidence of allele-specific enrichment in this cell type (Verona et al., 2008).

To understand if these allele-specific modifications are a cause or consequence of transcription at the *H19* locus, Verona et al. used F1 hybrid MEFs and neonatal livers harboring a 3.8 kb deletion that spans the entire *H19* ICR and the intervening sequence between the ICR and the promoter. In this system, when the deletion is inherited maternally, *H19* is not expressed in MEFs, but is expressed in neonatal liver. The investigators found that activating histone modifications at the promoter were only present in neonatal liver where *H19* was expressed, but not in MEFs, regardless of the presence of the 3.8 kb deletion. This indicates that allele-specific histone modifications,

at least at this locus, are established due to transcription and not due to the presence of the ICR (Verona et al., 2008). Interestingly, failure to reprogram these allele-specific histone modifications at this locus may explain a paternal-specific embryonic lethality phenotype in a mouse model where the human *H19* ICR was knocked into the endogenous mouse locus (Hur et al., 2016).

1.2.7 Imprinted genes in health and disease

The importance of proper monoallelic expression of imprinted genes is exemplified by their misregulation in human imprinting disorders and the abnormal phenotypes described in various genetic mouse models where imprinted gene dosage or ICR mutations have been constructed. For example, in patients where there is an abnormal gain of methylation at the *H19* ICR (in humans, imprinting control region 1 (IC1), *H19* is silenced and *IGF2* is biallelically expressed, resulting in an overgrowth disorder known as Beckwith-Wiedemann Syndrome (Cooper et al., 2005). This epimutation accounts for about 5%-10% of Beckwith-Wiedemann patients, whereas hypomethylation at the *KvDMR* (in humans: IC2) accounts for nearly 50% of these patients (Elhamamsy, 2017). Other abnormalities including uniparental disomy, ICR duplications or deletions, as well as deletions in regulatory regions also contribute to imprinting disorders such as transient neonatal diabetes, Silver-Russell syndrome, Prader-Willi syndrome, Angelman syndrome, and Pseudohypoparathyroidism type 1b (Elhamamsy, 2017). Together, these disorders highlight the tight regulation and expression required of imprinted genes for normal development. Moreover, imprinting disorders underscore the need to further understand how imprinted genes are regulated to begin to connect patient molecular diagnoses to phenotypes, which could aid in potential therapeutic discoveries in the future.

1.2.5 ICR methylation dynamics overview

While DNA methylation is a stable and heritable epigenetic mark, this modification is also highly dynamic, particularly during mammalian development. The global changes in DNA methylation after fertilization and in primordial germ cells (PGCs) are central to embryonic epigenetic reprogramming. Intriguingly, parent-specific DNA methylation marks at ICRs are also dynamically regulated during development (Fig 1.2). DNA methylation imprints are first set in the germline and maintained through fertilization and preimplantation development, despite a nearly complete demethylation of the genome. DNA methylation imprints are then erased in the developing PGCs of the embryo, which allows the establishment of sex-specific marks in the gametes (Macdonald and Mann, 2014). Below, I describe the epigenetic reprogramming, evidence for active DNA demethylation, details regarding the TET family of proteins and TDG, followed by a summary of the current knowledge regarding both reprogramming of the genome in general, as well as reprogramming of ICRs during embryonic development.

1.3 Epigenetic Reprogramming

Reprogramming in mammals consists of two main waves: the first occurs in the zygote and preimplantation embryo, and the second, in the developing germ line. In both cases, these waves include dramatic loss of DNA methylation, followed by subsequent de novo methylation. Histone modifications are also dynamically remodeled during these two waves of reprogramming and there may be mechanistic links between these two epigenetic processes (Hajkova et al., 2008; Saitou and Yamaji, 2012). Thus, epigenetic reprogramming refers to broad changes in epigenetic modifications, such as DNA methylation and histone modifications, which lead to changes in gene expression and cell potency. Here, I primarily focus on DNA methylation changes.

The concept of epigenetic reprogramming was initially recognized by Art Riggs when he proposed a role for DNA methylation in facilitating the process of X inactivation in female mammals (Riggs, 1975). In the 1980s, Jähner and Jaenisch observed that changes in gene expression were correlated with DNA methylation and postulated that DNA methylation “may be a condition for ‘resetting’ the genome” (Jähner and Jaenisch, 1984). Later, Monk et al. found that while sperm DNA is highly methylated, blastocysts had very low methylation. Gains of DNA methylation were observed from the blastocyst stage to embryonic day (E)6.5 in the epiblast. By E12.5 and E14.5, PGCs exhibited low levels of DNA methylation, while the somatic DNA methylation levels remained similar to E6.5 epiblasts. Monk and colleagues also observed methylation increases in certain repetitive sequences in male germ cells at E16.5 but not in female germ cells (Monk et al., 1987). This study demonstrated that the early embryo and the germline were likely undergoing dynamic DNA methylation changes.

Why would these reprogramming events be necessary for early mammalian development? In mammals, germ cells are specified from the epiblast (Anderson et al., 2000; Ginsburg et al., 1990). Therefore reprogramming of DNA methylation is required to erase the epiblast-specific pattern of DNA methylation enabling the subsequent acquisition of sperm- or egg-specific epigenetic marks (Monk et al., 1987). This is also true for the zygote, which must erase the cell-type specific DNA methylation marks that define the sperm and oocyte in order to facilitate DNA methylation patterns characteristic of somatic cells. DNA methylation erasure is also postulated to ensure that abnormal epigenetic marks are not transmitted to the next generation (Heard and Martienssen, 2014; Surani, 1999). Lastly, erasure of DNA methylation in the fetal germ line provides a blank slate so that parental specific imprinting marks can be properly established according to the sex of the developing embryo (Tada et al., 1997).

1.3.1 Evidence for active DNA demethylation

Breaking a carbon-carbon bond between the methyl group and the cytosine ring was thought to be impossible given the extreme thermodynamic input required in a physiological setting. However, evidence that DNA methylation could be removed was first demonstrated by Gjerset and Martin, who described demethylation in nuclear extracts from erythroleukemia cells where 5mC was replaced with an unmodified cytosine. This demethylation occurred in the absence of DNA synthesis, was proportional to the amount of protein added to the reaction, and was abolished by the addition of both proteinase K and heat inactivation, indicating an enzymatic activity (Gjerset and Martin, 1982). This demethylation was specific to DNA methylated CpGs (Razin et al., 1986; Razin et al., 1988). Likewise, HeLa cell extract exhibited such an activity and additionally demonstrated newly generated abasic sites in the template, indicating glycosylase involvement (Vairapandi and Duker, 1993). Lastly, it was shown that fusion of somatic cells with germ cells caused extensive DNA demethylation of somatic nuclei (Surani, 1999). This early evidence pointed to an active process whereby 5mC is replaced without DNA replication. While many candidate proteins and pathways have been described as the origin of a demethylating activity (for further information see (Bochtler et al., 2017; Dean, 2016; Ooi and Bestor, 2008)), one of the most promising discoveries involves a family of proteins called the Ten-eleven translocation (TET) family, described below.

1.3.3 Oxidative Demethylation by TET1, TET2, and TET3

In 2002, a fusion protein containing part of the mixed lineage leukemia (MLL) histone methyltransferase and a previously uncharacterized protein, called leukemia-associated protein with a CxxC domain (LCX), was described in patients with MLL (Ono et al., 2002). However, it was not until 2009 that the relevance of this new protein became apparent (Kriaucionis and Heintz, 2009; Tahiliani et al., 2009). A newly

described cytosine modification in mammals, 5-hydroxymethylcytosine (5hmC), was an oxidation product of 5mC and was reported in Purkinje neurons and mouse ESC DNA (Kriaucionis and Heintz, 2009; Tahiliani et al., 2009). Crucially, Tahiliani et al. demonstrated that LCX, now known as ten-eleven translocation methylcytosine dioxygenase 1 (TET1), was responsible for generating 5hmC and that this activity depended on a functional catalytic domain as well as Fe(II) and alpha-ketoglutarate. The two other TET family members, TET2 and TET3, were also shown to catalyze the 5hmC reaction, and all three family members can further oxidize 5hmC to 5-formylcytosine (5fC) and 5-carboxylcytosine (5caC) (He et al., 2011; Ito et al., 2010; Ito et al., 2011). The use of *Dnmt3a/3b* null mice revealed a reduction in 5fC, suggesting that 5fC accumulation was likely dependent on 5mC first being oxidized by TET to 5hmC (Pfaffeneder et al., 2011). Together, these important studies supported the idea that the TET family proteins are responsible for 5mC oxidation and thus led to the prevailing view that TETs are a major regulator of DNA demethylation.

1.3.4 TETs: Gene and Protein Structure and Function

All three TET family members contain a cysteine-rich domain and a double-stranded beta helix domain, together forming the catalytic domain of these proteins (Kohli and Zhang, 2013). The crystal structure of the TET2 catalytic domain revealed that the enzyme works by using a base-flipping mechanism. The methyl group of cytosine does not participate in the DNA-enzyme interaction and thus the active site can accommodate the larger oxidized cytosine bases (Hu et al., 2013). The active site of the TET enzyme does show different efficiencies of hydrogen abstraction, with 5hmC and 5fC adopting positions less favorable for the reaction. This structural finding indicates that catalytic efficiency is better converting from mC to 5hmC, than from 5hmC to 5fC, or from 5fC to 5caC (Hu et al., 2015).

Both TET1 and TET3 contain a CxxC domain that lacks the KFGG motif found in some other CxxC domain containing proteins, such as Dnmt1, whereas TET2 lacks this domain entirely. Instead, IDAX, a genomic neighbor of TET2, contains this domain, indicating that IDAX may have arisen from a gene duplication event (Ko et al., 2013). This structural difference is thought to create a more flexible mode of DNA binding compared to CxxC domain proteins containing the KFGG motif (Long et al., 2013). Studies of the TET CxxC domain have led to conflicting reports on its effect on the preferred sequence context of TET (Frauer et al., 2011; Xu et al., 2011; Zhang et al., 2010). Recent data supports the idea that the human TET1 CxxC domain will bind CpN with a slight preference for CpG, and only weakly binds hemi-methylated CpG sites, or hemi-5hmCpG sites (Xu et al., 2018; Zhang et al., 2017). TET1 ChIP-seq data from ESCs does demonstrate that TET1 localizes to regions of high CpG density, including DNA hypomethylated CpG-rich promoters (Williams et al., 2011; Wu et al., 2011a).

In mice, the *Tet1* gene is located on chromosome 10 and has two annotated refseq isoforms. These isoforms contain 11 or 12 exons, respectively, and the entire gene spans 75,445 base pairs. Interestingly, additional *Tet1* isoforms have been recently reported in the literature, including a N-terminal truncation that initiates transcription from exon 2 using an alternative promoter. This shortened isoform lacks the upstream sequence and CxxC domain of TET1. The full length isoform is expressed in ESCs, PGCs, and early embryos, while the truncated form is expressed later in development and in adult tissues (Zhang et al., 2016b). Zhang and colleagues expressed Flag-tagged full-length and short isoforms, as well as different isolated domains of TET1 in the background of *Tet1;Tet2* double knockout ESCs. They found that the short isoform of TET1 could still bind chromatin, although to a lesser extent than the full-length isoform. Of note, the N-terminal domain without the CxxC domain was also found to bind to chromatin. Thus

the authors conclude that the N-terminal domain, named before CxxC domain (BC), plays an additional, previously unappreciated role in chromatin binding (Zhang et al., 2016b).

1.3.5 TDG and base excision repair

Thymine DNA glycosylase (TDG) was originally described for its DNA glycosylase activity on G/T mismatches. Nevertheless, there had been hints that this enzyme was also involved in DNA demethylation (Jost et al., 2001; Vairapandi and Duker, 1993; Zhu et al., 2000). It is now appreciated that TDG cleaves 5fC and 5caC rapidly in vitro, whereas the enzyme shows no activity on 5hmC (He et al., 2011). This cleavage results in an abasic site that is subsequently repaired by base excision repair. Indeed, inhibition of base excision repair proteins downstream of TDG such as apurinic/apyrimidinic endonuclease 1 (APE1) or poly(ADP-ribose) polymerase 1 (PARP1) (Ciccarone et al., 2012; Hajkova et al., 2010; Kawasaki et al., 2014) in cultured mouse zygotes leads to accumulations of 5mC in zygotes (Hajkova et al., 2010). Other experiments that inhibited PARP pharmacologically in pregnant dams also led to increases in DNA methylation at certain imprinted genes in fetal PGCs. TDG null embryos die around E12.5 (Cortázar et al., 2011; Cortellino et al., 2011), further underscoring this protein's role in a critical developmental pathway.

1.4 Preimplantation DNA Methylation Reprogramming

1.4.1 Genome-Wide DNA Demethylation

After fertilization, the paternal pronucleus undergoes rapid demethylation before the onset of DNA replication whereas the maternal genome demethylates more slowly over multiple cell divisions. These kinetics indicate that the paternal genome is actively demethylated whereas the maternal genome is demethylated in a passive, replication-dependent manner (Seah and Messerschmidt, 2017). Multiple groups have described

TET3 activity as well as the accumulation of all three oxidized cytosine bases in both parental pronuclei (Shen et al., 2014; Tsukada et al., 2015). This accumulation depends on TET3 as well as TET1 as depletion of TET3 in the oocyte leads to an impairment of 5hmC accumulation, whereas depletion of both TET1 and TET3 leads to a complete absence of 5hmC at the 8-cell stage (Gu et al., 2011; Kang et al., 2015; Wossidlo et al., 2011). It is likely that 5hmC, 5fC, and 5caC are removed by passive dilution as these bases are only found on one half of the paternally-derived chromatids (Inoue and Zhang, 2011; Inoue et al., 2011).

Interestingly, the oxidation of 5mC in the zygote may not be necessary for the global demethylation as previously thought. Shen and colleagues demonstrated that demethylation still occurred in paternal pronuclei despite a conditional oocyte-specific *Tet3* knockout, suggesting that zygotic TET3 was partially responsible for demethylating the paternal genome and that only certain regions were dependent on TET3 for 5mC oxidation. When wild-type zygotes were treated with the replication inhibitor aphidicolin, 5mC levels did not decrease, despite the continued activity of TET3 as evidenced by the presence of the oxidized bases 5hmC, 5fC, and 5caC, suggesting a role for DNA replication (Shen et al., 2014). Further evidence that 5hmC accumulation does not drive DNA demethylation was demonstrated by precise staging of zygotes and detection of 5mC and 5hmC using antibody staining (Amouroux et al., 2016). This experiment demonstrated that the global wave of DNA demethylation is complete by pronuclear stage (PN)3, corroborating earlier reports (Amouroux et al., 2016; Santos et al., 2002). It was further demonstrated that the accumulation of 5hmC was dependent on previously underappreciated activities of both maternally inherited DNMT3A and DNMT1 (Amouroux et al., 2016). Thus, the role of TET3 in the zygote may not be connected to the initial DNA demethylation of the genomes after fertilization, but may be

serving to protect normally unmethylated regions from inappropriate acquisition of DNA methylation (Amouroux et al., 2016).

1.4.2 Imprinted Regions Escape Preimplantation DNA Methylation Reprogramming

Even before the discovery of imprinted genes, it was appreciated that the functional differences between maternal and paternal genomes remained intact during genome-wide demethylation that occurred in the zygote (Surani et al., 1986). Now, it is clear that a generalized feature of ICRs is the maintenance of DNA methylation and simultaneous protection from demethylation after fertilization. How are ICRs protected? Developmental pluripotency associated 3 (DPPA3, also known as STELLA or PGC7) is a highly expressed protein in oocytes, PGCs, and both pronuclei in the zygote (Sato et al., 2002). When DPPA3 is deleted, both maternal and paternal genomes lose methylation. This is also apparent for ICRs. *Dppa3* maternal-null zygotes partially lose imprinted DNA methylation at the *H19* (Table 1.1), *Peg1*, *Peg3*, *Peg10*, and *Rasgrf1* ICRs. In contrast, the *IG-DMR*, *Snrpn*, and *Peg5* ICRs remained methylated, indicating that DPPA3 is partially responsible for the maintenance of DNA methylation at a subset of ICRs (Nakamura et al., 2007). It has been suggested that DPPA3 exerts a maintenance function by binding to and inhibiting the activity of the C-terminal catalytic domain of TET2 and TET3 (Bian and Yu, 2014). Bian and Yu also demonstrated that approximately 60% of TET3 chromatin immunoprecipitation followed by deep sequencing (ChIP-seq) peaks overlapped with DPPA3 peaks, and vice versa. Analysis of the DNA sequence bound by DPPA3 indicated a motif preference found in the ICRs of *Peg1*, *Peg3*, *Peg10*, and *H19*. (Bian and Yu, 2014). However, results from this study should be interpreted with caution as the co-immunoprecipitations were conducted in human embryonic kidney 293T cells (Bian and Yu, 2014), which express low levels of TET proteins endogenously (Grosser et al., 2015; Wu and Zhang, 2011). Additionally, DPPA3 can bind

to H3K9me2, which is enriched on the methylated allele of imprinted genes, further explaining the targeting and protection of ICRs afforded by DPPA3 binding (Nakamura et al., 2012).

Perhaps a more compelling factor that is involved in the protection of ICR methylation during preimplantation development is zinc finger protein 57 (ZFP57) (Li et al., 2008). Null embryos from *Zfp57* heterozygous matings show a partial lethality phenotype (Li et al., 2008). Maternal-zygotic null zygotes exhibit changes in total expression of imprinted genes regulated by the *IG-DMR* and loss of ICR DNA methylation, but the ICR DNA methylation and imprinted gene expression at the *H19/Igf2* locus are unaffected (Table 1.1). The maternal-zygotic *Zfp57* mutants also lose methylation at the *Snrpn*, *Peg1*, *Peg3*, and *Peg5/Nnat* ICRs (Li et al., 2008). Interestingly, ZFP57 binds only to the methylated ICR and this methylation is necessary for its binding (Quenneville et al., 2011; Strogantsev et al., 2015). The allele-specific binding is neither observed at secondary DMRs (Fig 1.2) nor at DMRs unrelated to imprinted genes in the germline (Strogantsev et al., 2015). CHIP-seq experiments demonstrated that a six-base pair motif, TGCCGC, is found at almost all of the known ICRs. This motif is sufficient to maintain DNA methylation at the *Snrpn* ICR when it is integrated away from its endogenous locus, but mutations of the motif cause a loss of methylation maintenance in this system (Anvar et al., 2015).

The ability of ZFP57 to serve an ICR methylation maintenance function lies in its interacting partners. ZFP57 binds tripartite motif-containing 28 (TRIM28, also known as KAP1 or TIF1-beta), which is a corepressor that recruits repressive histone modifiers like histone deacetylases (HDACs), the histone methyltransferase SETDB1, and DNA methyltransferases to chromatin (Messerschmidt, 2012). The recruitment of maternal DNMT1 is essential for imprint maintenance as maternal-zygotic *Dnmt1* mutation also

leads to demethylation at ICRs in zygotes (Hirasawa et al., 2008). *Trim28* hypomorphic zygotic mutants maintain imprinted DNA methylation at the *IG-DMR*, but loss-of-function zygotic mutants lose DNA methylation at *IG-DMR* in a partially penetrant manner, indicating the amount of TRIM28 is important for ICR protection.

Hypomorphic maternal-zygotic *Trim28* mutants exhibit biallelic expression of *H19* (Table 1.1), *Gtl2*, and *Snrpn* (Alexander et al., 2015). Additionally, single cell methylation analysis of six ICRs (*H19*, *IG-DMR*, *Igf2r*, *Snrpn*, *Peg3*, *Nnat*), demonstrated that maternal loss of *Trim28* resulted in highly variable demethylation of these ICRs within the same blastomere (Tables 1.1 and 1.2). This result suggests that maternal *Trim28* deficiency leads to an incompletely penetrant ICR demethylation phenotype (Lorthongpanich et al., 2013).

1.5 Peri-implantation De Novo Methylation of the Genome

Following zygotic epigenetic reprogramming, the blastocyst is hypomethylated with the exception of imprinted genes, Intracisternal A particle elements (IAPs), and a subset of gene promoters, including genes enriched in functions such as gamete generation and sexual reproduction (Kim et al., 2004; Saitou et al., 2012). Beginning at the early blastocyst stage and culminating by E6.5, the genome gains DNA methylation globally while certain CpG islands remain hypomethylated (Saitou et al., 2012; Smith et al., 2012). PGCs are specified from cells with this aforementioned methylated state, which then must be subsequently erased, as discussed in the following section.

1.6 PGC DNA Methylation Reprogramming

PGCs are specified at E7.25 in the mouse. After specification, PGCs proliferate and migrate from the epiblast towards the genital ridge. PGCs then undergo a second wave of demethylation to erase the epiblast cell fate and facilitate germ-cell fate. Here, DNA is demethylated at ICRs (Saitou and Yamaji, 2012). First, levels of genome-wide

methylation decrease as early as E8.0, while some regions maintain DNA methylation. A later, second wave targets these initially resistant regions, leading to the lowest levels of methylation in PGCs by E13.5. This two-step demethylation process may be important for suppressing premature differentiation of the germline (Hargan-Calvopina et al., 2016).

1.6.1 Bulk genome-wide demethylation in PGCs: The early wave

Numerous studies have demonstrated genome-wide demethylation in PGCs from E7.25 to E13.5. Immunofluorescence staining of 5mC showed that PGCs are globally demethylated starting as early as E8.0, concomitant with the onset of PGC migration. Genome-wide profiling confirmed these observations (Guibert et al., 2012; Popp et al., 2010; Seisenberger et al., 2012a). Demethylation is accompanied by global loss of H3K9me (Seki et al., 2005), downregulation of DNMT3A (Seki et al., 2005), and cytoplasmic localization of DNMT3B. DNMT1 is expressed and localized to the nucleus from E10.5 to E13.5 (Hajkova et al., 2002). In PGCs, *Uhrf1* mRNA is also consistently downregulated after E7.25, and UHRF1 protein expression is undetectable between E8.5 and E11.5 (Ohno et al., 2013), indicating impaired targeting for DNMT1 to the replication fork (Kurimoto et al., 2008). Passive dilution of DNA methylation was further demonstrated using hairpin bisulfite sequencing, where strand-specific DNA methylation can be determined. In PGCs, hemimethylated DNA strands significantly increased between E10.5 to E11.5 at long-interspersed nuclear elements-1 (LINE1) (Ohno et al., 2013). Overall, these observations indicate that a variety of mechanisms facilitate DNA demethylation, including downregulation and nuclear exclusion of de novo and maintenance DNA methylation machinery and absence of the targeting factors.

Does the oxidation of 5mC by TET proteins contribute to global DNA demethylation in PGCs? *Tet1* and *Tet2* mRNA and protein are detectable in PGCs

between ~E9.5-E12.5. Notably, *Tet3* mRNA and protein levels are undetectable, indicating 5hmC is most likely generated by TET1 and TET2 in PGCs (Hackett et al., 2013; Hajkova et al., 2010; Yamaguchi et al., 2012). PGCs assayed for 5mC and 5hmC with mass spectrometry showed increases in 5hmC starting at E8.75 through E12.5. However, immunostaining did not reveal changes in the levels of 5fC and 5caC, indicating that further oxidation of 5hmC is not involved in the bulk wave of DNA demethylation (Hackett et al., 2013; Yamaguchi et al., 2013). Consistently, in chromosome spreads, 5hmC was only detected on one sister chromatid suggesting that dilution of the oxidized base through passive replication is responsible for demethylation in PGCs (Yamaguchi et al., 2013). To determine the role of TET1 catalytic activity on DNA demethylation in PGCs, an allele without the catalytic domain of TET1 was generated (*Tet1^{Gt}*) and methylation was profiled in *Tet1^{Gt}* E13.5 PGCs. Overall, global levels of methylation were unchanged, suggesting that TET1 does not contribute to genome-wide demethylation but may play roles in locus-specific demethylation instead (Yamaguchi et al., 2012).

It is notable that while overall levels of DNA methylation decrease beginning at E8.0 in PGCs, and reach a minimum at E13.5, not all parts of the genome follow these demethylation kinetics. Certain regions are initially resistant to this wave of DNA methylation, indicating DNA methylation is maintained. These regions include ICRs, a subset of repetitive elements, and CpG islands on the X-chromosome (Hajkova et al., 2002; Kobayashi et al., 2013; Seisenberger et al., 2012a). In order for DNA demethylation resistant loci to maintain DNA methylation, two processes are required. First, the loci must be resistant to demethylation, possibly through the use of proteins that protect DNA from demethylation. Second, methylation must be maintained during cell division. DNMT1, despite the low levels of UHRF1 in PGCs (Seki et al., 2005),

methylates the *H19* ICR, *Snrpn* ICR, and IAP elements. This suggests that DNMT1 can localize to specific regions including IAPs and ICRs to maintain DNA methylation (Hargan-Calvopina et al., 2016).

1.6.2 Chromatin Landscape Dynamics during DNA Demethylation in PGCs

During DNA demethylation in PGCs, conflicting reports describe changes in the chromatin landscape. It is generally agreed that early PGCs are characterized by global depletion of H3K9me2, and enrichment in H3K27me3, H3K4me2/3, H3K9ac, and H4/H2AR3me2s as determined by immunofluorescence staining (Ancelin et al., 2006; Hajkova et al., 2008; Seki et al., 2005). However, one study found that by E11.5, the loss of the linker histone, H1, as well as the loss of many heterochromatin marks such as H3K9me3, H3K27me3, and HP1 coincided with a loosening of the overall chromatin structure and enlarged size of the nucleus. H3K9ac marks are also lost at this time point (Hajkova et al., 2008). Conversely, another study reported that at E11.5, there was no loss of the linker histone, no loss of chromocenters, and no loss of H3K27me3 (Kagiwada et al., 2013). These conflicting reports may be due to the use of small numbers of single cell suspensions of PGCs compared to quantification using whole-mount immunofluorescence in the second study (Kagiwada et al., 2013). Hajkova et al. reports that at E12.5, PGCs have regained bright DAPI-staining chromocenters, H1, H3K9me3, and slowly start to accumulated H3K27me3. The enzyme complex of BLIMP1-PRMT5 responsible for adding H4/H2AR3me2s is excluded from the nucleus at this time and this coincides with the loss of these marks (Ancelin et al., 2006). While the exact levels of different histone modifications during PGC reprogramming are not yet completely clear, these dynamic changes in chromatin modifications may be interrelated with the concurrent DNA demethylation and may be necessary for PGC reprogramming.

1.6.3 ICR demethylation in PGCs

As stated above, ICRs retain their methylation in PGCs until approximately E10.5 and then are demethylated in a gene-specific stereotypical pattern. This result was first demonstrated by assaying DNA methylation at individual imprinted genes. Early profiling studies in F1 hybrid mice demonstrated that the *H19* ICR was considerably demethylated on both the maternal and paternal allele by E13.5 in PGCs (Davis et al., 2000). Lee et al. generated embryos from PGC clones and used the imprinting status of these embryos as proxies for the imprinted status in the parental PGCs. ICRs in embryos derived from E11.5 PGCs had very different levels of methylation, indicating this demethylation of ICRs occurs somewhat stochastically across a population of PGCs. This result also suggested that each ICR had its own demethylation timing: the *Nnat* ICR was one of the earliest to demethylate, the *H19* ICR was “intermediate”, whereas the *Peg10* ICR was the slowest and thus the most resistant to DNA demethylation. The timing of DNA methylation in PGCs and PGC clones had good concordance (Lee et al., 2002). Additionally, locus-specific bisulfite sequencing of PGCs revealed that the *Peg3*, *Lit1*, *Snrpn*, and *H19* ICRs were demethylated between E11.5 to E12.5 and this demethylation persisted until E13.5 (Hajkova et al., 2002). Sato and colleagues sorted GFP transgenic PGCs and found *Igf2r* ICR methylation at E10.5, but demethylation initiated at E11.5 (Sato et al., 2003).

Simultaneous profiling of all ICR methylation in smaller cell numbers was greatly enhanced by whole-genome bisulfite sequencing. Using this technique, at E10.5, ICRs were approximately 40% methylated. At E13.5, in both males and female PGCs, none of the paternally methylated ICRs showed appreciable DNA methylation, confirming the results from earlier locus-specific approaches (Kobayashi et al., 2013). Hackett et al. also found that demethylation timing depended on the imprinted gene in question. Whereas

Peg10 and *Peg3* ICRs were slow to demethylate, *Igf2r* ICR and the *KvDMR* exhibited faster demethylation kinetics (Hackett et al., 2013). Thus, how long DNA methylation is retained depends on the ICR. Interestingly, despite locus specific timing of DNA demethylation at ICRs, chromatin accessibility from E11.5 to E13.5 in both male and female PCGs was found to be relatively constant at ICRs (Guo et al., 2017).

1.6.4 Repetitive Elements

Certain classes of repetitive elements are also resistant to DNA demethylation. For example, sequences retaining the highest levels of DNA methylation in PGCs at E13.5 include certain families of long terminal repeats (LTR) endogenous retroviruses. IAPs are partially demethylated by E12.5 but are not further demethylated by E13.5 (Crichton et al., 2014). While some partial resistance to DNA demethylation has been reported for LINE elements (Hajkova et al., 2002; Kobayashi et al., 2013), both LINES and short interspersed nuclear elements (SINES) are considered to be largely reprogrammed in the germline (Seisenberger et al., 2012a). Lastly, resistance to demethylation appears dependent upon CpG density (Kobayashi et al., 2013).

1.6.5 TET-mediated demethylation of ICRs in the second wave of PGC demethylation

The second wave of demethylation includes ICR demethylation. The expression of TET1 and TET2 in PGCs prompted investigators to examine whether these enzymes participate in ICR demethylation. Multiple lines of evidence were consistent with this idea. Fusion of embryonic germ cells derived from E12.5 PGCs with B cells resulted in ICR demethylation, which coincided with a rapid accumulation of 5hmC (Piccolo et al., 2013). *Tet1* depletion using short-hairpin RNA interference in this system caused a loss of 5hmC accumulation at the *H19* ICR, and the failure to demethylate, despite the presence of TET2 (Piccolo et al., 2013). Physiological experiments directly showed a role for TETs in ICR demethylation. Using glucosyltransferase-quantitative polymerase chain

reaction (Glu-qPCR) to measure locus-specific 5hmC, levels of DNA methylation loss correlated with 5hmC gains at the *KvDMR*, *Peg10*, *Igf2r*, and *Peg3* ICRs in PGCs (Hackett et al., 2013). 9.5 and 10.5 day embryos generated from a homozygous *Tet1^{Gt}* mouse mated to wild-type mouse (Yamaguchi et al., 2012), or from 13.5 day embryos generated from *Tet1;Tet2* double knockout mice mated to either *Tet1;Tet2* double heterozygous mice or to wild-type mice (Dawlaty et al., 2013) showed hypermethylation at ICRs as well as dysregulated total levels of imprinted gene expression (Tables 1.1 and 1.2) (Dawlaty et al., 2013; Yamaguchi et al., 2013). Together, evidence strongly suggests that TET1 may be a prominent mediator of ICR erasure. Work in this thesis further addresses the role of TET1 in mediating genomic imprinting (see Chapter 2).

Despite the accumulation of 5hmC in wild-type PGCs, dependent upon the catalytic activity of at least TET1, the further processing of this oxidized base may occur by replication-dependent dilution. Multiple studies report a decrease in 5hmC levels to be consistent with the predicted replication rate of PGCs (Hackett et al., 2013; Kagiwada et al., 2013). Indeed, levels of *Tdg* mRNA, the protein responsible for cleaving 5fC and 5caC from the genome, drop from E9.5 to E13.5 in PGCs (Kagiwada et al., 2013). Therefore, evidence for active processing of 5hmC at ICRs is still wanting.

1.7 Reacquisition of DNA Methylation at ICRs

Once PGCs have completed demethylation at E13.5, genome-wide and locus-specific remethylation initiates. This remethylation is essential for ICRs to acquire their parental-specific imprints during germ cell development. Male germ cells acquire DNA methylation at ICRs shortly after DNA demethylation ceases, and DNA methylation is completed mostly before birth. In contrast, maternal specific-imprints are acquired predominantly after birth during oocyte growth (Lucifero et al., 2004; Stewart et al., 2016).

While our understanding of how ICRs are targeted for remethylation in the developing germ cells is incomplete, well-validated observations have been made. First, DNA methylation imprints are acquired when the histone modifications H3K4me2/3 are low, levels of the histone demethylases KDM1A and KDM1B are high, and H3K36me3 is high (Gahurova et al., 2017). Additionally, transcription likely plays a major role in the timing of imprinting acquisition, although transcription is not sufficient to explain this timing (Henckel et al., 2011; Stewart et al., 2015; Stewart et al., 2016). A unique case is found at the *Rasgrfi* imprinted locus where piwi-interacting RNAs (piRNAs) have been proposed to play a role in DNA methylation establishment in the male germline (Watanabe et al., 2011). While DNMT3B, DNMT3A, and DNMT3L are required for methylating the *Rasgrfi* ICR, other ICRs, such as the *H19* and *Igf2r* ICRs, are targeted by DNMT3A and DNMT3L (Tables 1.1 and 1.2) (Stewart et al., 2016). Interestingly, the timing of acquisition of imprinted marks is not the same on the previously paternal and previously maternal alleles, indicating a non-equivalence of the underlying chromatin state, despite the lack of DNA methylation in PGCs (Davis et al., 2000; Lucifero et al., 2004). Thus, a complex interplay between DNA methylation regulators, chromatin regulators, transcription, and long-noncoding RNAs together function in a complex manner to methylate the regions crucial for imprinted expression in the next generation.

1.8 Beyond Epigenetic Reprogramming: Other Roles of 5hmC

5hmC is the second most abundant modified cytosine residue in DNA, ranging from 0.03%-0.7% of all cytosine bases in the genome, with the highest levels being present in the central nervous system (Globisch et al., 2010). Given the moderately high levels of this base, as well as tissue-specific levels and distribution, 5hmC has been proposed to be not just an intermediate of DNA demethylation, but perhaps a stable epigenetic mark in its own right (Guo et al., 2014b; Hahn et al., 2013; Hahn et al., 2014;

Nestor et al., 2012). In ESCs, 5hmC tends to be enriched across gene bodies, CpG-rich promoters, and distal regulatory elements. (Pastor et al., 2011; Williams et al., 2011; Wu et al., 2011b). Using *Tet1* and *Tet2* knockdown in ESCs, Huang et al. found that regions that lost 5hmC upon *Tet1* knockdown tended to be in promoters and that 5hmC in this region were negatively correlated with gene expression. In contrast, gene bodies tended to lose 5hmC upon *Tet2* knockdown, and this enrichment in gene bodies was positively correlated with gene expression (Huang et al., 2014). 5hmC, unlike 5mC, is not enriched in repetitive elements such as IAPs and minor satellite repeats (Williams et al., 2011). Lastly, in HEK293T cells, overexpression of full-length TET1 was found to decrease 5mC in sparsely methylated CGIs (1-10% 5mC) but not in regions with higher 5mC. Additionally, the increase in 5hmC specifically at the border of unmethylated CGIs led to the idea that 5hmC may protect CGIs from encroachment of DNA methylation (Jin et al., 2014; Williams et al., 2012). Taken together, depending on the cell type, which TET family members are expressed, and the particular genomic region in question, 5hmC may play roles in transcription and DNA methylation maintenance.

1.9 Summary

The discovery of the TET family of proteins has greatly expanded our understanding of crucial epigenetic processes, including epigenetic reprogramming. This dissertation aims to elucidate the role that TET1 plays specifically in the reprogramming of ICRs. Chapter two provides valuable additional details into the erasure of both male and female imprints in the germline and how this erasure affects the monoallelic expression of imprinted genes in subsequent generations. Lastly, chapter three will detail ongoing and future work to answer remaining questions regarding TET1 and its role in genomic imprinting.

1.10 Contributions

This chapter contains direct quotes and figures from SanMiguel and Bartolomei *et al.* published in 2018 in *Biology of Reproduction* (SanMiguel and Bartolomei, 2018).

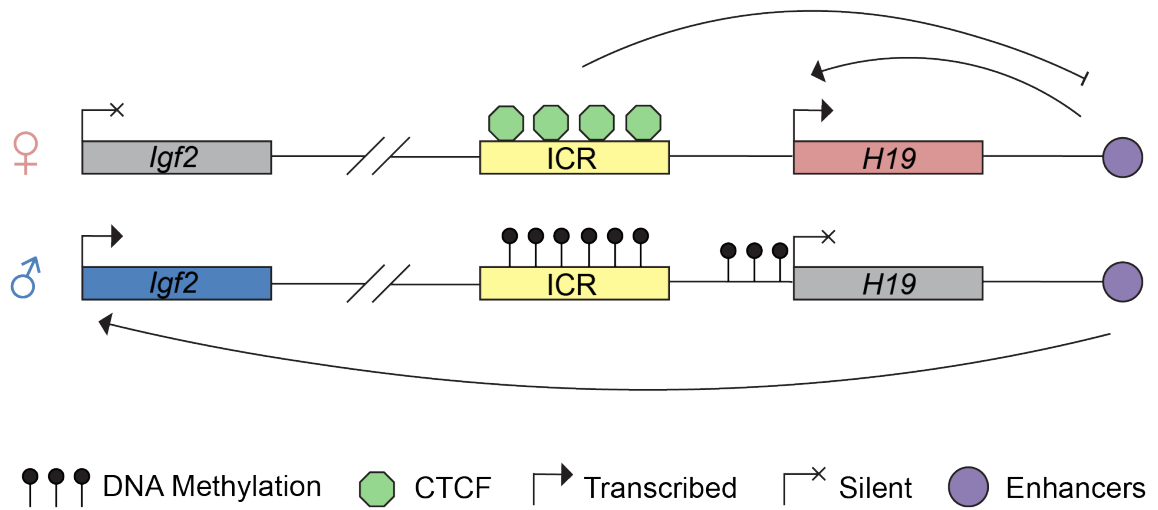


Figure 1.1. Schematic of the *H19* imprinted locus in mice. Arrows show enhancer activation of transcription. The blunt-ended arrow indicates the enhancer-blocker function of the insulator formed by the CTCF-bound unmethylated maternal ICR. The details of imprinted regulation at this locus are provided in the text.

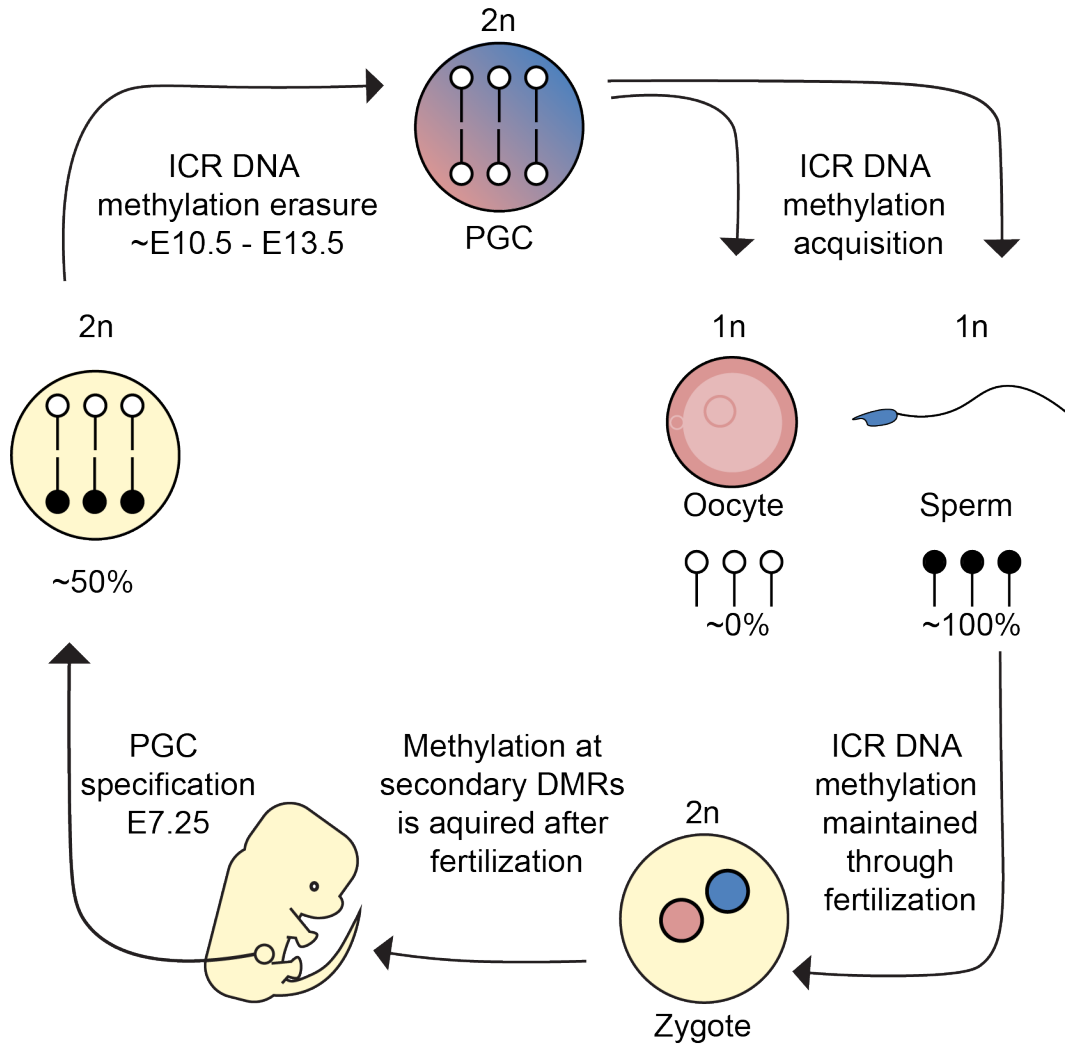


Figure 1.2. The life cycle of a DNA methylation imprint. ICRs obtain their parent-of origin-specific DNA methylation in the haploid genomes of germ cells. This differential methylation is maintained through fertilization. In contrast, secondary DMRs acquire DNA methylation after fertilization. PGCs are specified from the epiblast and thus need to erase imprinted methylation as PGCs develop, allowing a ground state for the acquisition of imprinted methylation in the germline.

Table 1.1. Genetic models of imprinted expression and DNA methylation regulators at the *H19* locus in mice

Genotype	Tissue	Allelic Expression	<i>H19</i> ICR DNA Methylation	Reference
<i>Dnmt1ⁿⁿ</i> (hypomorph)	E10.5 embryos	<i>H19</i> biallelic; <i>Igf2</i> repressed	ND	(Li et al., 1993b)
<i>Dnmt1^{s/s}</i> (replication foci targeting domain mutation)	E9.5 concepti	<i>H19</i> biallelic	ND	(Casparly et al., 1998)
<i>Dnmt1ⁿⁿ</i>	E9.5 concepti	<i>H19</i> biallelic; <i>Igf2</i> repressed	ND	(Weaver et al., 2010)
<i>Dnmt1⁺ⁿ</i>	E9.5 concepti	* <i>H19</i> biallelic	ND	
<i>Dnmt1^{+c}</i> (c = null)	E9.5 concepti	<i>H19</i> =	ND	
<i>Dnmt1^{mat/+}</i>	E3.5 blastocysts	ND	* <i>H19</i> ↓	(Hirasawa et al., 2008)
<i>Dnmt1^{mat/-}</i>	E3.5 blastocysts	ND	<i>H19</i> ↓	
<i>Uhrf1^{-/-}</i>	ESCs	ND	<i>H19</i> ↓	(Sharif et al., 2007)
<i>Uhrf1^{-/-}</i>	E9.5 embryos	<i>H19</i> biallelic; <i>Igf2</i> repressed	ND	
<i>Dnmt3a^{mat/-}; Dnmt3b^{+/-}</i>	E9.5 embryos	ND	<i>H19</i> =	(Hata et al., 2002)
<i>Dnmt3a^{2lox/1lox}, TNAP-Cre x</i> WT male (maternal deletion only)	E10.5 embryos	ND	<i>H19</i> =	(Kaneda et al., 2004)
<i>Dnmt3a^{2lox/1lox}, TNAP-Cre -/-</i> males	Spermatogonia (P11 Testis)	ND	<i>H19</i> ↓	
Paternal germline deletion <i>Dnmt3b</i>	Pups [#]	ND	<i>H19</i> =	
Maternal germline deletion <i>Dnmt3b</i>	Pups [#]	ND	<i>H19</i> =	
<i>Dnmt3a^{-/-}; Dnmt3b^{-/-}</i> DKO (Maternal-zygotic null)	E9.5 embryos	<i>H19</i> =	<i>H19</i> =	
<i>Dnmt3l^{-/-}</i>	Spermatogonia (P11 Testis)	ND	<i>H19</i> ↓	(Kaneda et al., 2004)
<i>Dnmt3l^{-/-}</i>	ESCs	ND	<i>Igf2</i> DMR2 ↓	(Hata et al., 2002)
<i>Dnmt3^{mat/-}</i>	E9.5 embryos	ND	<i>H19</i> =	
<i>Dnmt3^{mat/+}</i>	Embryos [#]	<i>H19</i> =; <i>Igf2</i> =	<i>H19</i> =	(Bourc'his et al., 2001)
<i>Dppa3^{mat/+}</i>	PN5 zygotes	ND	<i>H19</i> ↓	(Nakamura et al., 2007)
<i>Dppa3^{-/-}</i>	E12.5 PGCs	ND	<i>H19</i> =	(Nakashima et al., 2013)
<i>Zfp57^{-/-}</i> (zygotic only)	E11.5-E13.5 embryos	ND	<i>H19</i> =	(Li et al., 2008)
<i>Zfp57^{mat/-}</i> (maternal-zygotic)	E11.5-E13.5 embryos	ND	<i>H19</i> =	
<i>Zfp57^{+/-}</i>	Sperm	ND	<i>H19</i> =	
<i>Zfp57^{-/-}</i>	Sperm	ND	<i>H19</i> =	
<i>Trim28^{chatwo/chatwo}</i> (zygotic hypomorph)	E8.5 embryos	* <i>H19</i> biallelic; <i>Igf2</i> repressed	* <i>H19</i> ↓	(Alexander et al., 2015)
<i>Trim28^{L-L}</i> (zygotic null)	E7.5 embryos	<i>Igf2</i> repressed	* <i>H19</i> ↓	
Hypomorphic maternal-zygotic <i>Trim28</i>	E7.5 embryos	<i>H19</i> biallelic	ND	
<i>Trim28^{mat/+}</i> (maternal null)	8-cell stage embryos	ND	* <i>H19</i> ↓	(Lorthongpanich et al., 2013)
<i>Trim28^{mat/+}</i> (maternal null)	E12.5 embryos	ND	* <i>H19</i> ↓; * <i>H19</i> secondary DMR ↓	(Messerschmidt et al., 2012)

	E4.5 embryos	ND	*H19 ↓	
[Tet1 ^{-/-} ;Tet2 ^{-/-}] female x WT male	P1-2 pups	ND	*H19 ↑	(Dawlaty et al., 2013)
[Tet1 ^{+/-} ;Tet2 ^{+/-}] female x [Tet1 ^{-/-} ;Tet2 ^{-/-}] male	P1-2 pups	ND	*H19 ↑	
Table Key: * (partially penetrant); ND (no data); = (no change); ↓ (hypomethylated); ↑ (hypermethylated); # (age not explicitly stated) P (postnatal day); PN (Pronuclear stage); ESCs (Embryonic stem cells); PGCs (primordial germ cells)				

Table 1.2. Genetic models of imprinted expression and DNA methylation regulators at the *Igf2r* locus in mice

Genotype	Tissue	Allelic Expression	<i>Igf2r</i> ICR DNA Methylation	Reference
<i>Dnmt1^{n/n}</i> (hypomorph)	E10.5 embryos	<i>Igf2r</i> =	* <i>Igf2r</i> ↓	(Li et al., 1993b)
<i>Dnmt1^{s/s}</i> (replication foci targeting domain mutation)	E9.5 embryos	<i>Igf2r</i> repressed	ND	
<i>Dnmt1^{nc}</i> (c = null)	E9.5 embryos	<i>Igf2r</i> repressed	<i>Igf2r</i> ↓	
<i>Dnmt3a^{mat-/-};Dnmt3b^{+/-}</i>	E9.5 embryos	ND	<i>Igf2r</i> ↓	(Hata et al., 2002)
<i>Dnmt3a^{2lox/1lox}, TNAP-Cre</i> x WT male (maternal deletion only)	E10.5 embryos	<i>Igf2r</i> repressed	<i>Igf2r</i> ↓	(Kaneda et al., 2004)
<i>Dnmt3^{+/+}</i>	ESCs	ND	<i>Igf2r</i> =	(Hata et al., 2002)
<i>Dnmt3^{mat-/-}</i>	E9.5 embryos	ND	<i>Igf2r</i> ↓	
<i>Zfp57^{mat-/-}</i> (maternal-zygotic)	E11.5-E13.5 embryos	ND	* <i>Igf2r</i> ↓	(Li et al., 2008)
<i>Zfp57^{-/-}</i> (zygotic null)	E11.5-E13.5 embryos	ND	* <i>Igf2r</i> ↓	
<i>Zfp57^{+/-}</i>	Oocytes	ND	* <i>Igf2r</i> ↓	
<i>Zfp57^{-/-}</i>	Oocytes	ND	* <i>Igf2r</i> ↓	
<i>Trim28^{chatwo/chatwo}</i> (zygotic hypomorph)	E8.5 embryos	* <i>Airn</i> biallelic	ND	(Alexander et al., 2015)
<i>Trim28^{mat-/+}</i> (maternal null)	8-cell stage embryos	ND	* <i>Igf2r</i> ↓	(Lorthongpanich et al., 2013)
<i>Tet1^{Gt/Gt}</i> (catalytic domain removed)	E9.5 embryos	* <i>Airn</i> repressed	* <i>Igf2r</i> ↑	(Yamaguchi et al., 2013)

Table Key: *(partially penetrant); ND (no data); = (no change); ↓ (hypomethylated); ↑ (hypermethylated); # (age not explicitly stated) P (postnatal day); PN (Pronuclear stage); ESCs (Embryonic stem cells); PGCs (primordial germ cells)

CHAPTER 2: IMPRINTED GENE DYSREGULATION IN A *TET1* NULL MOUSE MODEL IS STOCHASTIC AND VARIABLE IN THE GERMLINE AND OFFSPRING

2.1 Introduction

Epigenetic reprogramming of ICRs in the germline is critical to the appropriate regulation of imprinted genes in offspring. Imprinted genes are uniquely expressed from only one parental allele and play important roles in growth and development (Plasschaert and Bartolomei, 2014). ICRs have DNA methylation on one parental chromosome that controls the monoallelic, parent-of-origin-specific expression of imprinted genes. By E13.5, ICRs are completely demethylated in the germline, which is necessary to allow the acquisition of the parent-of-origin specific DNA methylation patterns, either at maternally-methylated ICRs in the developing oocytes, or at paternally-methylated ICRs in the developing sperm (Stewart et al., 2016). This asymmetric DNA methylation of ICRs ensures proper monoallelic expression of imprinted genes in the resultant embryo.

The observation that DNA methylation at ICRs is resistant to the initial phase of demethylation in PGCs is consistent with ICR erasure being an active process. The discovery of the Ten-Eleven Translocation (TET) family of enzymes, TET1, TET2, and TET3, (Tahiliani et al., 2009) implicated their potential relevance to ICR DNA methylation erasure (Hill et al., 2014). All three TETs have the ability to progressively oxidize the methyl group on cytosines (5mC) to 5-hydroxymethylcytosine (5hmC), 5-formylcytosine (5fC), and 5-carboxylcytosine (5caC) (Ito et al., 2011; Tahiliani et al., 2009). This iterative oxidation is thought to play an active part in removing DNA methylation in conjunction with replication or base excision repair (Hajkova et al.,

2010). In PGCs, *Tet1* is the most highly expressed family member, while *Tet2* is expressed at a lower level, and *Tet3* is undetectable (Hackett et al., 2013; Hajkova et al., 2010; Kagiwada et al., 2013; Yamaguchi et al., 2012). Previous studies showed abnormal levels of DNA methylation and abnormal levels of total expression of imprinted genes in *Tet1*^{-/-} single and *Tet1*^{-/-}; *Tet2*^{-/-} double knockout mice (Dawlaty et al., 2013; Yamaguchi et al., 2013). However, most experiments in the Yamaguchi et al., 2013 study used a *Tet1* allele in which a fusion protein was generated. The catalytic domain of the endogenous TET1 protein was replaced with a β -galactosidase cassette, but the DNA-binding CxxC domain was retained (Yamaguchi et al., 2012). This study also focused primarily on the effects of *Tet1* on ICR methylation in the male germline. Additionally, the *Tet1*^{-/-}; *Tet2*^{-/-} mouse model did not allow the elucidation of the precise contribution of *Tet1* to ICR DNA methylation regulation (Dawlaty et al., 2013). Thus, our understanding of the role of *Tet1* in the regulation of genomic imprinting is incomplete. The goal of our study is to define the function of *Tet1* in both male and female germ cells using a null allele of *Tet1* in mice. Furthermore, we aim to elucidate how loss of *Tet1* affects the monoallelic expression of imprinted genes by studying offspring of male and female *Tet1* knockout animals. In addition to its requirement in the male germline, our work demonstrates for the first time, that *Tet1* is required for normal ICR methylation in female germ cells. Moreover, lack of *Tet1* in the germline leads to stochastic biallelic expression of imprinted genes across different stages of development in offspring. Importantly, we show that the reliance of TET1-mediated demethylation varies according to the imprinted locus, suggesting a complex relationship between TET1 demethylation and genomic context.

2.2 Results

2.2.1 Loss of *Tet1* leads to stochastic and variable DNA hypermethylation at ICRs in oocytes.

To examine how loss of *Tet1* affects DNA methylation (mCpG) in the female germline, we collected germinal vesicle stage oocytes from 3.5-week-old mice generated by mating heterozygous *Tet1* mutant mice. One pool of oocytes per mouse was bisulfite treated and ICR mCpG levels were subsequently analyzed by pyrosequencing (Fig. 2.1A). We investigated two of the three known paternally methylated ICRs in the mouse genome: *H19/Igf2* and *IG-DMR*. As expected, *Tet1* wild-type (WT) and heterozygous (Het) pools of oocytes had very low levels of mCpG at the *H19/Igf2* ICR and the *IG-DMR* while the maternally methylated *Peg3* ICR was nearly completely methylated and served as an internal control for somatic contamination. In contrast, *Tet1*^{-/-} (KO) oocyte pools showed stochastic hypermethylation at both the *H19/Igf2* and the *IG-DMR*, meaning some KO oocyte pools had mCpG levels comparable to WT and Het pools, while other KO oocyte pools had increased levels of mCpG (Fig 2.1B). The stochastic nature of the DNA methylation abnormalities was reflected in bimodal distributions in KO oocyte pools at each of the two paternally methylated ICRs (Fig. S2.1A,B). Affected KO oocyte pools were also variable in the severity of the hypermethylation phenotype, with each oocyte pool exhibiting different levels of abnormal mCpG, particularly at the *IG-DMR* (Fig. 2.1B and Table S2.1). Additionally, the variance in mCpG was significantly higher in the KO oocytes at *H19/Igf2* ICR and *IG-DMR* compared to controls (WT vs KO: $p = 0.008$, $p = 0.026$, respectively), whereas there was no difference in mCpG levels and variance at the *Peg3* ICR (Fig. 2.1C). Moreover, there was no correlation between abnormal methylation at *IG-DMR* and *H19/Igf2* in KO oocyte pools (Fig. S2.1C). Thus, consistent with the hypothesis that *Tet1* is required for proper DNA demethylation of

ICRs, lack of *Tet1* in the female germline leads to stochastic hypermethylation and significant increases in DNA methylation variance at paternally methylated ICRs.

2.2.2 Loss of *Tet1* leads to biallelic expression and changes in DNA methylation of imprinted genes in the offspring of female KO mice.

We speculated that the abnormalities in oocyte methylation might cause developmental defects in the resultant offspring. To address this question, we crossed either *Tet1* Het or KO females to WT *Tet1* males on the C57BL/6J(CAST7) (C7) background, which have a *Mus musculus castaneus* chromosome 7 on a C57BL/6J (B6) background (Fig. S2.2A,B). These F1 hybrid animals harbor SNPs on chromosome 7 that allow the parental origin of the RNA to be determined. Het *Tet1* females crossed to C7 males are hereafter referred to as mCON, and their offspring are either heterozygous or wild-type for *Tet1*. mKO refers to *Tet1* KO females crossed to C7 males. mKO offspring are all heterozygous for *Tet1*. We analyzed the number of live and resorbed embryos and placentas at E10.5 from mCON and mKO matings. By this developmental stage, there was a significant decrease in live embryos ($p = 0.005$) and a significant increase in resorbed embryos ($p = 0.011$) in mKO litters compared to mCON litters (Fig. 2.2A,B). This result indicates that offspring derived from *Tet1* KO females are more susceptible to fetal demise than those derived from mCON females at E10.5.

Next, we asked whether abnormal ICR methylation in the germline could affect the allele-specific expression of imprinted genes in the offspring of female *Tet1* KO mice. Given that each inherited *Tet1*^{-/-} parental allele contributing to an ICR in the offspring has a 50% chance of being unmethylated (previously maternal) or methylated (previously paternal and failed to erase in the germline), *a priori* we expect that the number of affected offspring would be 50%. Using restriction fragment length polymorphism analysis (RFLP), we quantified allele-specific expression at the *H19/Igf2*

locus (Fig. 2.2C and Table S2.2). Three mKO-derived embryos from independent litters exhibited biallelic expression of *Igf2* (3/36) whereas none of the mCON-derived embryos were affected (0/34) (Fig. 2.2D). This result shows the imprinting phenotype was neither present in every mKO embryo nor at the expected proportion of 50%. Additionally, in an affected conceptus, *Igf2* expression was biallelic in both the embryo and its placenta (Table S2.2).

To address how mCpG levels at the ICR may correspond to abnormal imprinted gene expression, we analyzed mCpG via pyrosequencing. We found that the mKO embryos with biallelic *Igf2* expression also showed DNA hypermethylation at the ICR (Fig. 2.2E). Additionally, we measured total expression of the imprinted genes *Igf2* and *H19*. Given hypermethylation of the ICR, the three biallelic mKO embryos had undetectable levels of *H19* expression, as expected. *Igf2* expression was less predictable but reflected increased total expression in the embryos that expressed *Igf2* biallelically and were hypermethylated at the *H19/Igf2* ICR. (Fig. 2.2F). As expected, *H19* expression in both mCON and mKO embryos and placentas was monoallelic or not expressed (Fig 2.2F, Table S2.2). Of note, two of the three affected embryos were female (Tables S2.2,S2.3). Together, these results indicate that *H19/Igf2* ICR hypermethylated oocytes can contribute to live embryos that have abnormal allele-specific expression of *Igf2*, which is associated with hypermethylation at the ICR.

We next determined if the mCpG and total expression patterns observed at the *H19/Igf2* locus were similar at the paternally methylated *IG-DMR* (Fig. 2.3A). There was a significant increase in proportion of hypermethylated E10.5 mKO embryos at the *IG-DMR* compared to mCON embryos (10/36 vs. 1/34, respectively, $p = 0.007$) (Fig. 2.3B). ICR hypermethylation was stochastic as not every KO embryo was affected and this proportion deviated from the expected 50%. Only one mKO embryo had

hypermethylation at both *H19/Igf2* and the *IG-DMR* (1/29, embryo “A”, see Figs 2.2C & 2.3B), whereas the rest of the affected embryos were hypermethylated at a single locus. This result reflects a lack of correlation between hypermethylation of the two loci in any given mKO animal.

Although we could not investigate allele-specific expression in our F1 hybrid model because the *IG-DMR* is on chromosome 12, we were able to measure total expression. Embryos that had abnormal hypermethylation at *IG-DMR* also had silenced *Meg3* expression, as expected given that *IG-DMR* methylation silences *Meg3* expression (Lin et al., 2003). Similar to *Igf2* total expression, however, total levels of *Dlk1* were variable, ranging from wild type levels of expression to 2.5-fold increases in expression compared to controls (Fig. 2.3C). Of 36 mKO offspring, 12 showed imprinting defects at the *H19/Igf2* locus, the *IG-DMR* locus, or both. Of these 12 affected offspring, nine were females and three were males, indicating a significant sex-biased effect early in development ($p = 0.033$, Table S2.3) despite the expected Mendelian ratio of male and female embryos. Thus, *Tet1* in the maternal germline is also required for proper *IG-DMR* mCpG levels in offspring and may preferentially affect female offspring.

To determine if the abnormalities we observed at the *H19/Igf2* ICR during embryogenesis were also present at birth, we isolated tissues from mKO and mCON pups at postnatal day (P)0 and measured allele-specific expression and mCpG levels. While the average number of mKO live-born pups was lower than mCON pups, this difference was not significant ($p = 0.067$) (Fig 4A). mCON tissues showed no biallelic expression (0/16). However, we observed biallelic expression of *Igf2* in mKO pups (2/31) and this change was consistent between tissues (tongue and liver, Fig. 2.4B). These affected pups were female (Tables S2.3,S2.4). There was no significant difference between the proportion of P0 mKO pups with biallelic *Igf2* compared to the proportion of E10.5 mKO

embryos with biallelic *Igf2* ($p = 1.00$), indicating these changes are present at the same frequency from mid-gestation through birth.

2.2.3 Loss of *Tet1* leads to stochastic DNA hypermethylation at ICRs in sperm.

Next, we addressed the effects of *Tet1* deletion on the male germline. We collected motile sperm from *Tet1* WT, Het, and KO adult males for mCpG analysis by pyrosequencing (Fig. 2.5A). WT and Het sperm showed the expected low levels of mCpG at the maternally methylated *KvDMR*, *Peg3*, *Snrpn*, and *Peg1* ICRs. The paternally methylated ICRs, *H19/Igf2* and *IG-DMR*, had the expected hypermethylation in sperm regardless of the paternal genotype. In contrast, mCpG levels were significantly increased at the *KvDMR*, *Peg1*, and *Peg3* ICRs in KO samples (WT vs KO, $p < 0.0001$, $p = 0.002$, $p = 0.003$, respectively). The *Snrpn* ICR had neither significant hypermethylation nor had significant differences in variance (WT vs KO, $p = 0.112$, $p = 0.91$, respectively) (Fig 2.5B). The pyrosequencing results were confirmed by bisulfite mutagenesis, followed by cloning and sequencing for the *H19/Igf2* and *Peg3* ICRs (Fig. S2.3A,B). Because the *Snrpn* ICR was demethylated in the *Tet1* KO sperm, we hypothesized that another protein, such as TET2, or a different demethylation pathway could be compensating in the absence of TET1. To test this hypothesis, we examined sperm from *Tet1/Tet2* double knockout mice (DKO) and saw no significant difference in DNA methylation level between KO and DKO sperm (Table S2.5), indicating TET1 is the primary enzyme responsible for DNA methylation imprint erasure at *KvDMR*, *Peg1*, and *Peg3* ICRs but TET1 and TET2 are dispensable for the erasure of the *Snrpn* ICR.

2.2.4 Loss of *Tet1* leads to biallelic expression and changes in DNA methylation of imprinted genes in the offspring of male KO mice.

We next asked how hypermethylated sperm affected allele-specific expression of imprinted genes and mCpG levels at ICRs in the offspring of *Tet1* KO male mice. Because

abnormal methylation at maternally methylated ICRs is thought to be less detrimental to normal development (Kawahara et al., 2007), we hypothesized that changes comparable to maternal *Tet1* deficiency would be observed at a slightly later time in gestation in paternal KO. Therefore, to collect F1 hybrid tissues for analysis, we mated *Tet1* Het or KO males with *Tet1* WT females on the C7 background to generate E12.5 paternal control offspring (pCON) or paternal KO offspring (pKO) (Fig. S2.2C,D). At E12.5, there were significantly fewer live pups ($p = 0.019$) and significantly more resorbed and delayed pups in the pKO offspring ($p = 0.011$) compared to pCON offspring (Fig. 2.6A,B). We then examined changes in allele-specific expression at the *KvDMR* in E12.5 pCON and pKO embryos (Fig. 2.6C). pKO embryos were more likely to express *Cdkn1c* biallelically (7/29) than pCON embryos (1/24) (Fig. 2.6D). Embryos with biallelic *Cdkn1c* expression exhibited DNA hypermethylation at the *KvDMR* (Fig. 2.6E). Notably, stochastic DNA hypermethylation of the *Peg3* ICR was also observed amongst pKO offspring (Table S2.6), but no single embryo had both *Peg3* and *KvDMR* hypermethylation (Fig. S2.4A). Because these loci are on opposite ends of chromosome 7, this result suggests meiotic recombination may dictate which pups within a litter are affected. The changes in allele-specific expression and DNA methylation were also observed in the corresponding placentas (Fig. S2.5 and Table S2.6). Unlike what was observed in the maternal offspring, male and female embryos from pKO crosses were equally affected ($p = 0.665$, Tables S2.3,S2.6).

Lastly, to determine if changes in allele-specific expression and mCpG levels at maternally methylated ICRs are detected at birth, we measured imprinted gene expression by RFLP and mCpG levels by pyrosequencing analysis in tissues from pCON and pKO P0 pups. pCON pups exhibited proper monoallelic expression of *Cdkn1c* while pKO pups had biallelic *Cdkn1c* expression (3/29) (Fig. 2.7A and Table S2.7). The pups

with biallelic expression also had hypermethylation at the *KvDMR*, which was consistent across three tissue types (Fig. 2.7B and Table S2.7). Similar to what was observed at E12.5, litter sizes at Po were significantly smaller in the pKO litters compared to pCON litters at birth ($p < 0.0001$) (Fig. 2.7C). This result suggests that embryonic lethality may contribute to a smaller proportion of affected animals at Po compared to E12.5. Lastly, as observed at E12.5, we also noted mutually exclusive hypermethylation of the *Peg3* ICR and the *KvDMR* (Fig. S2.4B). Together, these data show that the sperm hypermethylation in male KO animals was transmitted to a subset of offspring, resulting in defects in imprinted gene expression and ICR methylation.

2.3 Discussion

In the developing germline, DNA methylation at ICRs must be erased so that parent-of-origin specific imprints can be established according to the sex of the embryo. These sex-specific DNA methylation patterns are necessary for proper imprinted gene expression in the offspring. The importance of this process is highlighted in human imprinting disorders, where loss of imprinted gene expression or changes in DNA methylation at ICRs can lead to disorders such as Beckwith-Wiedemann, Angelman, and Prader Willi syndromes (Kalish et al., 2014). While DNA methylation at the global level has been well-studied (Guibert et al., 2012; Hajkova et al., 2002; Kagiwada et al., 2013; Seisenberger et al., 2012a; Seki et al., 2005), how imprints are effectively removed to allow imprinted gene expression in subsequent generations remains elusive. Only recently were the TET family of proteins discovered (Tahiliani et al., 2009). Subsequently, TET1, the predominantly expressed TET family member in PGCs, has been implicated in the ICR DNA demethylation process (Dawlaty et al., 2013; Yamaguchi et al., 2013). Until now, the role of TET1 in genomic imprinting was poorly understood, given the paucity of data involving the female germline and lack of allele-specific

expression analysis in the offspring. Here, we used a *Tet1* null allele to systematically investigate the function of TET1 in DNA demethylation of ICRs in both the maternal and paternal germlines. Furthermore, we determined the effect of *Tet1* loss on imprinted gene expression in the offspring of maternal and paternal *Tet1* KO mice.

We found variable levels of DNA methylation among *Tet1* KO oocyte pools collected from different females at the paternally methylated ICRs, *H19/Igf2* and *IG-DMR*. This variability could be attributed to a few different factors. First, because germ cells are derived from the diploid epiblast, each parental allele has an equal chance of being represented in the gamete. Thus, we expect two distinct populations within a pool of oocytes from a given *Tet1* KO female mouse. An allele originally derived from the unmethylated maternal allele will remain unmethylated and thus contribute with no apparent defect to subsequent offspring. However, an allele that was originally paternal and methylated may fail to erase in the absence of TET1, in which case, these oocytes will be hypermethylated. Therefore, the theoretical maximum DNA methylation level in a bulk pool of oocytes from one mouse will be 50%. However, meiotic defects have been reported in a gene-trap allele of *Tet1*; these defects were linked to increased levels of oocyte apoptosis during prophase I of meiosis (Yamaguchi et al., 2012). Consistent with this observation, we observe variable levels of hypermethylated oocytes at the paternally methylated ICRs. This hypermethylation includes deviations from the expected 50% levels of DNA methylation, including levels higher than 50%, which can be explained by stochastic oocyte apoptosis. Consistent with variable oocyte apoptosis, we see bimodal distributions of DNA methylation across analyzed oocyte pools (Fig S2.1A, B). Secondly, it is possible that loss of TET1 could affect PGC migration and/or proliferation timing. A number of genes have been reported to affect PGC proliferation and/or migration in a cell-autonomous manner (Saitou and Yamaji, 2012). Lack of *Tet1* may directly or

indirectly affect expression of these genes and thus affect the timing or migration patterns of PGCs. If a particular PGC can divide more frequently than another PGC, or is delayed in reaching the gonad where proliferation ceases, these PGCs would lose more DNA methylation due to replication in the absence of DNA methylation machinery than a PGC that divides more slowly or migrates to the gonad faster. Notably, TET1 binds to the *Dazl* promoter in ESCs (Williams et al., 2011), a critical factor in PGC development, survival, and differentiation (Haston et al., 2009; Lin and Page, 2005; Ruggiu et al., 1997; Schrans-Stassen et al., 2001). *Dazl* expression has also been demonstrated to be regulated by promoter methylation, and is hypermethylated in a PGC-like cell model where both *Tet1* and *Tet2* are simultaneously knocked down (Hackett et al., 2013). Lastly, we also see differences in the levels of hypermethylation between *H19/Igf2* and *IG-DMR* (Fig. 2.1). This result further emphasizes that a number of the aforementioned factors may be contributing to the variability at these loci.

We additionally identified ICR hypermethylation alterations in the offspring of female *Tet1* KO mice. Notably, the proportion of affected E10.5 mKO embryos mirrors the relative percent hypermethylation of each ICR in the oocytes. The presence of these abnormalities in both oocytes and E10.5 embryos suggests that abnormalities established in the germline are maintained throughout fertilization and the early epigenetic reprogramming of the preimplantation embryo. Furthermore, offspring with hypermethylation of the *H19/Igf2* ICR and/or the *IG-DMR* show close to 100% methylation, indicating that passive loss of methylation or TET2 and TET3 activity are unlikely and/or unable to compensate in the window between gametogenesis and E10.5 at these loci. One mCON animal also exhibited hypermethylation at the *IG-DMR* and this may be because the dam was heterozygous for the *Tet1* allele.

In addition to expanding *Tet1*'s role to regulation of DNA methylation in the female germline, we report for the first time that loss of TET1 leads to biallelic expression of paternally expressed genes when the deletion is inherited from the maternal lineage. At E10.5, we observe completely biallelic expression of *Igf2*. This level of expression from the normally silent maternal allele corresponds to the level of dysregulation of ICR methylation, which is close to 100% methylated in all of the affected offspring. Biallelic expression of *Igf2* is also observed at the newborn PO stage and is consistent across tissues from different germ layers. The proportion of animals with biallelic expression is consistent between the embryonic stage and the newborn stage. These results suggest that alterations at the *H19/Igf2* locus are compatible with late gestation development and live birth, consistent with the fact that biallelic *Igf2* is detected in a subset of Beckwith-Wiedemann patients (Kalish et al., 2014). It will be interesting to determine if animals with biallelic *Igf2* expression develop human imprinting disorder-like phenotypes postnatally. Such a result would indicate that misregulation of *Tet1* may be a cause of idiopathic cases of human imprinting disorders.

To date, previous studies regarding *Tet1* and genomic imprinting have relied on measuring total expression of imprinted genes. Our data demonstrate that hypermethylation of the *H19/Igf2* ICR and the *IG-DMR* is associated with silencing of the maternally-expressed genes, *H19* and *Meg3*, respectively. However, total levels of expression of the corresponding paternally expressed genes, *Igf2* and *Dlk1*, do not perfectly predict biallelic expression. This is consistent with other reports in the literature describing inconsistencies between total and allele-specific expression (Eckersley-Maslin and Spector, 2014). Moreover, our results contrast with Yamaguchi et al., 2013, where decreases in total expression of both maternally and paternally expressed genes at the *IG-DMR* were observed in E19.5 placentas of resorbed embryos.

These discrepancies could potentially be due to differences in the quality of the input material from resorption sites.

In this study, we demonstrate that despite equal sex ratios of *Tet1* mKO offspring at each developmental stage examined, imprinting phenotypes are biased towards females at the *H19/Igf2* ICR and the *IG-DMR*. This result is unexpected, as sex-biased imprinting phenotypes have yet to be described by other groups working with mouse models of *Tet1* (Dawlaty et al., 2013; Yamaguchi et al., 2013; Zhang et al., 2016b).

However, the nature of this sex-biased effect is unclear. While there have been previous reports of sex-specific differences in total expression of certain imprinted genes such as *H19* and *Igf2* in the E14.5 brain, these changes were not observed before sex-determination at E10.5 (Faisal et al., 2014). As our bias is observed before sex differentiation, it is likely that differences in sex steroids are not playing a major role in our animals. One possibility is that both male and female mKO offspring have hypermethylation at the *H19/Igf2* ICR and the *IG-DMR*, but this abnormal methylation is not maintained in males. It is also possible that imprinting abnormalities at the *H19/Igf2* ICR and the *IG-DMR* as well as defects at another locus (or multiple loci) are both embryonic lethal but affect each sex independently. In this circumstance, we envision that dysregulated imprinting at the *IG-DMR* and the *H19/Igf2* ICR is more detrimental in males, but methylation or expression defects elsewhere caused by loss of *Tet1* may be more detrimental in females. This scenario is compatible with the early lethality we observed at E10.5 and is also consistent with the equal sex ratios we observed at this developmental stage. Further studies are warranted to understand this mechanism.

In addition to our female germline and offspring analysis, we also investigated the function of TET1 in the male germline. We demonstrate that lack of TET1 leads to

hypermethylation of the maternally methylated ICRs, *KvDMR*, *Peg1*, and *Peg3*. The hypermethylation of *KvDMR* is consistent with reduced-representation bisulfite sequencing data from Yamaguchi et al., 2013. Additionally, Dawlaty et al., 2013 reported hypermethylation of *Peg1*, *Peg3*, and the *KvDMR* by methylated DNA immunoprecipitation and sequencing analysis. We additionally detected no significant difference in hypermethylation between *Tet1* KO and combined *Tet1/Tet2* double knockout sperm (Table S2.5) providing support to the role of TET1 as the primary isoform responsible for imprint erasure.

While three of the ICRs investigated in our study demonstrated dependency of TET1 for DNA methylation erasure in sperm, *Snrpn* was unique in that it was demethylated regardless of presence of TET1. Both our study and that of Dawlaty et al., 2013 find that the *Snrpn* ICR is not hypermethylated in the absence of TET1 or with the combined deletion of *Tet1* and *Tet2*. This finding is also consistent with experiments using an aorta-gonad-mesonephros organ culture that recapitulates endogenous PGC ICR demethylation *in vitro*. Using this system, the investigators inhibited PGC proliferation through the use of a PI3-kinase inhibitor and found that *Snrpn* was unable to demethylate, while the *H19/Igf2* ICR did lose DNA methylation (Calvopina et al., 2015). Together, these results indicate that the *Snrpn* ICR relies on passive demethylation via replication. While the mechanism underlying TET1-independent demethylation is unknown, the high density of Alu elements belonging to the SINE family of retroelements surrounding the *Snrpn* ICR may be relevant (Huq et al., 1997). SINEs, unlike other repetitive elements, are not resistant to DNA demethylation in the germline (Seisenberger et al., 2012b) and thus, may influence how *Snrpn* is demethylated. Overall, these results show that DNA demethylation of some maternally methylated ICRs requires TET while others do not.

Consistent with DNA methylation results from *Tet1* KO sperm, *Tet1* pKO offspring also showed hypermethylation of the *Peg3* ICR and *KvDMR*, whereas no changes in DNA methylation were observed at the *Snrpn* ICR at both E12.5 and at Po. Hypermethylation at the *KvDMR* was coincident with biallelic expression of *Cdkn1c*. Unlike the consistent levels of biallelic *Igf2* expression observed in offspring of mKO animals, the amount of abnormal maternal expression of *Cdkn1c* in pKO offspring was variable among affected individuals at both time points investigated. For all developmental stages tested, the variable level of biallelic expression closely mimicked the levels of DNA hypermethylation and both loss of imprinting and DNA hypermethylation were consistent across tissues. Given these findings, the variability in loss of imprinted expression suggests that at the *KvDMR* locus, activity of the other TET family members and/or passive dilution may be able to partially compensate between fertilization and the blastocyst stage when the extraembryonic tissues are specified. Moreover, this biallelic expression was more prevalent in the embryonic stages compared to the newborn stage. Given the smaller litter size of *Tet1* pKO offspring compared to pCON offspring at E12.5 and at birth, it is possible that embryonic loss could reduce the number of affected offspring at the later developmental stage. Similar to our maternal TET1 KO data, the molecular phenotype of pKO offspring was highly variable. In both male and female offspring, variability in the levels of imprinted genes at the embryonic stages examined could not be explained by changes in mRNA levels of *Dnmt1*, *Dnmt3a*, *Dnmt3b*, *Dnmt3l*, *Uhrf1*, *Tet2*, or *Tet3* (data not shown). One potential source of stochasticity could be due to the unique properties of individual imprinted loci. ICRs can differ in size, genomic and chromatin contexts, sequence, number and identity of *trans*-factor binding sites, as well as differences in mechanisms of genomic imprinting. For example, the *KvDMR* is large, highly enriched in LINE

elements, and very CpG rich (Engemann et al., 2000). These inherent differences may underlie some of the stochastic phenotypes observed in our study. Additionally, stochasticity of the imprinting phenotypes may be due to meiotic recombination. Even though some ICRs are on the same parental chromosome, hypermethylation of both loci is not correlated in a given pup (Fig S2.4). This observation is incompatible with a model of random segregation of parental alleles. For example, we observe either normal methylation at the *KvDMR* and the *Peg3* ICR, or hypermethylation of one locus but not the other, but never hypermethylation at both loci in the same animal. These phenotypes represent three of the four possible recombination states of meiosis on chromosome 7, as mice tend to have one or two recombination events per chromosome (Koehler et al., 2002). Given the proportions of animals we observe with hypermethylation of one of the two loci, the probability of seeing both hypermethylated loci in one animal is very low. However, we cannot exclude the possibility that hypermethylation of the *KvDMR* and the *Peg3* ICR produces a synthetically lethal effect. Lastly, TET1 is a large protein that is known to interact with epigenetic regulators such as SIN3A, HDAC1, HDAC2, OGT (Vella et al., 2013; Williams et al., 2011), pluripotency factors like NANOG (Costa et al., 2013), and has been suggested to play roles in recruiting the EZH2 subunit of the Polycomb Repressive Complex 2 to distinct sites in the genome (Wu et al., 2011a). Loss of these interactions may lead to inadequate or inappropriate targeting of these complexes, contributing to further dysregulation of the epigenome in *Tet1* KO animals.

In sum, we present a detailed analysis of the previously unexplored maternal germline and describe for the first time, allele-specific expression abnormalities in *Tet1* KO offspring. Together with sperm and paternal KO studies, we determine that *Tet1* is an important regulator of genomic imprinting in both the maternal and paternal lineages and ICRs.

2.4 Contributions

This chapter contains direct quotes and figures from SanMiguel *et al.* published in 2018 in *Development* (SanMiguel et al., 2018). The authors would like to thank Dr. Guo-Liang Xu and Dr. Mingjiang Xu for the *Tet1/Tet2* DKO sperm samples. Statistical advice was provided by Anthony Angueira. Lara Abramowitz was critical with intellectual contributions to the concept and design of this project, the analysis of the *Tet1/Tet2* DKO sperm samples, as well as revisions. Blake Caldwell assisted with Po *Tet1* pKO analyses.

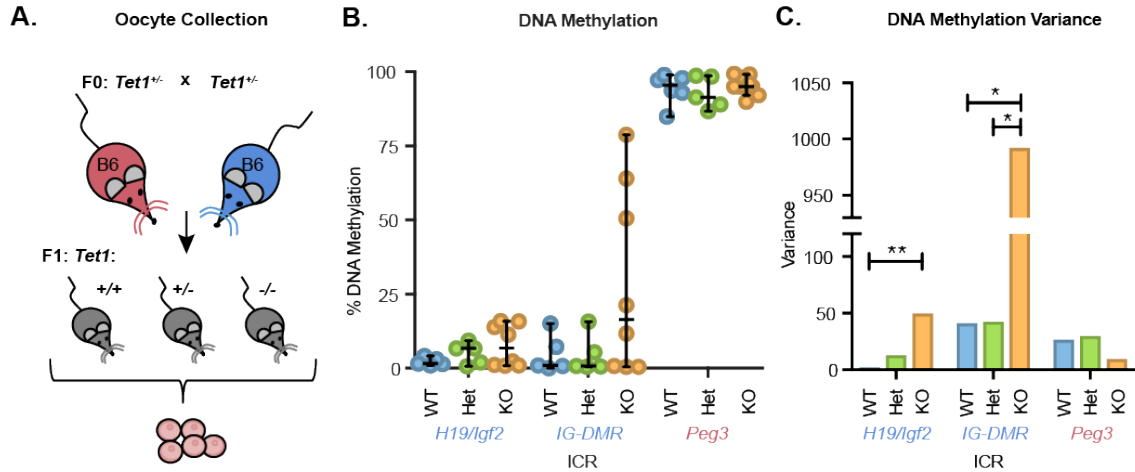


Figure 2.1. Hypermethylation occurs stochastically in $Tet1^{-/-}$ oocytes at the $H19/Igf2$ ICR and the IG-DMR.

(A) Schematic depicting the breeding scheme used to collect oocytes from 3.5-week-old mice. (B) Average DNA methylation at various ICRs. Individual dots represent the percent DNA methylation from one pool of oocytes collected from one mouse. ICR labels are color coded according to which parental allele is normally methylated: blue = the paternal allele; pink = the maternal allele. Line = median, bars = 95% confidence interval. WT = wild-type (blue); Het = heterozygous (green); KO = $Tet1^{-/-}$ (yellow). *H19/Igf2* & *IG-DMR*: (n) WT = 5, Het = 5, KO = 8; *Peg3* (n) WT = 6, Het = 5, KO = 9. (C) Calculated variance for each ICR per genotype is graphed. * $p < 0.05$, ** $p < 0.01$ (Fligner-Killeen Test).

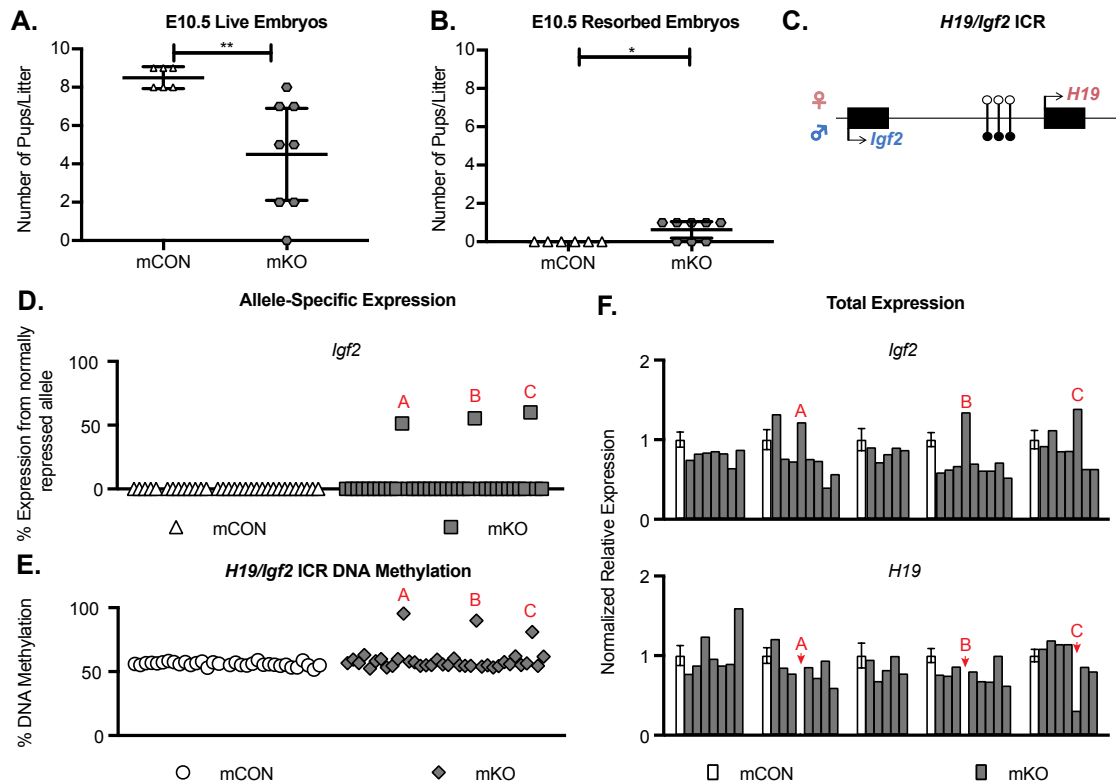


Figure 2.2. Abnormal allele-specific expression and methylation of *Igf2* in E10.5 mKO offspring.

(A) The number of live embryos per litter at E10.5. ** $p < 0.01$, unpaired 2-tailed t-test (unequal variance). Litters (n) mCON = 5; mKO = 8. (B) The number of resorbed embryos per litter at E10.5. * $p < 0.05$, unpaired 2-tailed t-test (unequal variance). (n) mCON = 5 litters; mKO = 8 litters. (A&B) Line = mean, bars = 95% confidence interval. (C) Schematic of the *H19/Igf2* locus. The maternal allele with maternal-specific *H19* expression is represented on the top (pink) and the paternal allele with paternal-specific *Igf2* expression is represented on the bottom (blue). Genes = black boxes. Black lollipops = methylated DNA at the ICR, white lollipops = unmethylated DNA at the ICR. (D) Allele-specific expression of *Igf2*. Abnormal mKO embryos are denoted with red letters which are consistent between Figures 2.2 and 2.3. All embryos are in the same order from left to right in Figures 2.2D, 2.2E, and 3.2B. *Igf2* (n) mCON = 32 embryos from 4 litters. mKO = 36 embryos from 7 litters. (E) Average percent DNA methylation at the *H19/Igf2* ICR, (n) mCON = 32 embryos from 4 litters; mKO = 36 embryos from 7 litters. (F) Total expression from qPCR analysis of *Igf2* and *H19*. White columns indicate the average of one of each of the five mCON litters (n = 8, 8, 8, 9, 9 respectively from left to right), which were normalized to the expression of *Rplpo*, *Nono*, and *Rpl13a* and set to 1. Bars represent \pm biological S.E.M. The gray columns represent individual mKO embryos that were run on the same plate as the adjacent mCON column. All mCON litters and embryos are in the same order in F as in Figure 2.3C. In the *H19* plot, *H19* expression in embryos A and B is undetectable.

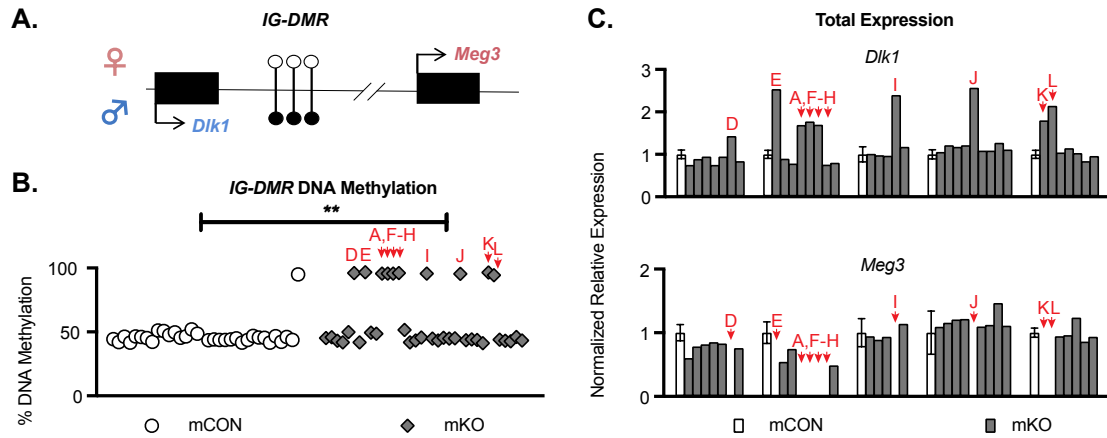


Figure 2.3. Abnormal methylation and total expression at the *IG-DMR* in E10.5 mKO offspring.

(A) Schematic of the *IG-DMR* locus. The maternal allele and maternal-specific *Meg3* expression is represented on the top (pink) and the paternal allele and paternal-specific *Dlk1* expression is represented on the bottom (blue). See Figure 2.2 legend for details. (B) Percent DNA methylation at the *IG-DMR*. All embryos are in the same order from left to right in both Figures 2.3B, 2.2D, and 2.2E. (n) mCON = 32 embryos from 4 litters; mKO = 36 embryos from 7 litters. ** $p < 0.01$, Fisher's Exact Test. (C) Total expression from qPCR analysis of *Dlk1* and *Meg3*. All mCON litters and embryos are in the same order between Figures 2.2F and 2.3C. See Figure 2.2 legend for details. In the *Meg3* plot, *Meg3* expression in embryos A, D, E, F, G, H, I, J, K, and L is undetectable.

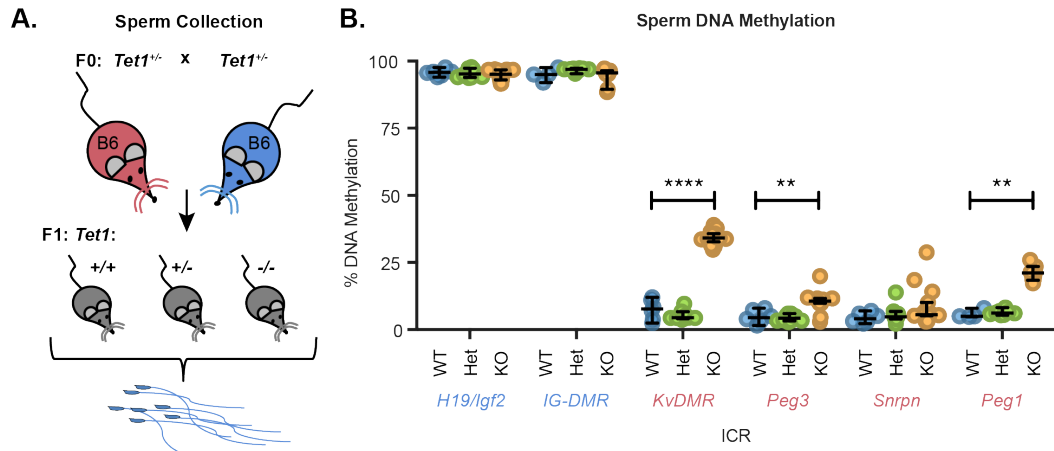


Figure 2.5. Hypermethylation occurs at a subset of ICRs in *Tet1*^{-/-} sperm.

(A) Schematic depicting the breeding scheme used to collect mature sperm. (B) Individual dots represent the percent DNA methylation for sperm collected from one adult mouse. ICR labels are color coded according to which parental allele is normally methylated: blue= the paternal allele; pink = the maternal allele. Line = median, bars = 95% confidence interval. ** = $p < 0.01$, **** = $p < 0.0001$, WT vs KO, Two-tailed Mann-Whitney Rank-Sum Test. *H19/Igf2* (n) WT = 5, Het = 9, KO = 14; *IG-DMR* & *Peg1* (n) WT = 4, Het = 8, KO = 11; *KvDMR* & *Snrpn* (n) WT = 6, Het = 10, KO = 15; *Peg3* (n) WT = 6, Het = 10, KO = 14.

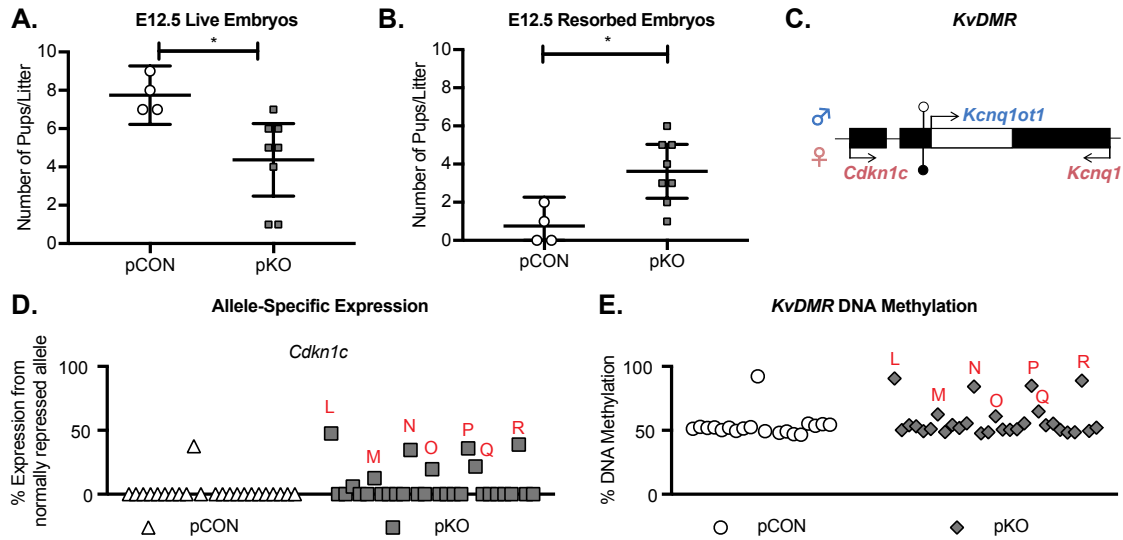


Figure 2.6. Biallelic expression of *Cdkn1c* is prevalent in E12.5 pKO offspring.

(A) The number of live embryos per litter at E12.5. (B) The number of resorbed embryos per litter at E12.5. (A&B) (n) pCON = 4 litters; pKO = 5 litters. Line = mean, bars = 95% confidence interval. * $p < 0.05$, unpaired two-tailed t-test. (C) Schematic of the *KvDMR* locus. The maternal allele and maternal-specific *Cdkn1c* and *Kcnq1* expression is represented on the top (pink) and the paternal allele and paternal-specific *Kcnq1ot1* expression is represented on the bottom (blue). Genes = black boxes with the exception of *Kcnq1ot1*, which is represented as white box within the gene body of *Kcnq1*. Black lollipops = methylated DNA at the ICR, white lollipops = unmethylated DNA at the ICR. (D) Allele-specific expression of *Cdkn1c*. (n) pCON = 23 embryos from 3 litters; pKO = 25 embryos from 7 litters. Abnormal embryos are indicated with red letters, which is consistent in graphs D and E. All embryos are in the same order from left to right in D and E. (E) Percent DNA methylation at the *KvDMR*. (n) pCON = 19 embryos from 3 litters; pKO = 29 embryos from 7 litters.

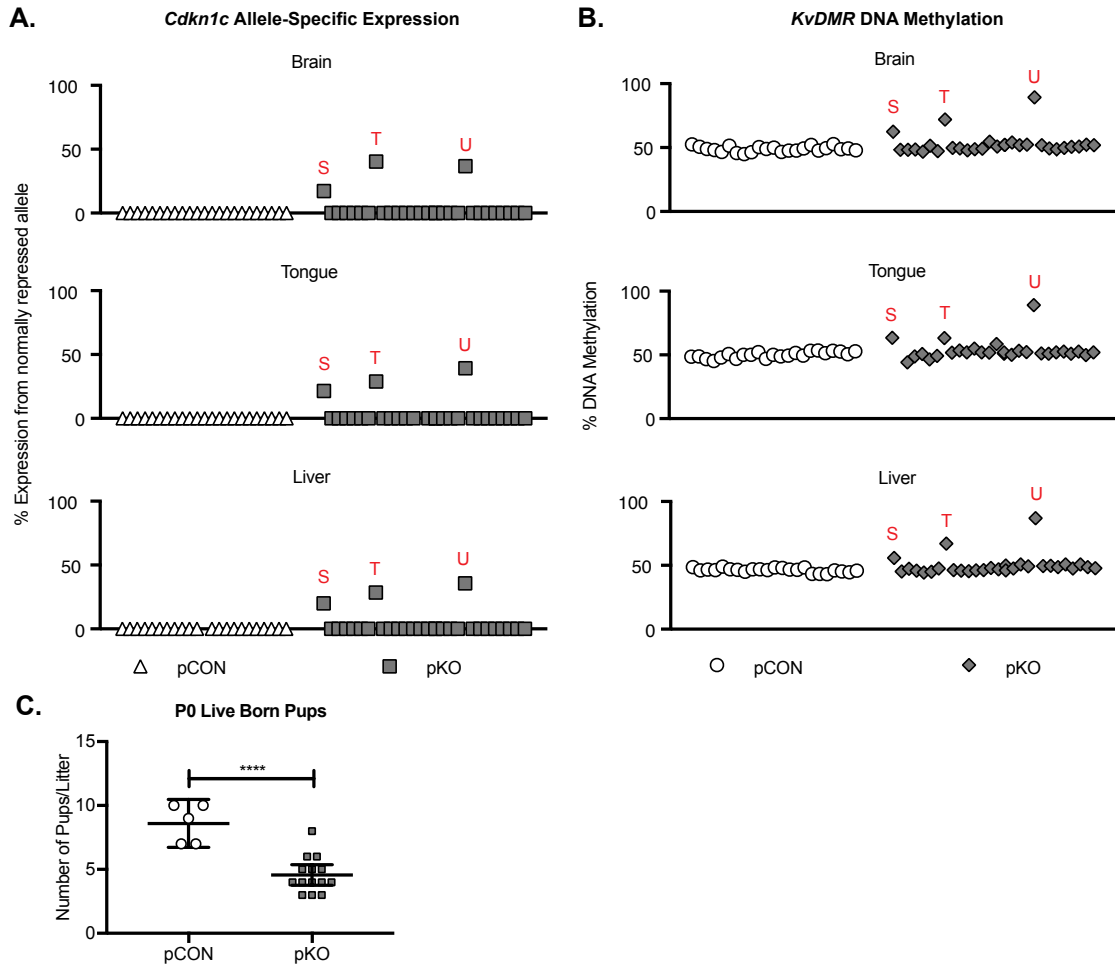
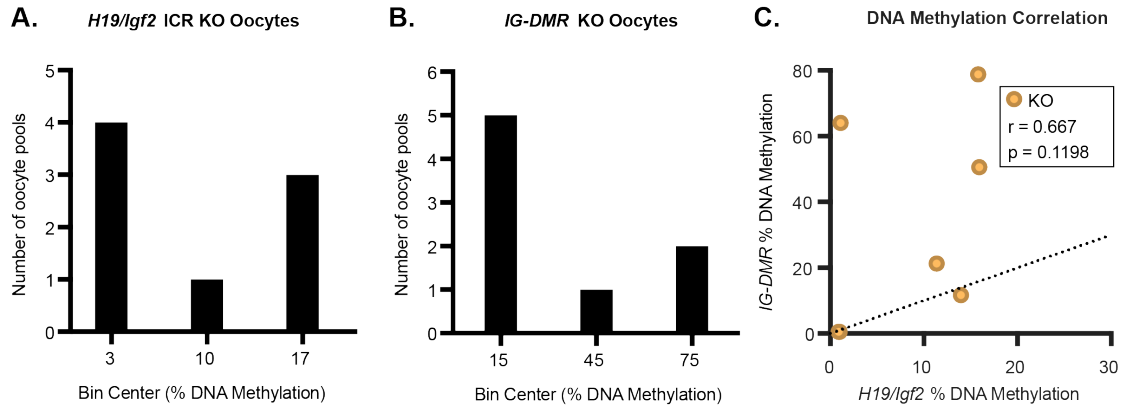
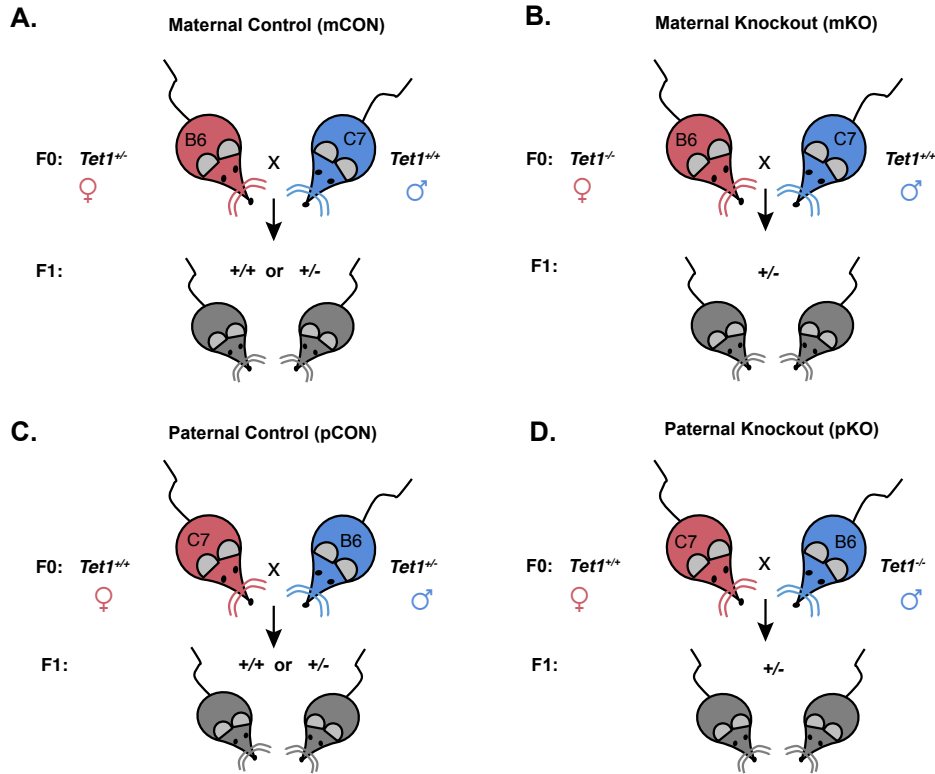


Figure 2.7. Po pKO pups show biallelic *Cdkn1c* expression and methylation defects across tissues.

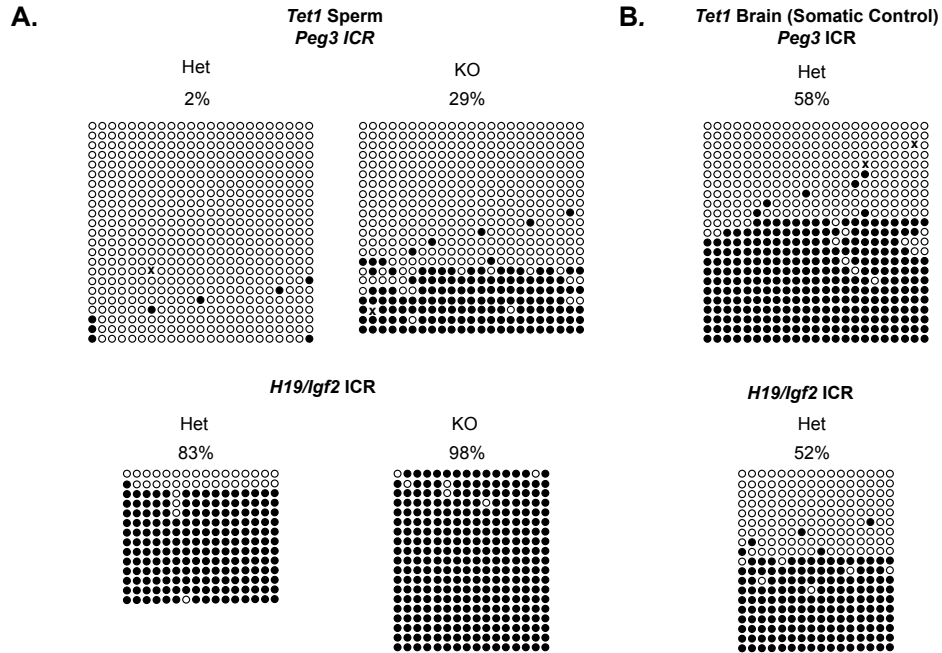
(A) Allele-specific expression of *Cdkn1c* in Po brain, tongue, and liver. (n) pCON = 23 pups from 4 litters; pKO = 29 pups from 5 litters. Abnormal pups are denoted with unique red letters, which are consistent in parts A and B. All pups are in the same order from left to right in all graphs in both parts A and B. (B) Percent DNA methylation at the *KvDMR*. (n) pCON = 19 pups from 4 litters; pKO = 29 pups from 5 litters. (C) The number of live pups per litter at Po, **** $p < 0.0001$, unpaired two-tailed t-test. (n) pCON = 5 litters; pKO = 13 litters. Line = mean, bars = 95% confidence interval.



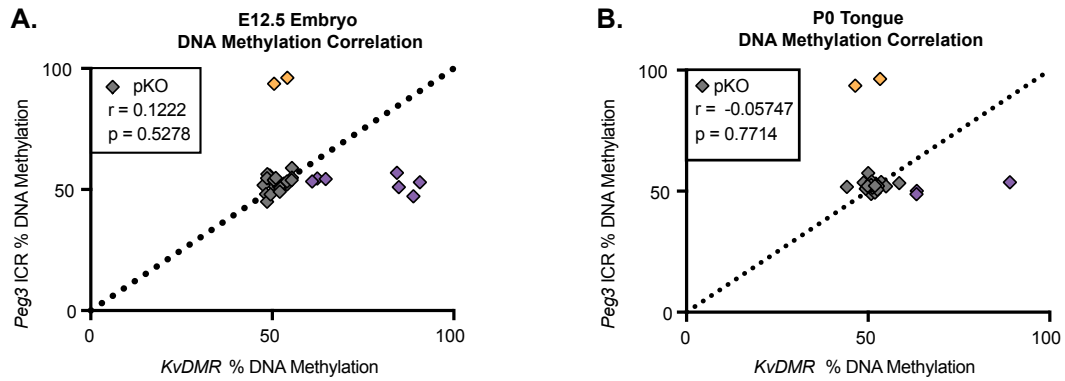
Supplemental Figure 2.1. Further characterization of oocyte DNA methylation. The DNA methylation data from Figure 2.1 (A) KO oocytes at the *H19/Igf2* ICR and (B) KO oocytes at the *IG-DMR* are plotted as histograms. (C) Correlation plot between KO oocyte pools at the *H19/Igf2* ICR versus the *IG-DMR*. $r =$ Spearman correlation coefficient. Dashed line represents a hypothetical perfect correlation.



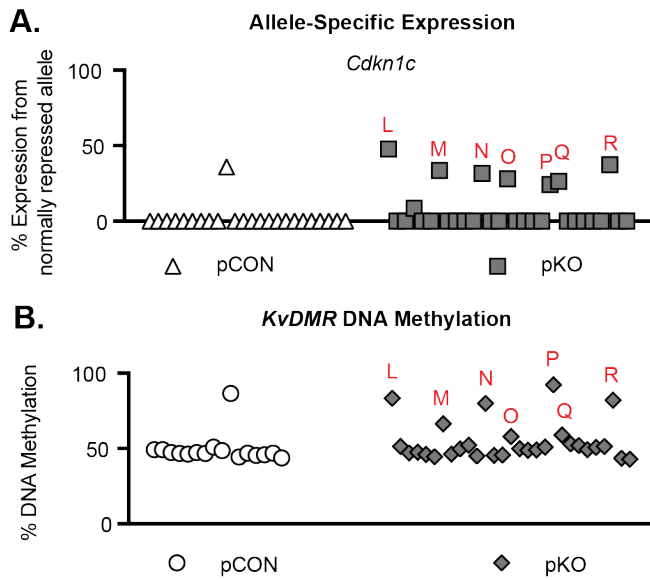
Supplemental Figure 2.2. F1 hybrid breeding schemes for analyzing allele-specific expression. (A) $Tet1^{+/-}$ female mice on the B6 background were mated to $Tet1^{+/+}$ mice on the C7 background to generate maternal control offspring (mCON) for analysis. (B) $Tet1^{-/-}$ female mice on the B6 background were mated to $Tet1^{+/+}$ mice on the C7 background to generate maternal KO offspring (mKO) for analysis. (C) $Tet1^{+/+}$ females on the C7 background were crossed to $Tet1^{+/-}$ males on the B6 background to generate paternal control offspring (pCON) for analysis. (D) $Tet1^{+/+}$ females on the C7 background were crossed to $Tet1^{-/-}$ males on the B6 background to generate paternal KO offspring (pKO) for analysis.



Supplemental Figure 2.3. Bisulfite sequencing validation of *Tet1* sperm DNA methylation. (A) Bisulfite sequencing of the *Peg3* ICR for both control heterozygous sperm and KO sperm. Bisulfite plots for the *H19/Igf2* ICR is shown as a control. (B) Bisulfite sequencing of a somatic control brain showing the expected methylation pattern at the *Peg3* ICR as a control. Each circle represents a CpG, white = unmethylated, black = methylated. Each row represents one cloned strand of DNA. Each bisulfite plot represents one animal and results from two technical PCR replicates.



Supplemental Figure 2.4. Hypermethylation at the *KvDMR* and *Peg3* ICRs is mutually exclusive in E12.5 pKO embryos and P0 newborns. (A) Correlation plot showing DNA methylation per E12.5 pKO embryo at the *KvDMR* and *Peg3* ICRs. (B) Correlation plot showing DNA methylation per P0 pup (tongue) at the *KvDMR* and *Peg3* ICRs. Gray diamonds show unaffected pKO pups. The orange diamonds highlight pups with *Peg3* hypermethylation. The purple diamonds highlight pups with *KvDMR* hypermethylation. r = Spearman correlation coefficient. Dotted line represents hypothetical perfect correlation.



Supplemental Figure 2.5. Abnormal biallelic expression and DNA hypermethylation are consistent in the E12.5 placental tissues. (A) Allele-specific expression of *Cdkn1c* in the E12.5 placenta (corresponding to the embryos from Figure 6 in the main text). *Cdkn1c* (n) pCON = 24 placentas from 3 litters; pKO = 29 placentas from 7 litters. (B) Percent DNA methylation at the *KvDMR*. (n) pCON = 16 placentas from 2 litters; pKO = 29 placentas from 7 litters. Abnormal placentas are indicated with red letters and this lettering is consistent between all graphs in Figures 2.6B and 2.6C and Supplemental Figures 2.5A and 2.5B. All placentas are in the same order from left to right in A and B.

Table S2.1: % DNA methylation at ICRs in Tet1 oocytes with inclusion data.

Mouse #	Genotype	ICR DNA Methylation (% Average)										H19/Igf2 and/or IG-DMR?	Number of Control ICRS	TOP 2 avg >90%	Both Criteria Met?
		Paternally Methylated					Maternally Methylated (Control)								
		H19	IG-DMR	Peg3	Snrpn	Peg1	KvDMR	H19/Igf2 and/or IG-DMR?							
5629A	WT	1.4	0.0	97.2		97.4						yes	2	97.3	yes
5826	WT		0.8	93.7	98.2	75.6						yes	3	95.9	yes
W956	WT	4.1	7.2	93.0	97.9	96.0						yes	3	96.9	yes
W1096	WT	3.1	15.1	84.9	92.6	94.5						yes	3	93.5	yes
W1542	WT	1.0	0.9	97.9		92.7						yes	2	95.3	yes
5442	Het	6.7	0.5	98.7	81.1	95.6						yes	3	97.1	yes
Het442	Het	2.0	0.8	89.0	97.7	81.9	64.9					yes	4	93.4	yes
H1095	Het	6.7	0.6	86.7	76.7	95.7						yes	3	91.2	yes
H1550	Het	0.7	5.5	91.4		94.6						yes	2	93.0	yes
LEP	KO	2.3		95.0		60.8	96.8					yes	3	95.9	yes
5619	KO	1.0	0.5	99.1	85.3	83.5						yes	3	92.2	yes
5828	KO	1.1	64.0	95.0	98.1	94.6						yes	3	96.5	yes
5834B	KO	0.9	0.5	98.0	98.0	94.7						yes	3	98.0	yes
Mut554A	KO	14.0	11.7	89.9	97.5	80.5	67.8					yes	4	97.8	yes
Mut445	KO	11.4	21.3	95.0	97.8	74.4						yes	3	96.4	yes
M1097	KO		0.8	96.1	98.3	91.9						yes	3	97.2	yes
M1027	KO	15.9	50.6	99.3	92.4	100.0						yes	3	99.6	yes
M1541	KO	15.8	78.8	92.1	89.5	100.0						yes	3	96.0	yes

Bold type indicates the top two most highly methylated maternally methylated ICRs

Table S2.2: Litter (denoted with unique letters), sex (M= male, F = female), allele-specific expression, and DNA methylation data for all E10.5 mCON and mKO embryo and placentas.

Cross	Original ID	Paper ID	Sex	Litter	Allele-Specific Expression- % Expression from normally repressed allele				ICR DNA Methylation - (% Average)									
					H19 Embryo	H19 Placenta	Igf2 Embryo	Igf2 Placenta	H19/Igf2 Embryo	H19/Igf2 Placenta	IG-DMR Embryo	IG-DMR Placenta	Peg3 Embryo	Peg3 Placenta	KvDMR Embryo	KvDMR Placenta		
mCON	1		F	A	0.0	0.0	0.0	0.0	56.1	58.2	44.3	54.3					52.3	46.8
mCON	2		M	A	0.0	0.0	0.0	0.0	55.2	55.1	42.1	63.0					52.5	48.1
mCON	3		F	A	0.0	0.0	0.0	0.0	56.6	53.7	46.2	42.3					53.4	49.4
mCON	4		F	A	0.0	0.0	0.0	0.0	57.0	57.6	41.6	62.7					51.5	50.3
mCON	5		M	A	0.0	0.0	0.0	0.0	56.4	56.8	46.6	42.7					49.7	47.6
mCON	6		M	A		0.0			57.4		46.2						51.0	
mCON	7		M	A	0.0	0.0	0.0	0.0	58.5	55.3	45.3	51.0					51.9	47.4
mCON	8		F	A	0.0	0.0	0.0	0.0	57.6	58.0	42.2	53.3					51.9	48.0
mCON	9		F	B	0.0	0.0	0.0	0.0	55.7	60.5	51.3	60.0					48.8	52.2
mCON	10		M	B	0.0	0.0	0.0	0.0	57.5	57.2	50.7	69.4					49.2	54.6
mCON	11		M	B	0.0	0.0	0.0	0.0	55.1	55.4	47.6	60.9					50.5	56.0
mCON	12		M	B	0.0	0.0	0.0	0.0	56.6	60.3	49.7	43.4					50.1	55.1
mCON	13		M	B	0.0	0.0	0.0	0.0	57.9	62.1	45.3	59.5					53.8	53.5
mCON	14		F	B	0.0	0.0	0.0	0.0	53.2	57.0	46.4	48.4			51.2		50.6	53.8
mCON	15		M	B		0.0			57.2		52.1						49.8	
mCON	16		M	B	0.0	0.0	0.0	0.0	56.2	61.6	48.7	62.5			50.0		52.6	52.4
mCON	17		M	B	0.0	0.0	0.0	0.0		56.0		47.3						53.4
mCON	24		F	C	0.0	0.0	0.0	0.0	55.2		43.5		49.0				50.6	
mCON	25		F	C	0.0	0.0	0.0	0.0	57.2	58.7	44.3	52.2	48.5	55.9			50.2	51.5
mCON	26		M	C	0.0	0.0	0.0	0.0	55.3	59.1	43.8	46.5	48.8	49.6			51.1	48.5
mCON	27		M	C	0.0	0.0	0.0	0.0	54.7	57.9	43.7	46.8	49.8	50.7			51.3	53.9
mCON	28		F	C	0.0	0.0	0.0	0.0	56.2	61.2	44.1	48.9	50.8	49.9			51.7	52.7
mCON	29		M	C	0.0	0.0	0.0	0.0	59.0	59.6	45.0	51.4	50.3	51.1			50.1	53.2
mCON	30		M	C	0.0	0.0	0.0	0.0	55.4	59.0	41.5	48.1	48.9	47.8			50.3	51.4
mCON	31		M	C	0.0	0.0	0.0	0.0	55.8	57.4	43.7	56.4	50.2	50.6			50.7	51.6
mCON	32		F	D	0.0	0.0	0.0	0.0	55.3		47.0		46.2				48.6	
mCON	33		M	D	0.0	0.0	0.0	0.0	54.6		45.7		46.2				49.9	
mCON	34		F	D	0.0	0.0	0.0	0.0	55.3		45.4		49.8				50.9	
mCON	35		F	D	0.0	0.0	0.0	0.0	53.4		41.7		48.0				48.0	
mCON	36		F	D	0.0	0.0	0.0	0.0	53.2		46.6		50.6				52.3	
mCON	37		F	D	0.0	0.0	0.0	0.0	58.8		42.4		45.5				49.9	
mCON	38		M	D	0.0	0.0	0.0	0.0	55.1		46.1		51.3				53.4	
mCON	39		F	D	0.0	0.0	0.0	0.0	51.7		43.9		47.4				50.2	
mCON	40		F	D	0.0	0.0	0.0	0.0	55.0		95.0		51.9				50.2	
mCON	49		M	E														
mCON	50		F	E														
mCON	51		M	E														
mCON	52		F	E														
mCON	53		M	E														
mCON	54		M	E														
mCON	55		F	E														
mCON	56		F	E														
mCON	57		M	E														
mKO	1		M	F	0.0	0.0	0.0	0.0	56.6	55.6	45.3	40.9					52.7	47.9
mKO	2		M	F	0.0	0.0	0.0	0.0	59.5	58.0	46.0	55.5					50.6	50.1
mKO	3		F	F	0.0	0.0	0.0	0.0	56.7	59.4	43.2	50.1					50.5	49.7
mKO	4		M	F	0.0	0.0	0.0	0.0	62.9	57.9	41.9	58.9					53.2	49.8
mKO	5		F	F	0.0	0.0	0.0	0.0	52.5	52.5	49.9	46.4					51.0	47.2
mKO	6	D	F	F	0.0	0.0	0.0	0.0	58.2	61.3	96.0	80.7					50.7	49.1
mKO	8		F	F	0.0	0.0	0.0	0.0	59.9	58.1	41.9	47.0					50.6	46.9
mKO	9	E	M	G	0.0	0.0	0.0	0.0	53.3	57.0	96.7	86.5					51.2	56.7
mKO	10		M	G	0.0	0.0	0.0	0.0	54.6	50.7	49.4	69.4					49.4	51.5
mKO	11		F	G	0.0	0.0	0.0	0.0	60.0	62.3	48.7	47.6					49.9	48.2
mKO	12	A	F	G	0.0	0.0	51.5	52.4	95.5	93.2	95.7	84.5					49.9	53.0
mKO	13	F	F	G	0.0	0.0	0.0	0.0	57.9	65.1	95.7	82.2					51.1	52.1
mKO	14	G	F	G	0.0	0.0	0.0	0.0	57.4	59.0	95.7	86.2					52.3	49.5
mKO	15	H	F	G	0.0	0.0	0.0	0.0	54.6		96.0						49.1	
mKO	16		F	G	0.0	0.0	0.0	0.0	55.0	58.3	51.6	55.9					50.7	49.9
mKO	18		F	H	0.0	0.0	0.0	0.0	55.3	56.1	41.7	51.4	50.6	46.9			53.3	47.6
mKO	19		M	H	0.0	0.0	0.0	0.0	59.3	59.7	43.4	56.2	50.8	51.4			53.0	53.2
mKO	20		M	H	0.0	0.0	0.0	0.0	55.7	58.4	45.7	61.9	50.8	51.6			52.0	53.2
mKO	21	I	F	H	0.0	0.0	0.0	0.0	55.1	57.0	95.7	83.0	51.0	52.1			50.9	51.6
mKO	22		F	H	0.0	0.0	0.0	0.0	60.3	57.2	44.8	52.7	49.1	49.9			50.4	51.5
mKO	23		M	I	0.0	0.0	0.0	0.0	55.0		43.4						50.5	
mKO	25		M	I	0.0	0.0	0.0	0.0	54.5		45.5						51.3	
mKO	26		M	J	0.0	0.0	0.0	0.0	54.5		44.9						53.1	
mKO	27	B	F	J	0.0	0.0	53.3	55.5	90.0		45.0						51.3	
mKO	28	J	F	J	0.0	0.0	0.0	0.0	54.0		95.4						50.2	
mKO	29		M	J	0.0	0.0	0.0	0.0	55.1		43.5						50.1	
mKO	30		M	J	0.0	0.0	0.0	0.0	53.2		44.3						50.3	
mKO	31		F	J	0.0	0.0	0.0	0.0	54.4		43.8						50.3	
mKO	33		M	J	0.0	0.0	0.0	0.0	57.4		41.1						51.4	
mKO	34	K	M	K	0.0	0.0	0.0	0.0	55.8	49.3	96.4	87.1	50.3	36.0			53.5	47.8
mKO	35	L	F	K	0.0	0.0	0.0	0.0	61.9	54.3	94.5	84.7	55.1	44.7			52.9	46.9
mKO	36		M	L	0.0	0.0	0.0	0.0	55.2	54.8	43.9	46.6	51.1	48.5			56.8	49.1
mKO	37		M	L	0.0	0.0	0.0	0.0	56.4	53.3	43.1	53.8	50.3	45.8			52.2	47.5
mKO	39	C	M	L	0.0	0.0	60.1	60.0	81.1	78.5	42.7	65.6	51.7	39.6			53.7	43.5
mKO	40		F	L	0.0	0.0	0.0	0.0	54.5	53.1	46.0	53.0	52.8	46.4			49.6	51.5
mKO	41		M	L	0.0	0.0	0.0	0.0	61.8	57.0	43.3	46.1	51.5	50.6			50.2	47.9

Table S2.3: Sex ratio information for both maternal and paternal Tet1 offspring.

Maternal E10.5 mCON				Maternal E10.5 mKO															
	Observed	Expected	TOTAL		Observed	Expected	TOTAL												
Male	21	17	38	Male	18	18	36												
Female	13	17	30	Female	18	18	36												
TOTAL	34	34	68	TOTAL	36	36	72												
Two-tailed Chi-Square: $p = 0.170$ Sex ratio is not significantly different				Two-tailed Chi-Square: 1.000 Sex ratio is not significantly different															
				<table border="1"> <thead> <tr> <th colspan="3">Maternal E10.5 mKO</th> </tr> <tr> <th></th> <th>Affected</th> <th>Unaffected</th> </tr> </thead> <tbody> <tr> <td>Male</td> <td>3</td> <td>16</td> </tr> <tr> <td>Female</td> <td>9</td> <td>8</td> </tr> </tbody> </table> <p>The two-tailed P value = 0.033 The association between rows and columns is significant.</p>				Maternal E10.5 mKO				Affected	Unaffected	Male	3	16	Female	9	8
Maternal E10.5 mKO																			
	Affected	Unaffected																	
Male	3	16																	
Female	9	8																	
Maternal P0 mCON				Maternal P0 mKO															
	Observed	Expected	TOTAL		Observed	Expected	TOTAL												
Male	8	8	16	Male	14	15	29												
Female	8	8	16	Female	16	15	31												
TOTAL	16	16	32	TOTAL	30	30	60												
Two-tailed Chi-Square: $p = 1.000$ Sex ratio is not significantly different				Two-tailed Chi-Square: $p = 0.715$ Sex ratio is not significantly different															
				<table border="1"> <thead> <tr> <th colspan="3">Maternal P0 mKO</th> </tr> <tr> <th></th> <th>Affected</th> <th>Unaffected</th> </tr> </thead> <tbody> <tr> <td>Male</td> <td>0</td> <td>16</td> </tr> <tr> <td>Female</td> <td>3</td> <td>13</td> </tr> </tbody> </table> <p>Affected = J, K, and # (see Table S2.6) Two-tailed Fisher's Exact Test: $p = 0.226$ The association between rows and columns is not significant.</p>				Maternal P0 mKO				Affected	Unaffected	Male	0	16	Female	3	13
Maternal P0 mKO																			
	Affected	Unaffected																	
Male	0	16																	
Female	3	13																	
Paternal E12.5 pCON				Paternal E12.5 pKO															
	Observed	Expected	TOTAL		Observed	Expected	TOTAL												
Male	11	11.5	22.5	Male	10	14.5	24.5												
Female	12	11.5	23.5	Female	19	14.5	33.5												
TOTAL	23	23	46	TOTAL	29	29	58												
Two-tailed Chi-Square: $p = 0.835$ Sex ratio is not significantly different				Two-tailed Chi-Square: $p = 0.095$ Sex ratio is not significantly different															
				<table border="1"> <thead> <tr> <th colspan="3">Paternal E12.5 pKO</th> </tr> <tr> <th></th> <th>Affected</th> <th>Unaffected</th> </tr> </thead> <tbody> <tr> <td>Male</td> <td>3</td> <td>7</td> </tr> <tr> <td>Female</td> <td>4</td> <td>15</td> </tr> </tbody> </table> <p>Two-tailed Fisher's Exact Test: $p = 0.665$ The association between rows and columns is not significant.</p>				Paternal E12.5 pKO				Affected	Unaffected	Male	3	7	Female	4	15
Paternal E12.5 pKO																			
	Affected	Unaffected																	
Male	3	7																	
Female	4	15																	
Paternal P0 pCON				Paternal P0 pKO															
	Observed	Expected	TOTAL		Observed	Expected	TOTAL												
Male	13	11.5	24.5	Male	17	14	31												
Female	10	11.5	21.5	Female	11	14	25												
TOTAL	23	23	46	TOTAL	28	28	56												
Two-tailed Chi-Square: $p = 0.532$ Sex ratio is not significantly different				Two-tailed Chi-Square: $p = 0.257$ Sex ratio is not significantly different															
				<table border="1"> <thead> <tr> <th colspan="3">Paternal P0 pKO</th> </tr> <tr> <th></th> <th>Affected</th> <th>Unaffected</th> </tr> </thead> <tbody> <tr> <td>Male</td> <td>0</td> <td>17</td> </tr> <tr> <td>Female</td> <td>3</td> <td>8</td> </tr> </tbody> </table> <p>Two-tailed Fisher's Exact Test: $p = 0.050$ The association between rows and columns is not significant.</p>				Paternal P0 pKO				Affected	Unaffected	Male	0	17	Female	3	8
Paternal P0 pKO																			
	Affected	Unaffected																	
Male	0	17																	
Female	3	8																	

Table S2.4: Litter (denoted with unique letters), sex (M= male, F = female), allele-specific expression, and DNA methylation data for all P0 mCON and mKO brain, liver, and tongue.

Cross	Original ID	Paper ID	Sex	Litter	Allele-Specific Expression- % Expression from normally repressed allele						ICR DNA Methylation- (% Average)											
					H19			Igf2			H19/Igf2			IG-DMR			Peg3			KvDMR		
					Brain	Liver	Tongue	Brain	Liver	Tongue	Brain	Liver	Tongue	Brain	Liver	Tongue	Brain	Liver	Tongue	Brain	Liver	Tongue
mCON	5313-1		F	A	0.0	0.0	0.0	0.0	0.0			63.3			51.9			53.1			57.1	
mCON	5313-2		M	A	0.0	0.0	0.0	0.0	0.0			57.1			49.9			50.8			51.8	
mCON	5313-3		M	A	0.0	0.0	0.0	0.0	0.0			58.9			48.3			52.8			52.2	
mCON	5313-4		F	A	0.0	0.0	0.0	0.0	0.0			57.5			45.8			51.2			52.1	
mCON	5313-5		M	A	0.0	0.0	0.0	0.0	0.0			57.7			45.6			51.5			51.1	
mCON	5313-6		F	A	0.0	0.0	0.0	0.0	0.0			55.4			48.4			51.5			51.8	
mCON	5314-1		F	B	0.0	0.0	0.0	0.0	0.0			57.6			49.5			51.5			51.4	
mCON	5314-2		M	B	0.0	0.0	0.0	0.0	0.0			58.4			49.8			53.0			52.0	
mCON	5314-3		M	B	0.0	0.0	0.0	0.0	0.0			61.6			48.6			52.4			52.7	
mCON	1330-1		F	C	0.0	0.0	0.0	0.0	0.0			59.8			48.1			51.6			54.6	
mCON	1330-2		F	C	0.0	0.0	0.0	0.0	0.0			57.0			46.6						55.1	
mCON	1330-3		F	C	0.0	0.0	0.0	0.0	0.0			55.9			44.2			54.0			49.7	
mCON	1330-4		M	C	0.0	0.0	0.0	0.0	0.0			59.4			46.2			51.9			50.7	
mCON	1330-5		M	C	0.0	0.0	0.0	0.0	0.0			55.6			48.1			52.6			51.0	
mCON	1330-6		F	C	0.0	0.0	0.0	0.0	0.0			55.6			47.4			51.0			53.3	
mCON	1330-7		M	C	0.0	0.0	0.0	0.0	0.0			57.7			45.9			52.7			53.0	
mKO	5106-1		M	D	0.0	0.0	0.0	0.0	0.0			58.3			48.9			53.2			52.7	
mKO	5106-2		F	D	0.0	0.0	0.0	0.0	0.0			57.5			52.6			53.4			52.6	
mKO	5106-3		M	D	0.0	0.0	0.0	0.0	0.0			58.6			48.3			50.7			52.7	
mKO	5106-4		F	D	0.0	0.0	0.0	0.0	0.0			58.4			46.8			50.3			51.3	
mKO	5106-5		M	D	0.0	0.0	0.0	0.0	0.0			50.6			49.3			50.0			53.4	
mKO	5106-6		F	D	0.0	0.0	0.0	0.0	0.0			60.0			51.9			52.6			51.6	
mKO	5108-1		F	E	0.0	0.0	0.0	0.0	0.0			55.1			46.4			51.5			51.2	
mKO	5108-2		M	E	0.0	0.0	0.0	0.0	0.0			55.7			45.1			51.1			50.6	
mKO	5108-3		M	E	0.0	0.0	0.0	0.0	0.0			58.4			46.1			53.2			49.8	
mKO	5108-4		F	E	0.0	0.0	0.0	0.0	0.0			58.7			45.4			52.9			53.7	
mKO	5108-5	J	F	E	0.0	0.0	39.4	52.1				86.0			43.5			52.1			48.7	
mKO	5108-6		F	E	0.0	0.0	0.0	0.0	0.0			55.7			47.2			52.9			52.3	
mKO	5106-7		F	F	0.0	0.0	0.0	0.0	0.0			62.6			48.0			43.8			52.4	
mKO	5106-8		M	F	0.0	0.0	0.0	0.0	0.0			53.5			44.0			53.2			51.3	
mKO	5106-9		M	F	0.0	0.0	0.0	0.0	0.0			58.8			45.3			56.1			53.2	
mKO	5106-10		F	F	0.0	0.0	0.0	0.0	0.0			49.1			42.0			40.6			64.6	
mKO	5106-11		M	F	0.0	0.0	0.0	0.0	0.0			57.5			41.6			51.0			52.1	
mKO	5106-12		F	F	0.0	0.0	0.0	0.0	0.0			56.4			47.3			52.5			51.5	
mKO	5106-13		M	F	0.0	0.0	0.0	0.0	0.0			62.7			47.1			53.3			47.6	
mKO	mKO-8		F	G	0.0	0.0	0.0	0.0	0.0			60.4			46.6			51.9			51.2	
mKO	mKO-9		F	G	0.0	0.0	0.0	0.0	0.0			57.0			51.1			51.8			51.3	
mKO	mKO-10		F	G	0.0	0.0	0.0	0.0	0.0			57.1			49.4			52.4			54.6	
mKO	912-1	# (See IG-DMR & Table S2.5)	F	H	0.0				0.0			57.6			94.2			52.6			54.1	
mKO	912-2		F	H	0.0	0.0	0.0	0.0	0.0			57.2			50.4			52.0			52.8	
mKO	912-3		M	H	0.0	0.0	0.0	0.0	0.0			58.9			50.4			50.8			55.3	
mKO	912-4		M	H	0.0	0.0	0.0	0.0	0.0			59.1			53.2			51.7			56.1	
mKO	912-5		F	H	0.0	0.0	0.0	0.0	0.0			59.1			49.4			51.7			52.3	
mKO	912-6		M	I	0.0	0.0	0.0	0.0	0.0			57.8			49.0			50.5			52.1	
mKO	912-7		M	I	0.0	0.0	0.0	0.0	0.0			57.2			48.8			51.5			51.8	
mKO	976-2	K	F	J	0.0	0.0	6.7	11.7				60.2			50.2			50.8			52.5	
mKO	976-3		M	J	0.0	0.0	0.0	0.0	0.0			58.9			52.4			51.7			53.7	

Table S2.5: % DNA methylation at ICRs in Tet1 Sperm

Sample ID	Genotype	ICR DNA Methylation (% Average)					
		Paternally Methylated		Maternally Methylated			
		<i>H19/Igf2</i>	<i>IG-DMR</i>	<i>KvDMR</i>	<i>Peg3</i>	<i>Peg1</i>	<i>Snrpn</i>
W5062	WT	94.6		8.5	7.3		5.1
W5068	WT	95.7		2.5	1.6		2.3
WT1	WT	96.0	95.0	11.0	8.0	5.0	7.0
WT2	WT	96.0	95.0	12.0	4.0	5.0	3.0
WT3	WT	94.0	92.0	7.0	5.0	8.0	6.0
WT5183	WT	97.6	97.6	3.8	3.3	4.8	3.2
H4852	Het	95.4	96.9	4.0	3.4	5.8	4.2
H5059	Het	93.7	97.4	4.4	2.9	5.4	4.5
H5069	Het	97.7		9.6	5.3		13.8
H5103	Het	95.9	95.4	4.5	3.6	6.4	6.8
H5104	Het	94.0	97.3	4.8	6.0	6.9	4.6
H5105	Het	95.0	96.3	3.8	3.3	5.5	5.9
H5184	Het	94.1	97.0	4.4	6.0	6.1	2.3
Hep3	Het	93.9		6.7	5.0		5.3
Het5787	Het	97.4	96.9	5.3	5.3	8.2	5.0
Het5791	Het	97.1	97.2	4.4	3.4	6.6	3.9
M4848	KO	95.2		29.8	3.0		5.6
M4851	KO	93.7		33.6			18.5
M4859	KO	95.0		30.9	4.6		14.2
M5060	KO	94.8	95.1	33.9	10.6	20.4	5.1
M5064	KO	96.8	95.9	32.7	10.3	21.5	5.9
M5109	KO	91.6		39.0	9.8		28.8
M5311	KO	92.6	96.1	33.8	10.8	18.9	6.1
Mutep3	KO	93.0	96.4	34.3	11.6	23.5	7.0
Mutep4	KO	96.9	95.6	31.3	10.7	21.2	3.1
Mut5339	KO	91.7	88.4	36.5	19.9	26.0	10.1
Mut5781	KO	96.8	96.2	34.4	11.7	19.8	5.4
Mut5318	KO	95.2	89.4	37.9	11.9	21.4	5.5
Mut5333	KO	96.2	95.5	34.2	10.4	18.4	5.2
Mut5058	KO	96.5	95.1	35.8	11.2	21.4	5.2
Mut5728	KO	96.8	97.2	35.5	9.8	17.3	3.1
DKO 1	DKO	94.0	93.0	23.0	6.0	10.0	7.0
DKO 2	DKO	96.0	96.0	30.0	5.0	20.0	8.0
DKO 3	DKO	96.0	93.0	37.0	9.0	22.0	11.0
		<i>H19/Igf2</i>	<i>IG-DMR</i>	<i>KvDMR</i>	<i>Peg3</i>	<i>Peg1</i>	<i>Snrpn</i>
KO vs DKO, Mann-Whitney (p-value)		0.985	0.440	0.360	0.065	0.660	0.203

Table S2.6: Litter (denoted with unique letters), sex (M= male, F = female), allele-specific expression, and DNA methylation data for all E12.5 pCON and pKO embryo and placenta.

Cross	Original ID	Paper ID	Sex	Litter	Cdkn1c Embryo	Cdkn1c Placenta	Kcnq1ot1 Embryo	Kcnq1ot1 Placenta	H19 Embryo	H19 Placenta	Igf2 Embryo	Igf2 Placenta	ICR-DNA Methylation - (% Average)												
													H19/Igf2 Embryo	H19/Igf2 Placenta	Ig-DMR Embryo	Ig-DMR Placenta	IG-DMR Embryo	IG-DMR Placenta	Peg3 Embryo	Peg3 Placenta	KUDMR Embryo	KUDMR Placenta	Peg1 Embryo	Peg1 Placenta	Srrpn Embryo
pCON	CE2		F	A	0.0	0.0	0.0	0.0	0.0	0.0	0.0	0.0	50.6	45.4	41.6	42.8	47.7	45.1	51.3	49.2	49.3	41.0	44.1	39.1	
pCON	CE3		F	A	0.0	0.0	0.0	0.0	0.0	0.0	0.0	0.0	49.2	49.4	38.7	39.0	47.8	46.2	49.3	49.3	49.8	41.2	43.9	38.8	
pCON	CE4		F	A	0.0	0.0	0.0	0.0	0.0	0.0	0.0	0.0	51.4	48.8	40.7	39.3	48.9	46.5	52.0	52.0	50.2	42.8	43.4	39.9	
pCON	CE5		F	A	0.0	0.0	0.0	0.0	0.0	0.0	0.0	0.0	50.9	50.4	38.9	36.5	48.9	45.1	52.3	46.7	49.7	42.2	42.5	41.6	
pCON	CE6		M	A	0.0	0.0	0.0	0.0	0.0	0.0	0.0	0.0	53.3	48.1	42.4	39.6	46.7	46.7	50.3	46.2	50.5	42.1	43.0	39.5	
pCON	CE7		M	A	0.0	0.0	0.0	0.0	0.0	0.0	0.0	0.0	50.1	52.4	42.0	41.4	51.0	46.9	52.1	47.3	50.9	44.2	44.7	39.5	
pCON	CE18		M	B	0.0	0.0	0.0	0.0	0.0	0.0	0.0	0.0	48.6	51.4	42.5	40.0	48.5	49.5	46.6	49.0	42.3	44.9	41.5		
pCON	CE19		M	B	0.0	0.0	0.0	0.0	0.0	0.0	0.0	0.0	50.8	50.9	44.0	54.2	47.5	51.4	51.0	49.4	47.8	43.9	42.6		
pCON	CE20		M	B	37.7	35.9	0.0	0.0	0.0	0.0	0.0	0.0	49.9	48.9	47.7	48.1	52.5	49.1	52.6	48.7	51.6	42.7	45.8	42.0	
pCON	CE21		M	B	0.0	0.0	0.0	0.0	0.0	0.0	0.0	0.0	48.5	59.3	46.4	52.7	50.4	53.4	52.2	86.5	50.4	46.3	37.2	41.3	
pCON	CE22		M	B	0.0	0.0	0.0	0.0	0.0	0.0	0.0	0.0	52.2	52.7	54.7	52.0	52.7	48.2	49.4	44.5	49.8	46.5	45.9	40.9	
pCON	CE23		M	B	0.0	0.0	0.0	0.0	0.0	0.0	0.0	0.0	51.6	51.6	46.8	46.8	48.4	48.4	47.0	47.0	42.7	42.7	39.5		
pCON	CE24		F	B	0.0	0.0	0.0	0.0	0.0	0.0	0.0	0.0	52.7	54.0	50.5	53.2	51.3	49.4	48.0	45.5	51.4	45.0	44.9	41.7	
pCON	CE25		M	B	0.0	0.0	0.0	0.0	0.0	0.0	0.0	0.0	54.5	53.2	49.3	49.3	50.4	45.9	49.3	45.9	50.7	43.6	48.6	40.2	
pCON	CE26		M	B	0.0	0.0	0.0	0.0	0.0	0.0	0.0	0.0	52.1	51.5	47.1	46.7	50.7	48.4	47.1	46.8	49.8	39.1	42.9	39.2	
pCON	CE27		M	C	0.0	0.0	0.0	0.0	0.0	0.0	0.0	0.0	53.4	47.2	43.1	51.7	50.5	45.3	46.6	43.9	49.8	42.6	48.0	40.8	
pCON	CE28		F	C	0.0	0.0	0.0	0.0	0.0	0.0	0.0	0.0	55.4	53.6	53.6	54.2	54.2	55.4	55.4	55.4	55.4	49.5	49.5	49.5	
pCON	CE29		F	C	0.0	0.0	0.0	0.0	0.0	0.0	0.0	0.0	56.0	50.7	50.7	54.2	54.2	54.2	53.7	53.7	53.7	48.5	48.5	48.5	
pCON	CE30		F	C	0.0	0.0	0.0	0.0	0.0	0.0	0.0	0.0	55.1	49.4	49.4	53.4	53.4	53.4	54.8	54.8	54.8	49.5	49.5	49.5	
pCON	CE31		M	C	0.0	0.0	0.0	0.0	0.0	0.0	0.0	0.0	55.1	49.4	49.4	52.2	52.2	52.2	54.4	54.4	54.4	49.6	49.6	49.6	
pCON	CE32		F	C	0.0	0.0	0.0	0.0	0.0	0.0	0.0	0.0	55.1	49.8	49.8	52.2	52.2	52.2	54.4	54.4	54.4	49.6	49.6	49.6	
pCON	CE33		F	C	0.0	0.0	0.0	0.0	0.0	0.0	0.0	0.0	55.1	49.8	49.8	52.2	52.2	52.2	54.4	54.4	54.4	49.6	49.6	49.6	
pCON	CE34		M	C	0.0	0.0	0.0	0.0	0.0	0.0	0.0	0.0	55.1	49.8	49.8	52.2	52.2	52.2	54.4	54.4	54.4	49.6	49.6	49.6	
pKO	ME1	L	F	D	47.5	47.7	0.0	0.0	0.0	0.0	0.0	0.0	51.5	53.7	45.5	52.9	53.1	50.8	90.7	83.3	49.3	44.6	40.1	40.1	
pKO	ME2		F	D	0.0	0.0	0.0	0.0	0.0	0.0	0.0	0.0	47.5	46.5	42.4	44.1	52.2	48.3	50.2	51.3	58.0	43.6	46.4	40.8	
pKO	ME3		F	D	0.0	0.0	0.0	0.0	0.0	0.0	0.0	0.0	49.4	56.5	42.9	47.1	52.1	49.5	54.1	47.2	57.9	45.7	45.1	37.9	
pKO	ME4		F	D	6.1	8.5	0.0	0.0	0.0	0.0	0.0	0.0	51.5	53.7	38.5	39.8	52.4	50.4	53.2	47.6	51.5	42.0	42.8	37.5	
pKO	ME6		F	D	0.0	0.0	0.0	0.0	0.0	0.0	0.0	0.0	52.8	57.4	44.4	52.8	55.9	51.9	49.3	46.2	51.7	43.5	43.9	43.2	
pKO	ME7		F	D	0.0	0.0	0.0	0.0	0.0	0.0	0.0	0.0	52.7	47.1	45.6	58.0	54.2	49.2	44.5	51.3	44.8	47.6	46.6	36.0	
pKO	ME8	M	F	D	12.6	33.5	0.0	0.0	0.0	0.0	0.0	0.0	53.1	52.1	43.9	50.2	54.5	54.3	62.4	66.3	53.5	44.7	45.1	43.4	
pKO	ME24		F	E	0.0	0.0	0.0	0.0	0.0	0.0	0.0	0.0	50.8	47.5	50.3	44.5	56.4	48.7	46.3	46.3	52.1	42.6	43.6	39.6	
pKO	ME25		F	F	0.0	0.0	0.0	0.0	0.0	0.0	0.0	0.0	51.7	48.9	43.5	50.2	96.2	77.5	54.2	49.7	52.9	45.7	45.1	40.7	
pKO	ME26		F	F	0.0	0.0	0.0	0.0	0.0	0.0	0.0	0.0	53.1	54.0	46.5	51.6	51.2	48.7	51.9	52.3	53.6	44.2	45.7	42.9	
pKO	ME28		F	F	0.0	0.0	0.0	0.0	0.0	0.0	0.0	0.0	57.5	47.0	66.3	38.2	59.0	46.8	55.4	45.0	54.9	41.3	45.6	38.7	
pKO	ME29	N	M	F	34.6	31.6	0.0	0.0	0.0	0.0	0.0	0.0	47.0	45.3	43.5	38.2	59.0	56.9	48.3	84.4	80.0	54.8	41.5	52.6	39.1
pKO	ME30		M	F	0.0	0.0	0.0	0.0	0.0	0.0	0.0	0.0	51.6	43.8	46.5	44.6	51.8	47.1	47.6	45.6	45.6	42.8	42.8	41.3	
pKO	ME32		M	F	0.0	0.0	0.0	0.0	0.0	0.0	0.0	0.0	53.1	55.7	46.3	40.2	54.7	48.0	48.6	45.6	52.8	42.8	42.8	41.3	
pKO	ME34	O	M	G	19.6	28.0	0.0	0.0	0.0	0.0	0.0	0.0	53.2	50.4	50.7	46.0	53.4	49.4	61.0	58.1	53.2	45.7	48.5	42.8	
pKO	ME35		F	G	0.0	0.0	0.0	0.0	0.0	0.0	0.0	0.0	53.5	48.7	50.0	47.9	53.6	52.2	50.7	49.8	53.2	51.4	47.3	43.9	
pKO	ME38		F	G	0.0	0.0	0.0	0.0	0.0	0.0	0.0	0.0	55.3	52.1	47.8	53.9	53.9	52.8	50.5	48.7	53.3	45.7	46.6	43.8	
pKO	ME41		F	G	0.0	0.0	0.0	0.0	0.0	0.0	0.0	0.0	53.9	50.7	49.9	55.0	54.8	53.2	50.9	49.1	55.9	46.7	46.1	42.7	
pKO	ME43		M	H	0.0	0.0	0.0	0.0	0.0	0.0	0.0	0.0	54.9	54.7	52.1	50.9	54.9	52.1	55.4	50.9	59.8	57.4	50.4	47.0	
pKO	ME44	P	F	H	36.0	24.2	0.0	0.0	0.0	0.0	0.0	0.0	57.1	56.9	48.2	56.9	51.0	53.0	84.9	92.3	56.9	60.3	48.4	48.9	
pKO	ME46	Q	F	H	21.8	26.4	0.0	0.0	0.0	0.0	0.0	0.0	57.1	56.9	50.1	52.3	54.4	52.4	64.7	59.1	64.0	54.4	47.4	48.9	
pKO	ME48		M	H	0.0	0.0	0.0	0.0	0.0	0.0	0.0	0.0	57.7	55.6	52.7	55.1	53.3	54.9	54.1	53.0	58.1	53.5	47.2	44.4	
pKO	ME50		F	H	0.0	0.0	0.0	0.0	0.0	0.0	0.0	0.0	53.5	52.5	50.8	59.8	52.5	55.4	52.0	61.6	52.0	51.6	52.6	50.1	
pKO	ME52		F	I	0.0	0.0	0.0	0.0	0.0	0.0	0.0	0.0	49.5	49.8	45.7	48.7	93.7	90.3	50.5	49.3	47.9	42.5	46.3	42.5	
pKO	ME54		M	I	0.0	0.0	0.0	0.0	0.0	0.0	0.0	0.0	47.8	55.0	42.8	52.7	48.1	48.9	48.3	50.7	47.7	42.7	42.4	37.7	
pKO	ME55		F	I	0.0	0.0	0.0	0.0	0.0	0.0	0.0	0.0	46.6	50.7	39.2	42.8	45.0	50.0	48.6	51.4	40.1	48.2	38.0	41.2	
pKO	ME56	R	F	I	39.0	37.5	0.0	0.0	0.0	0.0	0.0	0.0	49.1	52.0	42.3	51.1	47.2	46.2	88.9	82.2	51.7	41.2	42.3	36.4	
pKO	ME57		M	J	0.0	0.0	0.0	0.0	0.0	0.0	0.0	0.0	49.4	50.1	41.8	39.6	48.0	47.2	49.5	43.6	49.1	46.5	42.4	41.2	
pKO	ME63		F	J	0.0	0.0	0.0	0.0	0.0	0.0	0.0	0.0	51.3	49.8	46.9	42.5	49.1	46.5	52.1	42.9	51.9	37.8	46.8	39.2	

CHAPTER 3: FUTURE DIRECTIONS

Our lab's experiments and other recent studies employing knockdown and knockout models have explored whether the TET enzymes may play a role in the two waves of DNA methylation that occur during development. These studies demonstrated that lack of TET1 led to aberrant levels of DNA methylation at ICRs, abnormal total expression of imprinted genes, and loss of imprinting (Dawlaty et al., 2013; SanMiguel et al., 2018; Yamaguchi et al., 2013). However, *Tet1* and *Tet2* are both expressed in PGCs. While evidence from our sperm DNA methylation studies (see Chapter 2) indicates TET2 is not contributing to the normal DNA demethylation in PGCs, without dissecting 5hmC from 5mC profiles, we cannot definitively rule out contributions from TET2 during PGC reprogramming. Additionally, it remains unclear how TET1 is recruited to chromatin during PGC demethylation. Given the importance on monoallelic imprinted gene expression to healthy mammalian development, it is critical to understand what factors regulate TET1 binding and thus affect ICR demethylation. Moreover, understanding the role of TET1 in this important developmental process may lead to further insight into human imprinting disease etiologies.

3.1 Parse the requirements of individual TET proteins for ICR demethylation during PGC reprogramming in mice.

Tet1 homozygous null sperm and oocytes show defects in erasing DNA methylation at ICRs. This hypermethylation phenotype was not significantly worse in *Tet1*; *Tet2* double knockout sperm. However, this methylation was assayed by bisulfite treatment followed by pyrosequencing, and this method cannot distinguish 5mC from 5hmC. Thus, the possibility still remains that despite similar total levels of modified 5mC/5hmC, the ratios may actually be different between the groups. If this were true,

this would point to a role for *Tet2* in this demethylation of ICRs as well. While seemingly not a player in PGCs due to its low to undetectable expression in PGCs, if any amount of TET3 were present, this could also potentially lead to low levels of compensation and may partially explain the variability in phenotype in some of our offspring. Indeed, despite undetectable levels of TET3 in ESCs, another cell type with TET expression similar to PGCs, in *Tet1; Tet2* DKO, 2% of 5hmC remained as assayed by mass spec. Only when all three family members were deleted did the 5hmC levels drop to 0% (Lu et al., 2014). Therefore, deleting *Tet3* after its described role in the early embryo may also be worth examining.

Previously, levels of 5hmC in WT PGCs were measured using Glu-qPCR and showed 5hmC accumulation at four ICRs during demethylation. However, this technique relies on a single CCGG site within a locus and these experiments did not address how 5hmC accumulation changes in the *in vivo* context of *Tet* deletions in mice (Hajkova et al., 2010). Additionally, 5mC was analyzed in *Tet3; TNAP-cre* sperm and oocytes using *TaqI* or *BstUI* digestion and showed normal WT levels of 5mC. However, these analyses again depend on only one TCGA site, and the number of biological replicates appears to be n=1 (Gu et al., 2011). Therefore, to determine the precise roles of each TET family member, it will be crucial to examine 5hmC and 5mC levels in the context of different *Tet* deletions. Additionally, profiling 5hmC during different time points in PGCs as they demethylate will address whether hypermethylation at ICRs is a direct effect of losing of TET1. Given the low numbers of PGCs, this analysis has until now been difficult. However, the development of a new, bisulfite-free method of marking 5hmC in genomic DNA, called Apobec-coupled epigenetic sequencing (ACE-seq), is highly amenable to low input, long reads, and can be analyzed by any sequencing method, including whole genome sequencing or pyrosequencing (Schutsky et al., under review and personal

communication). To address these questions, we would profile 5hmC using ACE-seq in both WT and TET1 KO PGCs from E10.5- E13.5. To accomplish this goal, the *Tet1* allele has been crossed into a *Oct4-eGFP* reporter line that drives GFP expression specifically in germ cells starting at E9.5 (Fig 3.1) (Hargan-Calvopina et al., 2016; Lengner et al., 2007). My current efforts have involved collecting gonads at E13.5 and E12.5. We have successfully dissociated the gonads and used flow cytometry to measure EGFP. The next steps will be to use fluorescence-activated cell sorting (FACS) to collect these cells for analysis (Fig 3.1). In addition to our *Tet1* KO mouse model, floxed alleles of both *Tet2* and *Tet3* exist. Thus, it would also be useful to address their contribution by using the *TNAP-Cre* line which expressed Cre recombinase as early as E9.5 in PGCs. This conditional approach would bypass the early embryo requirement for *Tet3* and would eliminate or reduce any confounding effects from reducing *Tet* expression in other cell types. Both male and female PGCs should be profiled in order to determine the effects of *Tet1* deletion on maternally methylated, and paternally methylated ICRs, respectively.

Given that no imprinting defects have been reported for *Tet2* KO mice, and our data in sperm thus far, I do not expect to see a difference in levels of 5hmC at the ICRs between the WT mouse and the *Tet1* KO mouse germ cells. However, measuring 5hmC levels in PGCs in the context of different TET deletions would conclusively determine the precise contributions of each TET protein to this process. A potential drawback with this approach would be if Cre recombination is variable between mice, particularly at the early E10.5 time point, which could potentially confound our results. An alternative would be to use a ubiquitous Cre driver to delete *Tet2* early in development, but this would preclude analysis of *Tet3* KO PGCs. Another drawback may be profiling in bulk PGCs. As the technology develops, applying single-cell ACE-seq to PGCs may help elucidate the underlying causes of stochasticity and variability in our mice.

3.2 Determine if epigenetic factors control TET1 binding at specific ICRs during demethylation.

TET1 binding sites have been defined in embryonic stem cells (ESCs), a proxy for the inner cell mass of the early embryo. However, in ESCs, TET1 is not present at ICRs as determined by ChIP-seq (Fig 3.3) (Williams et al., 2011). Despite evidence that 5hmC can accumulate at a subset of ICRs in PGCs during DNA demethylation (Hackett et al., 2013), how and when TET1 is recruited to ICRs in PGCs remains unknown.

Multiple lines of evidence suggest that histone modifications play a role in ICR methylation dynamics. For example, H3K4me3 has been shown to prevent binding of DNMT3A and its cofactor DNMT3L during DNA methylation reestablishment in germ cells, but when H3K4 is unmethylated, DNMTs can bind and reestablish DNA methylation patterns (Fournier et al., 2002). Additionally, a progressive loss of H3K9me2/3 occurs concurrently with the DNA demethylation wave in PGCs, while concomitant accumulation of H3K27me3 also occurs (Hajkova et al., 2008; Seki et al., 2005). Strong evidence suggests that H3K9me2/3 may play a potential role in TET1 demethylation at ICRs; firstly, both of these marks are enriched on the methylated ICR and are associated with heterochromatin (Bannister et al., 2001; Delaval et al., 2007; Fournier et al., 2002; Henckel et al., 2009; Lachner et al., 2001). In addition, deletion of the enzymes responsible for establishing these marks resulted in altered DNA methylation at imprinted genes (Dong et al., 2008; Leung et al., 2014; Tachibana et al., 2008; Xin et al., 2003). DPPA3 binds to H3K9me2 in zygotes and this binding helps protect ICRs from erasure during the first wave of demethylation. Lastly, in ESCs, the histone methyltransferases G9a and GLP are required for recruitment of DNMTs to imprinted loci, and this recruitment antagonizes TET activity at these loci (Zhang et al.,

2016a). Taken together, I hypothesize that particular chromatin environments are permissive or repressive to TET1 interactions and this is what controls the timing of TET1 binding and demethylation of ICRs in PGCs.

Our *Tet1* KO sperm data demonstrates that TET1 is required at both an early- and a late-DNA demethylating ICR (*KvDMR* and *Peg3* ICR, respectively (Hackett et al., 2013))(SanMiguel et al., 2018). Because both of these loci depend on TET1 for demethylation, but are demethylated asynchronously, these ICRs are likely to have differences in chromatin states during DNA demethylation in PGCs. As such, these ICRs can be used as model loci to determine how histone modification enrichment, specifically, H3K9me2/3 marks, correlate with TET1 occupancy given the relationship of these PTMs to DNA methylation at ICRs. To specifically test a causal role for changes in these modifications, the CRISPR-Cas9 system can be used. This system allows efficient targeting of fusions to specific genomic loci using an engineered guide RNA (Dong et al., 2008; Xin et al., 2003). By targeting writers and erasers of H3K9me2/3 to *KvDMR* and *Peg3* ICR, respectively, it may be possible to determine if perturbing the chromatin environment in *in vitro* primordial germ cell-like cells (PGCLCs) alters TET1 recruitment using 5hmC as a proxy and DNA demethylation dynamics using bisulfite sequencing. These experiments will test the hypothesis that TET1 is recruited or blocked from binding to specific sites in PGCs depending on H3K9me2/3 presence or absence and will be an important step in understanding how demethylation is regulated.

To isolate PGCs for this analysis, the *Pou5f1*-EGFP reporter mouse will be used as described in section 3.1. First, PGCs will be isolated by microdissecting gonadal regions of embryos at time points corresponding to early, middle, and late DNA demethylation: E10.5 (early), E11.5 (late), and E12.5 (demethylated). FACS sorting will be used to separate the EGFP⁺ PGCs from the EGFP⁻ somatic cells. The somatic cells do not express

Tet1 highly at this stage nor do they undergo demethylation at these time points (Hayashi et al., 2011). PGCs and somatic cells will be pooled respectively for downstream analyses.

In order to perturb histone modifications in a relevant cell type, PGCLCs can be used (Hayashi and Saitou, 2013; Hayashi et al., 2011). Briefly, these cells are derived from ESCs and are induced to an epiblast-like state in two days. On the second day, the cells are subsequently cultured for six days in floating conditions in GMEM with a defined cocktail of growth factors. At this time, the cells express PGC-specific genes, exhibit globally decreased H3K9me2 as shown by dot blot analysis, and have decreased DNA methylation at the early-demethylated imprinted ICR *KvDMR* (Hayashi et al., 2011). To verify that the PGCLCs recapitulate many of the epigenetic changes that occur *in vivo* and are the most relevant cell type in which to test the fusion proteins, it will be important to assay H3K9me2/3 by ChIP, and 5mC and 5hmC levels via pyrosequencing and ACE-seq in PGCs and PGCLCs in our own laboratory. It will be important to use low-cell number ChIP-qPCR (Sachs et al., 2013) for H3K9me2, H3K9me3, and TET1 if possible (see below), as well as total histone H3 (H3) and IgG control antibodies at the early-demethylating ICRs, *KvDMR* and *Igf2*, and compare them to the late-demethylating ICRs *Peg3* and *Peg10* in PGCs and somatic cells isolated directly from mice. We have also designed negative and positive control ChIP-qPCR primers for the factors of interest. For these protocols as few as 10,000 cells can be used per ChIP immunoprecipitation (Sachs et al., 2013). As uniform sonication of chromatin will be essential, up to 50,000 PGCs or somatic cells should be pooled for sonication. These pools can then be divided into aliquots for the aforementioned ChIP experiments. Replicates of the ChIP should be performed with an independent cohort of mice. PGCLCs can generate up to 10^5 to 10^6 cells (Hayashi and Saitou, 2013; Hayashi et al.,

2011), which can also be sonicated and aliquoted for ChIP experiments as described for the PGCs.

I expect H3K9me2/3 enrichment to inversely correlate with 5hmC accumulation and thus TET1 binding and demethylation timing. To specifically test whether addition or removal of these marks from ICRs alters TET1 activity at these sites and thus TET1 dependence for DNA methylation erasure, targeted epigenomic modifiers could be used. For example, fusion of the catalytic domains of the histone methyltransferases, G9A and SUV39H1 (both previously used in zinc-finger protein (Couture et al., 2007; Snowden et al., 2002) as well as the histone demethylase KDM4A (Couture et al., 2007), to the catalytically-inactive Cas9 protein (dCas9) under the control of an inducible tetracycline responsive element (TRE) promoter could be generated (Kearns et al., 2013; Ochiai et al., 2015). Multiple single guide RNAs (sgRNAs) are complementary to *KvDMR* and *Peg3* ICRs as determined by using the CRISPR design website <http://crispr.mit.edu/> which is based on the sequence specificities as determined by Hsu et al. 2013 (Hsu et al., 2013). These sgRNAs recruit the dCas9 fusion proteins to a specific genomic locus to alter the chromatin environment. The CRISPR-Cas9 approach may be the most effective epigenomic modifying system as it appears to bind DNA irrespective of its DNA methylation state. Additionally, the use of this platform allows for multiple sgRNAs to be generated in a short amount of time, as well as the ability to simultaneously co-transfect multiple guide RNAs to enhance the levels of histone modification changes across a broader region of the locus. The use of an inducible promoter will allow control of expression of the fusion proteins only when the PGCLCs have completed their differentiation so that the addition or removal of the repressive histone modifications occurs only when DNA demethylation proceeds in these cells (Bisht et al., 2017).

It will be important to test both transient transfection using Lipofectamine 2000 and lentiviral transduction of plasmids containing the dCas9- fusions, various guide RNAs and rTTA into ESCs. Pilot ESCs transfections and transductions to select which sgRNAs afford the best dCas9 recruitment and levels and timing of doxycycline induction needed. The efficiency of the CRISPR fusions can be assayed by measuring H3K9me2 and H3K9me3 by ChIP-qPCR, as well as pyrosequencing and ACE-seq. Once conditions have been optimized, ESCs can be differentiated into PGCLCs and CRISPR construct expression can be induced with doxycycline. By targeting dCas9-G9A or dCas9-SUV39H1 to the *KvDMR*, it will be possible to test if retention of one or both of these marks can prevent TET1 binding and demethylation of this ICR. Following the same cloning and cell derivation strategy, it can be determined if targeting the histone demethylase domain of the KDM4A promotes earlier TET1 binding and earlier erasure of the TET1-dependent ICR of *Peg3*. To determine if the effects of the CRISPR fusions are specific to the catalytic activity and not simply chromatin binding, a dCas9 fused to a dominant negative version of the G9A catalytic domain (Gyory et al., 2004) as well as dCas9 fused to a known point mutant which abolishes demethylation activity should be included as controls (Yamane et al., 2006).

Given the strong evidence linking DNA methylation to the repressive histone marks H3K9me2 and H3K9me3, I expect to find that these histone marks are present at ICRs, correlating with DNA methylation and with little to no overlapping enrichment of TET1 and/or 5hmC. Inversely, I expect that immediately prior to or as demethylation begins, there will be little H3K9me2/3 correlating with enrichment of TET1. As such, I would expect that targeting G9A (H3K9me2 writer) or SUV39H1 (H3K9me3 writer) to early demethylating ICRs in PGCLCs would prevent TET1 binding and thus prevent the ICR from becoming demethylated. Consistently, I would expect that targeting the eraser

of H3K9me2/3 to lead to the late-demethylating ICRs will promote earlier TET1 binding and DNA demethylation (Fig 3.4). These results would support the hypothesis that the local chromatin environment can prevent or facilitate TET1 binding, thus influencing DNA demethylation dynamics. These results would be consistent with the roles of histone modifications affecting other DNA methylation modifiers, such as the protective state of DPPA3 bound to H3K9me2, which protects ICRs during zygotic reprogramming following fertilization, as well as H3K4me3 which prevents the *de novo* DNA methyltransferase DNMT3A and its cofactor DNMT3L from reestablishing DNA methylation patterns. I would not expect any phenotypic consequence of changing an early-demethylated ICR to a late-demethylated ICR, or vice versa, other than the molecular phenotype in the *in vitro* system. This is because timing of erasure may be due to the underlying chromatin environment and/or accessibility of the locus. Therefore, if erasure is still complete at the proper developmental stage, the ICRs can then be properly methylated during subsequent germ cell development with appropriate timing. *In vivo*, chronic expression of the dCas9-G9A fusion could prevent ICRs from demethylating in the appropriate developmental window, and this could lead to abnormal expression of imprinted genes similar to the expected molecular phenotypes of the *Tet1* KO mice.

Reports have demonstrated that TET1 binding does not necessarily correlate with 5hmC enrichment in the genome (Zhang et al., 2016b). Thus, assaying 5hmC serves not only as a proxy for TET1 binding, but as a direct indicator of TET1 activity. However, it could also be possible that TET2 is compensating at ICRs. Thus, it may be necessary to study TET1 activity in the absence of TET2. The most straightforward way to do this would be to use the mice with a *Tet2* floxed allele and/or PGCLCs derived from ESCs null for *Tet2*. It is possible that there will not be any correlation with early erasure, TET1

binding, and lack of H3K9me2/3, or that different histone modifications are permissive/repressive to TET1 binding. If so, an unbiased approach using mass spectrometry could be used to determine histone modifications enriched in a TET1 pull-down using chromatin from FACS-sorted PGCs. Using histone modifications present in PGCs, but depleted from a TET1 pull-down, would generate a list of candidate histone marks to test. Additionally, recombinant TET1 could be used in conjunction with the MODified histone peptide array from Active Motif, which could also narrow down the list of modifications including combinatorial modifications that are permissive to TET1, leaving the rest as candidates that may repress TET1 binding *in vivo*. Additionally, TET1 might not bind directly to modifications but to a protective protein that does bind, such as DPPA3. Thus, assessing DPPA3 binding by ChIP-qPCR may also yield insights to how chromatin affects TET1 recruitment.

4.3 TET1 and Human Imprinting Disorders

Given the findings that mice with *Tet1* mutations are viable and fertile, yet have abnormal germ cells and thus transmit imprinting defects to F1 offspring, the hypothesis arises that *TET1* may play a similar role in the etiology of human imprinting disorders. While deleterious *TET1* mutations have been described in the context of somatic mutations in cancer (Li et al., 2016) and annotated in very rare instances in reference human populations (1000 Genomes project, the Exome Aggregation Consortium [ExAC, <http://exac.broadinstitute.org>], the Trans-Omics for Precision Medicine [TOPMed] Program [<https://www.nhlbi.nih.gov/science/trans-omics-precision-medicine-topmed-program>], and the Exome Sequencing Project [ESP, <http://evs.gs.washington.edu/EVS/>]), to date, no mutations in *TET1* have been reported to affect imprinted gene expression in humans (see Table 3.1). If this hypothesis were true, we would expect the following criteria in patients. First, because TET1 is

responsible for the erasure of DNA methylation during primordial germ cell reprogramming, the hypothetical patient's imprinting abnormality would be expected to be hypermethylation. Secondly, this hypermethylation would be expected to affect only maternal or paternal ICRs. Only in the case that both parents were homozygous for *TET1* mutations, or if one allele was mutated and the other allele was encompassed by a larger deletion, would we expect to see hypermethylation at both maternal and paternal ICRs. While this scenario seems unlikely, we cannot rule out this possibility. Thirdly, the patient would not be mosaic for the defect as this would indicate a problem post-fertilization, as opposed to the germline. Fourthly, the defect would not be explained by an underlying uniparental disomy (UPD) or a copy number variation at the ICR. Lastly, it is possible that patients could have a single hypermethylated locus but could also show abnormalities at more than one loci, such as has been reported in multi locus imprinting disorders (MLID). However, while most MLID cases consist of epimutations, they tend to fall under the category of loss of methylation and additionally tend to be mosaic (Mackay and Temple, 2017).

To explore the hypothesis that *TET1* plays a similar role in the etiology of human imprinting disorders as we have shown in mice, I searched through the available literature to determine if there are any patients that would satisfy the criteria outlined above. Surprisingly, most imprinting disorders are explained by copy number variation or uniparental disomy. Of those that are not explained by a deletion, duplication, or UPD and are purely “epimutations” at an ICR, most cases are reported to be loss of methylation as opposed to gain of methylation at ICRs (Court et al., 2013). Despite this, there are indeed reports, albeit rare, of hypermethylation epimutations including 5-10% of Beckwith–Wiedemann syndrome (BWS) with hypermethylation of H19, <1% of hypermethylation in Prader-Willi syndrome (PWS), and <5% “epimutations” for

Angelman syndrome (AS)(Elhamamsy, 2017; Mackay and Temple, 2017). Given these numbers, I looked in the primary literature to find examples of patients that supported our hypothesis.

In a cohort of 79 patients with growth restriction, four patients presented with hypermethylation at the *IGF2R* ICR with no concurrent methylation changes at IC1 (Turner et al., 2010). While *IGF2R* only exhibits imprinted expression in human fetal tissue and some Wilms' tumors (Yotova et al., 2008), the hypermethylation of the ICR and growth restricted phenotype of these patients would be consistent with overexpression of *IGF2R* during development and possibly affecting postnatal growth as a result. Further studies of these patients and their circulating levels of *IGF2* as well as levels of *IGF2R* are warranted (Turner et al., 2010). Additionally, in a cohort of 51 patients with PWS and 85 patients with AS, 19 PWS patients presented with hypermethylation of the PWS-IC, the imprinting control region at the *SNRPN* locus in humans (Ohta et al., 1999), with no underlying IC mutation. Intriguingly, microsatellite analysis determined that all 19 of the abnormally methylated paternal alleles were inherited from the grandmother, indicating a failure to erase in the paternal germline. These authors calculated that given the 1% occurrence of epimutations in PWS cases, which occur in 1 in 15,000 births, the likelihood of a sperm carrying an abnormally hypermethylated imprint at the PWS locus is 1 in 1,500,000 sperm (Buiting et al., 2003). Regardless of the rarity, these patients align with our hypothesis that abnormalities of this nature could be due to mutations or changes in expression or activity of *TET1* in the germline. In contrast, the AS patients with epimutations not explained by underlying deletions showed mosaicism as well as equal inheritance of the abnormal allele from their grandmothers and grandfathers, indicating that *TET1* was unlikely to underlie the etiologies of these AS patients. Two independent studies found four, and four out of 56

BWS patients, respectively, with hypermethylation at IC1 but no changes in *KvDMR* methylation (Blik et al., 2001; Smilinich et al., 1999). Therefore, there are clinical that support the hypothesis that *TET1* could be affecting a small but detectable proportion of imprinting disorder patients.

Why have *TET1* mutations not been reported in patients with imprinting disorders? This may be due the order and types of testing that are currently used in the clinical setting. For example, first pass molecular diagnoses are usually methylation studies of a single imprinted locus in question (Grafodatskaya et al., 2017). If further tests are required, they often are still single locus or single chromosome specific, involving FISH to look for common, large deletions, other types of CNV analysis, single gene mutation analysis, or UPD analysis, which is primarily performed by using microsatellite markers across the chromosome (Brioude et al., 2018; Grafodatskaya et al., 2017; Smith and Hung, 2017; Wakeling et al., 2016). When genome-wide technologies are used, they are typically karyotypes, genome-wide methylation arrays, or SNP arrays, which can detect uniparental disomy, (Court et al., 2013; Grafodatskaya et al., 2017), all of which lack the sensitivity to detect point mutations or insertions and deletions smaller than the size of an exon (Hjelm et al., 2010). Therefore, exomes are not the diagnostic choice for imprinting disorders (van Zelst-Stams et al., 2014). In the more limited cases where exomes are applied, common filtering strategies used will only account for de novo, X-linked, or autosomal dominant or recessive inheritance patterns that do not account for imprinted inheritance. Additionally, identification of a variant can be confounded by presence of mosaicism in the parent in trio-based exome strategies (Aten et al., 2016; Bodian et al., 2014; Palomares-Bralo et al., 2017). Indeed, because *TET1* mutations would be expected to present in a homozygous state in one unaffected

parent and in the heterozygous state in the affected offspring, this alteration would likely also be filtered out and remain undetected.

Having a molecular and clinical diagnosis for imprinting disorders is important for multiple reasons. For families, determining the recurrence rate for future family planning as well as for counseling other family members is crucial. Homozygous alterations at the *TET1* locus would lead to a very high recurrence rate for future pregnancies, and while the affected child would not pose a risk of their children being affected, their grandchildren could potentially be homozygous and thus great-grandchildren would be at high risk again for having an imprinting disorder. Secondly, being able to classify patients into subgroups can help with genotype-phenotype associations. For example, certain subtypes of imprinting disorders require different management strategies, such as in the case of hypermethylation at the *H19* locus where BWS patients have a higher risk of developing tumors compared patients with other molecular causes of BWS (Grafodatskaya et al., 2017).

Given the evidence above, I recommend that in cases of imprinting disorders characterized by hypermethylation, no underlying CNV, ICR deletion, or UPD, patients should be tested for heterozygous alterations in *TET1*. If parent samples are available, they should also undergo targeted *TET1* testing. However, despite the possibility of *TET1* potentially being a contributor to human imprinting disorders, it is also possible that this is not the case. *Tet1* homozygous null mutations are well tolerated in mice, but this may not be the case in humans. Additionally, the reproductive challenges imposed by *Tet1* mutations in female mice could be equally as bad or more severe in humans. Thus, human *TET1* alterations may contribute to impaired or complete infertility in mothers as opposed to imprinting disorders in their children. Lastly, the ICRs regulated by *TET1* in humans and in mice may vary. Data from our lab and others demonstrates that in mice,

TET1 does not regulate the demethylation of *Snrpn* in the germline. However, the strongest evidence for TET1 to be playing a role is at the PWS-IC. Therefore, more work is needed, in human PGC culture models for instance, to understand the similarities and differences between mouse and human TET1 function. By exploring TET1 as a potential cause of imprinting disorders, patients and families will benefit from not only the knowledge of their mutation but the additional counseling and potential treatments that may follow in the future.

3.4 Tet1 knockout by Tet1 knockout breeding

Previous evidence suggests it is possible to generate live pups from a *Tet1*^{-/-} by *Tet1*^{-/-} cross (Dawlaty et al., 2011; Yamaguchi et al., 2012). However, it has not been ascertained whether these offspring have imprinting defects, such as DNA methylation abnormalities at ICRs or loss of imprinting. These crosses would also shed light on whether it is possible to have both hypermethylated maternal and paternal ICRs in the same animal or if no combinations are seen, which abnormal ICR combinations could produce a synthetic lethal effect. I hypothesize that the live born animals would have only one or no imprinting defects. These animals may be the ones who escaped inheriting multiple hypermethylated imprinted alleles, as we see in our *Tet1*^{-/-} maternal or paternal knockout crosses. To begin to address these questions, we mated *Tet1*^{-/-} by *Tet1*^{-/-} animals and measured both weight and litter size at birth. Controls for these crosses were *Tet1*^{-/-} sires with either *Tet1*^{+/+} females or *Tet1*^{+/-} females. Our preliminary data indicates that indeed, live embryos were generated by the *Tet1*^{-/-} by *Tet1*^{-/-} breeding scheme (Table 3.2). Comparing our pups to weight and litter data from offspring of *Tet1*^{+/+} by *Tet1*^{-/-} crosses, we see no differences in weight or litter size (Fig. 3.5). However, the sample size will need to be significantly increased in order to determine if there are any true effects. Additionally, it may be informative to look at early embryonic stages as

changes in proportions of affected animals were detected at certain loci in our maternal or paternal *Tet1*^{-/-} matings.

The next steps for this project would be to measure DNA methylation by pyrosequencing in the tissues from pups. We could quantify the presence or absence of any ICR alterations, as well as correlate hypermethylation in one locus to the other imprinted loci. Additionally, to begin to understand not only changes in DNA methylation but also imprinted gene expression, the *Tet1* mice should be crossed into the C7 background for multiple generations. Thus, the F1 hybrid offspring would now have allele-specific SNPs, allowing for allele-specific expression to be determined.

Relatedly, another remaining question concerns how these imprinting abnormalities persist through generations. I hypothesize that a Het produced from a *Tet1*^{-/-} mouse mated to a WT mouse would have normal DNA methylation levels in their gametes and normal monoallelic expression of imprinted genes if they were to be mated to another Het or WT mouse. This is because the PGCs in the next generation would now have a WT copy of *Tet1* during DNA demethylation and thus the error should correct itself. The exception would be if the amount of WT TET1 is insufficient to demethylate two alleles instead of just one, in which case, this result would indicate that *Tet1* may be haploinsufficient in certain cases. This would also support data from Chapter 2 where we very rarely saw hypermethylated control offspring coming from a Het parent.

3.5 Conclusion

These proposed experiments will reveal key insights into TET1 recruitment at ICRs and how this protein promotes proper monoallelic imprinted gene expression. Additionally, my investigation through the literature reveals a rare, but possible link between TET1 abnormalities and human imprinting disorders. Overall, these studies will

shed light on proper epigenetic reprogramming as a key developmental process crucial for human health.

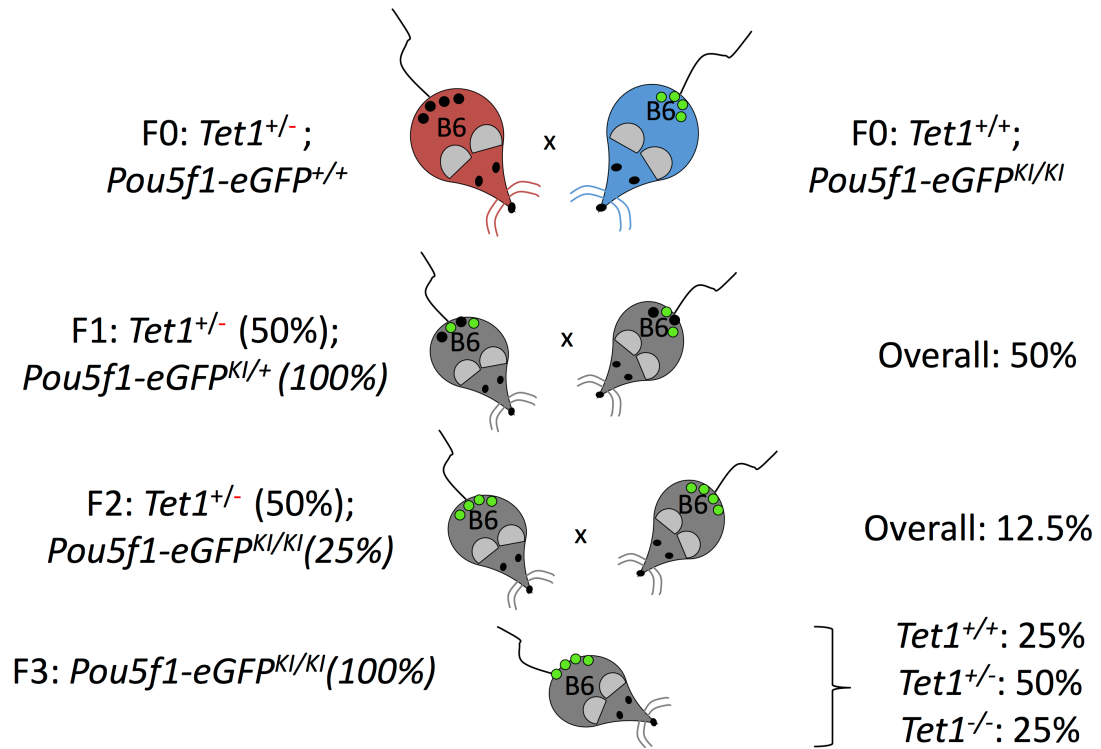


Figure 3.1. *Tet1*;*Oct4*-eGFP mouse crossing strategy. The left hand column describes the genotype of interest and the percentage of mice that will have the resultant alleles based on the cross depicted above it. The right hand column depicts the overall percentage of mice with the genotype of interest, taking into account both alleles. Green circles represent EGFP positive primordial germ cells.

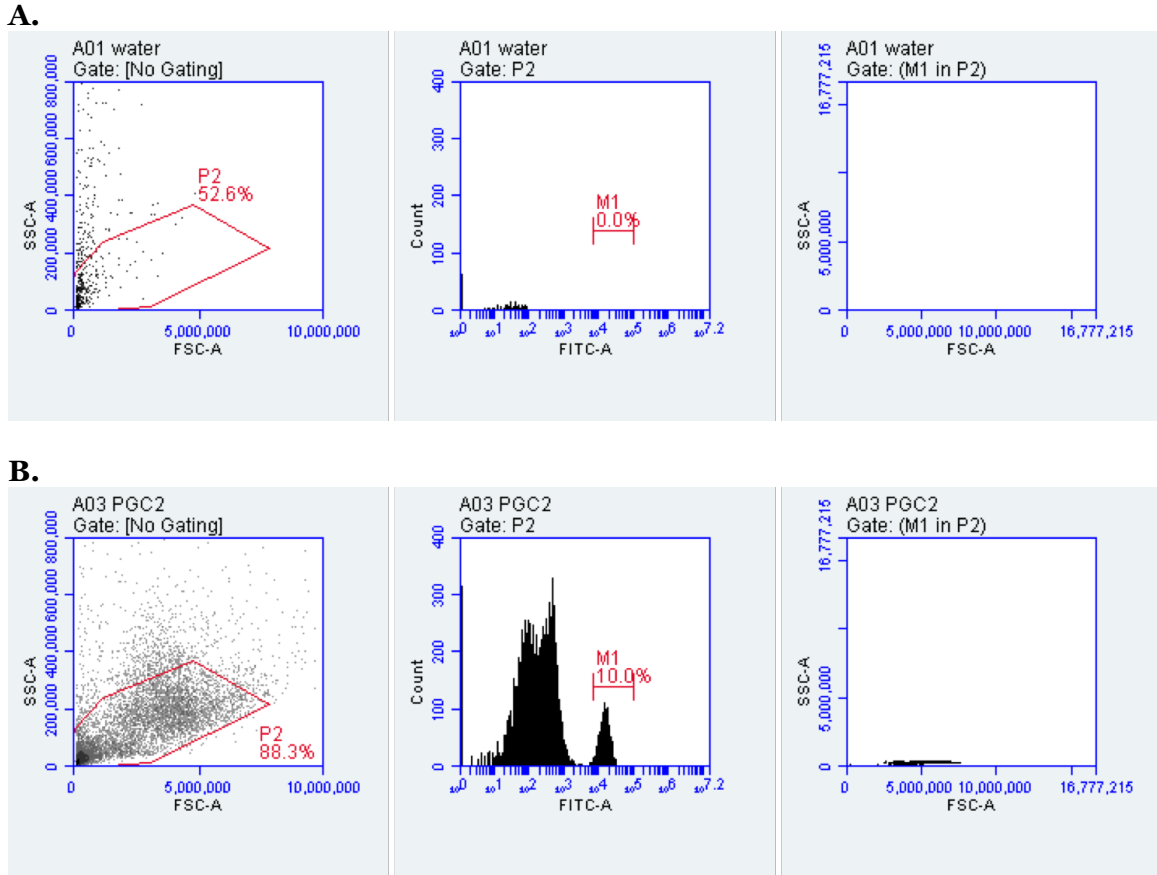


Figure 3.2. E13.5 PGC sorting using the EGFP reporter. (A) Negative control (water) plots and (B) E13.5 PGCs. First panel represents viable cells. Second panel indicates GFP signal on the x-axis and count on the y-axis. Third panel shows where M1 gated cells fall in the P2 gate in the first panel, indicating these cells are both viable and GFP⁺. GFP⁺ PGCs are the smaller peak, designated M1. 10% of the cells sorted are EGFP positive. Overall, for this particular sample, about 6,500 PGCs are EGFP positive from the two gonads from one embryo.

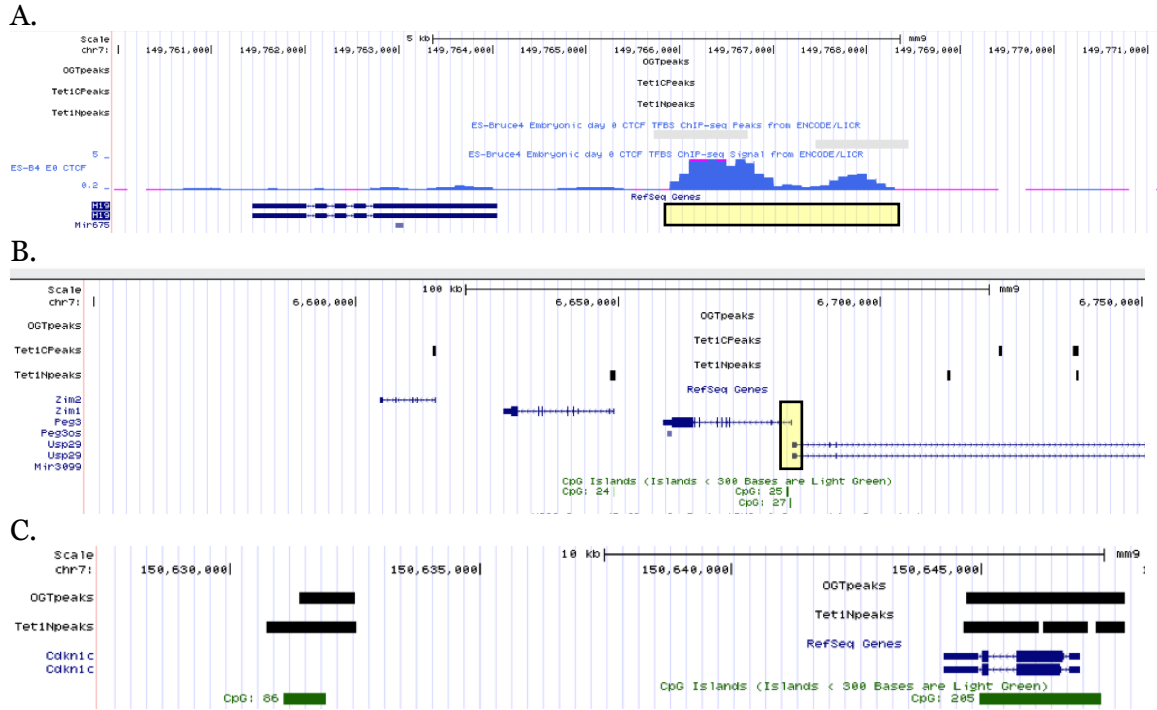


Figure 3.3. TET1 is not localized to ICRs but is localized at secondary DMRs in mouse ESCs.

(A) mm9 UCSC genome browser screen shot showing the *H19* gene, dark blue, and the corresponding intergenic ICR [highlighted in a yellow box (not to scale) and by the CTCF peaks shown in light blue]. There are no TET1 peaks in this region. (B) The *Peg3* locus with the ICR highlighted in yellow box, not to scale. TET1 peaks are visible in this screen shot (black boxes) but not at the ICR. (C) The *Cdkn1c* gene is shown in dark blue, CpG islands are shown in green, corresponding to the secondary DMR at this locus. TET1 and OGT peaks localize across the gene body and overlap annotated CpG islands in ESCs. ChIP-seq data from (Williams et al., 2011).

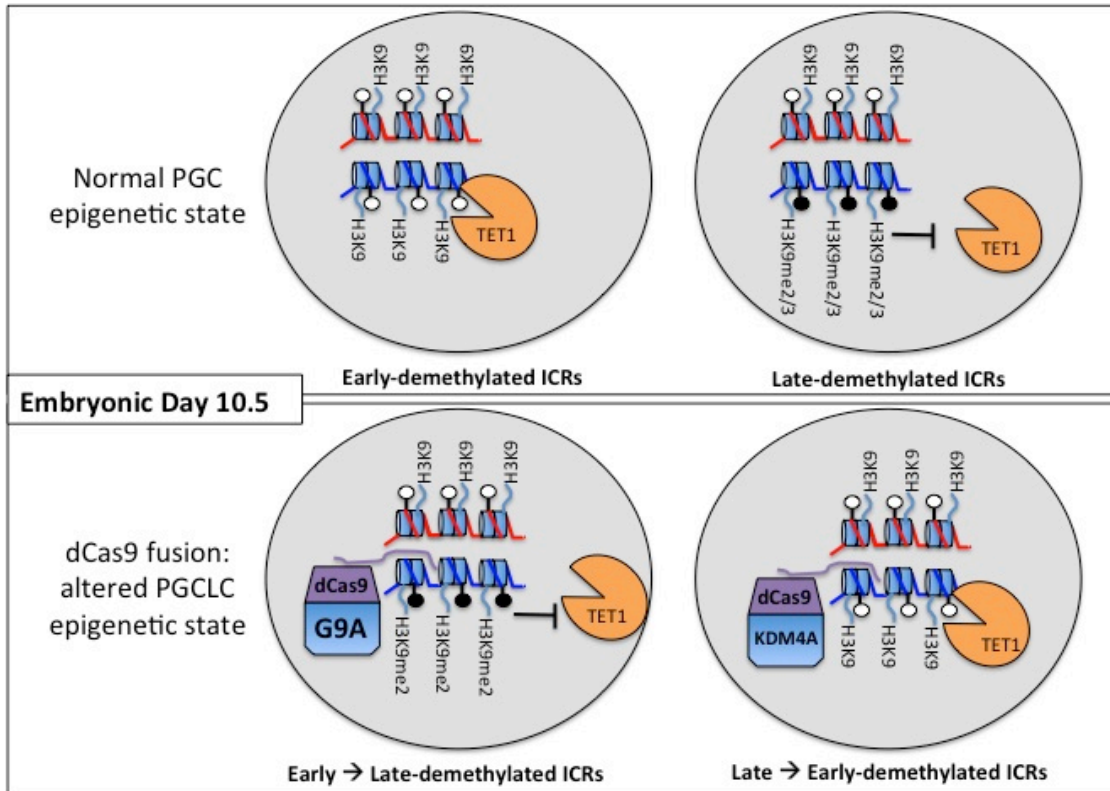


Figure 3.4. Models of how H3K9me2/3 might repress TET1, leading to early- and late-demethylated ICRs in PGCs and how perturbing these modifications using dCas9-fusions could lead to a switch in DNA methylation erasure timing in vitro PGCLCs.

Table 3.1. Potentially deleterious splice site, indel, and nonsense mutations reported for human <i>TET1</i> Gene (ENSEMBL transcript ENST00000373644.4)								
Variant ID	Chr: bp	Alleles	Global Minor Allele Frequency	Class	Evidence	Conseq. Type	AA	AA coordinates
rs903799822	10:68560748	T/C	(-)	SNP		splice region variant intron variant	-	-
rs939086876	10:68560750	G/A	(-)	SNP	-	splice region variant intron variant	-	-
rs750698861	10:68572345	C/T	(-)	SNP		stop gained	R/*	3
rs758126390	10:68572531	A/G/T	(-)	SNP		stop gained	K/*	65
rs771320434	10:68572657	C/T	(-)	SNP		stop gained	R/*	107
rs760021546	10:68573791-68573793	AAA/-	(-)	deletion		inframe deletion	K/-	485
rs528358468	10:68574012-68574014	CAC/-	(-)	deletion	-	inframe deletion	NT/N	558
rs765339037	10: between 68574051 & 68574052	-/TGGATCCCATTAAAAGTG...	(-)	insertion		frameshift variant	-/WIPLKVNK	572
rs866103110	10:68574091-68574093	AAG/-	(-)	deletion		inframe deletion	K/-	585
rs750883311	10:68574106	C/T	(-)	SNP		stop gained	R/*	590
rs903550402	10:68574234-68574236	TGT/-	(-)	deletion		inframe deletion	SV/S	632
rs183042361	10:68574255	A/G	0.000 (G)	SNP		splice region variant intron variant	-	-
rs545206990	10:68600981	G/A	0.000 (A)	SNP		missense variant splice region variant	V/I	639
rs747848417	10:68644691	T/C	(-)	SNP		splice region variant intron variant	-	-
rs34181473	10: between 68644898 & 68644899	-/G	(-)	insertion	-	frameshift variant	-/X	724
rs568996501	10:68644962	C/T	0.000 (T)	SNP		stop gained	R/*	745
rs757069841	10: between 68645222 & 68645223	-/ATTCCACA	(-)	insertion		frameshift variant	-/IPX	832
rs767271365	10: between 68645224 & 68645225	-/TTC	(-)	insertion		inframe insertion	C/CS	832
rs750350675	10: between 68645226 & 68645227	-/GCCT	(-)	insertion		frameshift variant	S/SLX	833
rs34797319	10: between 68645329 & 68645330	-/A	(-)	insertion	-	frameshift variant	P/PX	867
rs756042590	10:68645656-68645661	CCCTTT/-	(-)	deletion		inframe deletion	TLS/T	976
rs780168660	10: between 68645949 & 68645950	-/A	(-)	insertion		frameshift variant	E/EX	1074
rs1025734794	10:68646190-68646192	CAT/-	(-)	deletion		inframe deletion	PS/P	1154
rs35667415	10: between 68646206 & 68646207	-/A	(-)	insertion	-	frameshift variant	-/X	1160
rs748754173	10:68646936-68646938	TTT/-	(-)	deletion		inframe deletion	F/-	1403
rs754553353	10: between 68647012 & 68647013	-/AG	(-)	insertion		splice region variant intron variant	-	-
rs375405592	10:68647013	C/T	(-)	SNP		splice region variant intron variant	-	-
rs868611128	10:68651848	C/T	(-)	SNP	-	stop gained splice region variant	R/*	1427

- Frequency: The variant is reported to be polymorphic in at least one sample.
- ExAC: The variant was discovered in the Exome Aggregation Consortium
- ESP: The variant was discovered in the Exome Sequencing Project
- 1000 Genomes: The variant was discovered in the 1000 Genomes Project
- HapMap: The variant is polymorphic in at least one HapMap panel

Variant ID	Chr: bp	Alleles	Global Minor Allele Frequency	Class	Evidence	Conseq. Type	AA	AA coordinates
rs940218648	10:68652493	A/T	(-)	SNP	-	splice region variant intron variant	-	-
rs765813946	10:68652495	A/G	(-)	SNP		splice region variant intron variant	-	-
rs936986855	10:68652498	C/T	(-)	SNP		splice region variant intron variant	-	-
rs750890650	10:68652503	A/G	(-)	SNP		missense variant splice region variant	Y/C	1457
rs759890779	10:68667259	A/G	(-)	SNP		splice region variant intron variant	-	-
rs10998381	10:68672887	T/C	0.005 (C)	SNP		splice region variant intron variant	-	-
rs567513166	10:68672890	T/C	0.000 (C)	SNP		splice region variant intron variant	-	-
rs745380607	10:68672892	C/T	(-)	SNP		splice region variant intron variant	-	-
rs772497171	10:68672894	G/T	(-)	SNP		splice acceptor variant	-	-
rs776044335	10:68672897	G/A	(-)	SNP		missense variant splice region variant	R/H	1559
rs755912455	10:68673044	A/G	(-)	SNP		missense variant splice region variant	H/R	1608
rs1029571068	10:68673052	G/T	(-)	SNP		splice region variant intron variant	-	-
rs553813491	10:68681395	A/G	(-)	SNP		splice region variant intron variant	-	-
rs764225020	10:68681400	A/-	(-)	deletion		frameshift variant splice region variant	E/X	1609
rs866146478	10:68681486	C/T	(-)	SNP	-	stop gained splice region variant	Q/*	1638
rs376596485	10:68681491	A/G	(-)	SNP		splice region variant intron variant	-	-
rs374330506	10:68681492	T/C	(-)	SNP		splice region variant intron variant	-	-
rs377688387	10:68681494	T/C	(-)	SNP		splice region variant intron variant	-	-
rs200371130	10:68682971	G/A	0.000 (A)	SNP		missense variant splice region variant	V/M	1684
rs757571644	10:68686349	C/G/T	(-)	SNP		splice region variant intron variant	-	-
rs757571644	10:68686349	C/G/T	(-)	SNP		splice region variant intron variant	-	-
rs746023944	10:68686351	A/G	(-)	SNP		splice region variant intron variant	-	-

Variant ID	Chr: bp	Alleles	Global Minor Allele Frequency	Class	Evidence	Conseq. Type	AA	AA coordinates
rs187179634	10:68686353	C/T	0.003 (T)	SNP		splice region variant	-	-
						intron variant		
rs751689739	10:68686548	C/T	(-)	SNP		stop gained	Q/*	1749
rs754533175	10:68686674-68686676	AAC/-	(-)	deletion		inframe deletion	N/-	1791
rs764213448	10:68690802	G/C	(-)	SNP		splice region variant	-	-
						intron variant		
rs747815836	10: between 68690992 & 68690993	-/AAT	(-)	insertion		inframe insertion	-/N	1864
rs368275418	10:68691476	C/T	(-)	SNP		stop gained	R/*	2025

Table 3.2. Summary of litter size and sex from KO x KO and KO x Het control crosses

Mate Pair ID	Mating Pair Genotype	Litter # 1		Litter #2	
		# of pups	Sex	# of pups	Sex
1	KO (M) x KO (F)	2	1M, 1F	1	F
2	KO (M) x KO (F)	1	1M	-	-
3	KO (M) x KO (F)	2	1M, 1M?	3	1M?, 1F, 1F?
4	KO (M) x Het (F)	3	2M, 1F	-	-

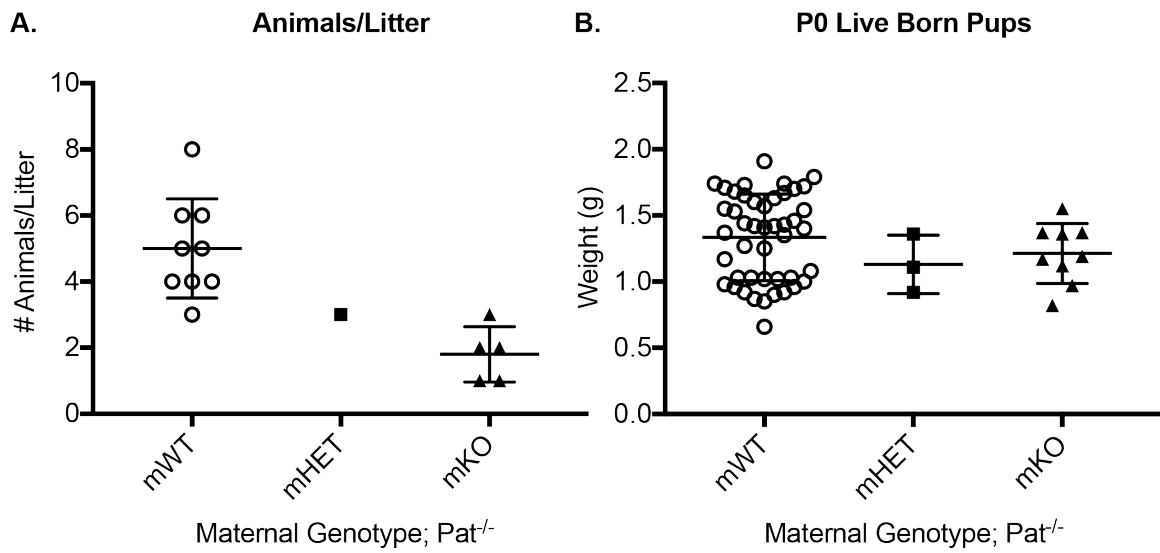


Figure 3.5. Preliminary data regarding differences in (A) litter size or (B) weight (g) of KO x KO pups. No statistical differences are detected by One-way ANOVA analyses. mWT data from the *Tet1*^{+/+} (C7) x *Tet1*^{-/-} (B6) crosses described in chapter two for comparison, whereas all other data is B6 x B6.

CHAPTER 4: MATERIALS AND METHODS

4.1 Animals

Tet1 mice were purchased from The Jackson Laboratory (Dawlaty et al., 2011: B6;129S4-*Tet1*^{tm1.1Jae/J}, Stock No: 017358). Mice were backcrossed at least 4 generations to C57BL/6J (Stock No: 000664) before analysis with the exception of sperm samples. *Tet1/2* double knockouts have the same allele as the *Tet1* single knockouts and the *Tet2* allele was originally generated by Li et al., 2011. *Tet1* knockout mice were generated by heterozygous mating or by mating *Tet1* heterozygotes on a *Oct4-GFP* heterozygous background (Lengner et al., 2007, B6;129S4-*Pou5f1*^{tm2Jae/J}, Stock No. 008214). *Tet1* animals were genotyped by lysing ear punches in fast lysis buffer A (25 mM NaOH, 0.2 mM EDTA, pH 8.0) at 95°C for one hour and subsequently adding an equal volume of fast lysis buffer B (40 mM Tris HCl). 2 µL of genomic DNA was used for genotyping PCR reactions. CAST7 mice are maintained in our mouse colony. Timed mating was determined by checking for a vaginal sperm plug. 12 PM (noon) was taken to be E0.5 on the day the plug was observed. Embryos were also visually staged upon dissection. All studies were performed in accordance with procedures approved by the University of Pennsylvania's Institutional Animal Care and Use Committee.

4.2 Germ Cell Collection

4.2.1 Oocytes

Pools of 20-100 germinal vesicle-stage oocytes were collected from the ovaries of one 26-28 day-old mouse. Cumulus cells were removed from oocytes by mouth pipetting and transferring into clean drops of M2 medium (Sigma-Aldrich, catalog number: M7167) supplemented with a final concentration of 2.5 µM milrinone. When necessary, oocytes were briefly incubated in a drop of M2 media containing a final concentration of

0.3 mg/mL of hyaluronidase to remove cumulus cells. Oocytes were snap frozen in liquid nitrogen.

4.2.2 Sperm

Adult male mice (> 8 weeks of age) were mated with a female for at least two days and then isolated for at least two days. After sacrifice, the epididymis was dissected. Epididymal sperm was collected on a needle and then incubated in room temperature PBS. Motile sperm were collected by removing the supernatant. Sperm were counted on a hemocytometer and then pelleted. The PBS was removed from the sperm pellet and was snap frozen in liquid nitrogen.

4.2.3 PGCs

E13.5 or E12.5 concepti were removed from the uterine horn and from the amniotic sac. The placenta was separated and each embryo was placed in ice cold PBS in individual wells of a 12 well plate. Gonads were isolated and moved to 1.5 mL eppendorf tubes on ice. When all gonads were collected, they were gently spun down and the remaining PBS was removed. 1 mL of 0.05 % Trypsin/EDTA was added to the gonads and incubated at 37 degrees either rotating in the hybridization oven or shaking in the 37 degree water bath. After incubation, the gonads were further dissociated by using a 1 mL syringe with an 18-gauge needle (5 times up and down) followed by a 23 gauge needle (5 times up and down). The reaction was then quenched with 0.5 mL of HBSS with 1% BSA. The tubes were spun down for 10 minutes at 4 degrees C, followed by another wash in the same solution, and finally, suspended in 0.5 mL of the HBSS with 1% BSA. Immediately before flow cytometry, the cell suspension went through five more times through a 23-gauge needle. Cell counts were additionally conducted independently of the flow cytometer using a hemocytometer at 10X magnification. Concurrent genotyping took place using embryonic tail or limb.

4.3 Tissue Homogenization

Embryonic tissue samples were homogenized in tail lysis buffer (50 mM Tris-HCl, pH 8, 0.5% SDS, 100 mM EDTA, pH 8) with a needle and syringe. Po newborn brain and tongue were homogenized in tail lysis buffer with a polytron (Kinematica, Model PT 10-35 GT). Po newborn livers were divided upon dissection and one half was homogenized with a needle and syringe directly in TRIzol Reagent, and the other half was homogenized in tail lysis buffer using the polytron and subsequently processed for DNA.

4.4 RNA and cDNA conversion

Tissue lysate was added to TRIzol reagent (Thermo Fisher Scientific, Cat # 15596026) and mixed thoroughly. TRIzol extraction was performed as specified in the manufacturer's protocol. RNA quantity was determined by nanodrop (ND-1000 Spectrophotometer) and RNA quality was assessed by running 500 ng on an agarose gel and confirming intact rRNA bands at the expected intensity ratio. Only samples with intact RNA were used for further analysis. 500-1000 ng of total RNA was treated with 1.5 μ L of RQ1 RNase-free DNase (Promega Cat # M6106) for 30 minutes at 37°C followed by addition of 1.5 μ L of Stop Solution and incubated for 10 minutes at 65°C. Two-thirds of the treated RNA was put into a 20 μ L cDNA conversion using SuperScript III Reverse Transcriptase (RT) (Thermo Fisher Scientific, Catalog number: 18080093) and random primers (Sigma-Aldrich, catalog number 11034731001). The remaining one-third of the treated RNA was used in a negative RT reaction.

4.5 qPCR Analysis

A cDNA dilution series was used to make a standard curve from which qPCR primer amplification efficiencies were determined using Power SYBR Green Master Mix

(ThermoFisher Scientific, catalog number 4368577). For primers and cycling conditions, see Tables S8,S9. cDNA was diluted to a final amount of 5 ng/well for total expression analysis. Samples were run in triplicate on a 7900 Fast Real-Time PCR System (Applied Biosystems) with non-template controls for each gene. Melt-curve analysis was performed to ensure specific amplification. For quality control, any individual Ct value within a triplicate that was > 0.5 Ct from the other two was removed. Data was normalized to the geometric mean of three housekeeping genes: *Rplp0*, *Nono*, and *Rpl13a*. The control animals were averaged and graphed with the individual *Tet1* mutant animals per qPCR plate.

4.6 Allele-Specific Expression Analysis

10 ng of cDNA were used per PCR reaction. For primers and PCR conditions, see Tables S8,S9. Linear range of amplification was determined for each tissue and developmental stage. Each assay used a different restriction enzyme: *H19*: *Cac8I* 37°C for 3 hours, heat-inactivated at 65°C for 20 minutes (NEB, Cat. No. R0579S); *Igf2*: *MluCI*, 37°C for 3 hours, no heat-inactivation (NEB, Cat. No. R0538S); *Peg3*: *MnlI* 37°C for 3 hours, heat-inactivated at 65°C for 20 minutes (NEB, Cat. No. R0163S); *Cdkn1c*: *Taq^{AI}* 65°C for 1 hour, heat-inactivated for 20 minutes at 80°C (NEB, Cat. No. R0149S); *Kcnq1ot1*: *StuI* 37°C for 3 hours, no heat-inactivation (NEB, Cat. No. R0187S). Digests were performed using the supplied buffer and 3-8 µL of PCR in a 20 µL reaction volume. Digests were run on 7% or 12% polyacrylamide gels. Band densitometry was analyzed using ImageJ software. Complete digestion was assessed by running pure parental strain cDNA PCR product digests as controls. *Snrpn* allele-specific analysis was performed using the LightCycler Real-Time PCR system (Roche) as described in Mann et al., 2004 with the following modifications: illustra PuReTaq Ready-To-Go PCR Beads were used

(GE healthcare, catalog number 27-9559-01) and hybridization probes were purchased from IDT.

4.7 DNA extraction

Tissue lysate was incubated overnight with Proteinase K (Sigma-Aldrich, P2308) at a final specific activity of 180 U/mL at 37°C. Sperm pellets were resuspended in sperm lysis buffer (20 mM Tris-HCl, pH 8, 200 mM NaCl, 20 mM EDTA, 4% SDS) with the addition of 5 μ L β -mercaptoethanol and Proteinase K at a final specific activity of 180 U/mL at 55°C overnight. DNA was subsequently phenol-chloroform extracted, followed by ethanol precipitation and resuspended in dH₂O or TE (10 mM Tris-HCL pH 8, 0.5 mM EDTA) buffer.

4.8 Bisulfite Treatment

1000 ng of sperm and mouse tissue DNA was bisulfite treated using the EpiTect Bisulfite Kit (Qiagen Cat No./ID: 59104) and eluted in 20 μ L of the supplied EB buffer. Oocyte pools were directly lysed using the LyseAll Lysis Kit (Qiagen) and bisulfite converted using the EpiTect Plus Bisulfite Kit (Qiagen, Cat No./ID: 59124). Oocyte bisulfite-treated DNA was resuspended in 13 μ L of the supplied EB buffer.

4.9 Pyrosequencing

Pyrosequencing PCRs and sequencing reactions were carried out as described in de Waal et al., 2014. For primers and PCR conditions, see Tables S8,S9. Briefly, 1-2 μ L of bisulfite treated DNA was used to set up pyrosequencing PCRs using the PyroMark PCR kit (Qiagen, Cat. No. 978703) using locus-specific primers. 2-4 μ L of PCR was used in each pyrosequencing reaction and sequenced on the Q96 machine. Pyrosequencing peaks were manually inspected for sequencing errors and matching to the reference expected peaks. CpGs that did not pass these quality control criteria were excluded from

the final analysis. Oocyte methylation data was further subjected to the following criteria to ensure there was no somatic cell contamination: For any given sample, two maternally methylated ICRs had to have an average % methylation $\geq 90\%$ and must have amplified at least *H19/Igf2* or *IG-DMR*. Samples that did not meet these criteria were excluded from the final analysis (Table S1).

4.10 Bisulfite, Clone, and Sequencing Analysis

Nested PCR reactions were performed using bisulfite-treated DNA (Tables S8,S9) as previously described (Market-Velker et al., 2010) with the following exceptions: illustra PuReTaq Ready-To-Go PCR Beads were used (GE healthcare, catalog number 27-9559-01). 1 μ L of bisulfite DNA was used for the first round of PCR, while 4 μ L of first round PCR seeded the second round PCR reaction. Two independent PCR reactions were set up for both first and second round PCRs. Second round PCR products were cloned using StrataClone PCR Cloning Kit (Agilent). At least 20 colonies per plate were picked and analyzed for the insert using EcoRI digestion. Clones containing the correct size insert were submitted for Sanger Sequencing analysis at the University of Pennsylvania DNA sequencing facility. Sequences were analyzed using the QUMA website (Kumaki et al., 2008, quma.cdb.riken.jp/).

4.11 Statistics

All analyses were completed using the Graphpad PRISM software with the following exceptions: Variance ($\sigma^2 = [\sum(x_i - \bar{x})^2]/[n-1]$) was calculated in Microsoft Excel using the VAR.S function, and the Fligner-Killeen Test of Homogeneity of Variances was calculated in R. Chi-square and Fisher's exact test were calculated on the Graphpad website (<https://graphpad.com/quickcalcs/chisquared1.cfm>, <https://graphpad.com/quickcalcs/contingency1.cfm>). Sample size was determined by

conducting smaller pilot studies. The investigators were not blinded to the identity of the samples during analysis.

Table 4.1: List of primers used for each assay in this study.				
Gene/Region	Primer	Primer Sequence	Assay	References
<i>Tet1</i>	13037	TCAGGGAGCTCATGGAGACTA	<i>Tet1</i> Genotyping	The Jackson Laboratory (https://www2.jax.org/protocols/dsbf?m=116.5.0-NO.5-P5-M. ASTER_PROTOCOL_ID_P5_JRS_CODE.25442.017358)
<i>Tet1</i>	13038	TTAAAGCATGGGGGGAGTC	<i>Tet1</i> Genotyping	
<i>Tet1</i>	13039	AACGATTCCTCGTGACAG	<i>Tet1</i> Genotyping	
<i>Kdm5c/Kdm5d</i>	<i>Smc1</i>	TGAAGCTTTTGGCTTTGAG	Sex Genotyping	(Jay and Claudio, 2013)
<i>Kdm5c/Kdm5d</i>	<i>Smc2</i>	CCACTGCCAAATCTTTGG	Sex Genotyping	
<i>H19</i>	<i>H19 F</i>	GTCTCGAAGAGCTCGACTG	qPCR	(Thorvaldsen et al., 2006)
<i>H19</i>	<i>H19 R</i>	ACTGGCAGGCACATCCAC	qPCR	
<i>Igf2</i>	<i>Igf2 F</i>	CGCTTCAGTTGTCTGTCG	qPCR	
<i>Igf2</i>	<i>Igf2 R</i>	GCAGCACTCTCCACGATG	qPCR	
<i>Meg3/Gli2</i>	<i>Meg3 F</i>	TTGCTGTGTGCTCAGGTC	qPCR	(Lin et al., 2011)
<i>Meg3/Gli2</i>	<i>Meg3 R</i>	ATCCTGGGTCTCAGCTCT	qPCR	
<i>Dlk1</i>	<i>Dlk1 F</i>	CGGGAATTCGCGAAATAG	qPCR	
<i>Dlk1</i>	<i>Dlk1 R</i>	TGTCAGGAGCATTCCTACT	qPCR	
<i>Rplp0</i>	<i>Arpo F</i>	TCCCACTTACTGAAAGGTCAGG	qPCR	
<i>Rplp0</i>	<i>Arpo R</i>	TCCGACTCTTCCTTTGCTTC	qPCR	
<i>Rpl13a</i>	<i>Rpl13a F</i>	ATCCCTCCACCCTATGACAA	qPCR	(Bouqault et al., 2008)
<i>Rpl13a</i>	<i>Rpl13a R</i>	GCCCCAGGTAAGCAAACTT	qPCR	
<i>Nano</i>	<i>Nano F</i>	GCTCGTGAAGCTGGAGAT	qPCR	(Plasschaert and Bartolomei, 2015)
<i>Nano</i>	<i>Nano R</i>	TTCTTGACCTCTCATAAATCC	qPCR	
<i>H19</i>	HE2 (F)	TGATGGAGAGGACAGAGGG	Allele-Specific Expression	(Thorvaldsen et al., 2006)
<i>H19</i>	HE4 (R)	TTGATTGAGAAGGACAGGAC	Allele-Specific Expression	
<i>Igf2</i>	<i>Igf2-18</i>	ATCTGTGACCTCTCTGACAGG	Allele-Specific Expression	(Fortier et al., 2008)
<i>Igf2</i>	<i>Igf2-20</i>	GGGTTGTTAGAGCCAATCAA	Allele-Specific Expression	
<i>Cdkn1c</i>	p57-L	GCCAAATGGCAAGCGTGGC	Allele-Specific Expression	(Weaver et al., 2010)
<i>Cdkn1c</i>	p57-4	TACACTGGGACAGCGTACTCC	Allele-Specific Expression	
<i>Peg3</i>	PG4	ATGCCACTCCCTCAGCG	Allele-Specific Expression	(Bhatnagar et al., 2014)
<i>Peg3</i>	PG7	GCTCATCTCTGGAAGTTTG	Allele-Specific Expression	
<i>Kcnq1ot1</i>	LI1 F	ATTGGGAAGCTGGGGTGGAGCC	Allele-Specific Expression	(Rivera et al., 2008)
<i>Kcnq1ot1</i>	LI1 R	GGCACACGGTATGAGAAAAGATTG	Allele-Specific Expression	
<i>Snrpn</i>	Sn1 (F)	CTCCACAGGAATTAGAGCC	Allele-Specific Expression (Light Cyler)	(Szabo and Mann, 1995)
<i>Snrpn</i>	Sn3 (R)	GCAGTAAGAGGGTCAAAAGC	Allele-Specific Expression (Light Cyler)	
<i>Snrpn</i>	SnMut (Snrpn sensor probe)	GAAGCAATTGAGGGAGAGAA-fluorescein	Allele-Specific Expression (Light Cyler Probe)	
<i>Snrpn</i>	SnAnc (Snrpn anchor probe)	LC-Red640-GGCTGAGATTATCAACTGTATCTTAGGGTC-P	Allele-Specific Expression (Light Cyler Probe)	
<i>H19/Igf2</i> ICR	<i>H19/Igf2</i> ICR F	GGTAGATATATGTATTTTGGGTTG	Pyrosequencing PCR	(de Waal et al., 2014)
<i>H19/Igf2</i> ICR	<i>H19/Igf2</i> ICR R-biotinylated	CTCATAAAACCACTAATAAATCAT	Pyrosequencing PCR	
<i>H19/Igf2</i> ICR	<i>H19/Igf2</i> ICR Sequencing	TGTAAGATTAGGGTTGT	Pyrosequencing Sequencing Primer	
<i>IG-DMR</i>	<i>IG-DMR</i> F	GTGGTTTGTATGGTAAAGTTT	Pyrosequencing PCR	
<i>IG-DMR</i>	<i>IG-DMR</i> R-biotinylated	CCCTCCCTCACTCCAAAATTTAA	Pyrosequencing PCR	
<i>IG-DMR</i>	<i>IG-DMR</i> sequencing	GTTATGGATTGGTGTAAAG	Pyrosequencing Sequencing Primer	
<i>Snrpn</i> ICR	<i>Snrpn</i> F	GGTAGTTGTTTTTTGGTAGGATAT	Pyrosequencing PCR	
<i>Snrpn</i> ICR	<i>Snrpn</i> R-biotinylated	ACTAAAATCCCAAAACCACTAACCT	Pyrosequencing PCR	
<i>Snrpn</i> ICR	<i>Snrpn</i> Sequencing	GTGTAGTTATGTTTTGGGA	Pyrosequencing Sequencing Primer	
<i>Peg3</i> ICR	<i>Peg3</i> F	GGTTTTAAGGGTAATTGATAAGG	Pyrosequencing PCR	
<i>Peg3</i> ICR	<i>Peg3</i> R-biotinylated	CCCTACACCTAAATAACATCCC	Pyrosequencing PCR	
<i>Peg3</i> ICR	<i>Peg3</i> Sequencing	AAATGATAAGGTTGATGAT	Pyrosequencing Sequencing Primer	
<i>KvDMR</i>	<i>KvDMR</i> F	TTTGTGTGATTTTATTTGGAGAGT	Pyrosequencing PCR	
<i>KvDMR</i>	<i>KvDMR</i> R-biotinylated	CCTCAAAACACCCCTACT	Pyrosequencing PCR	
<i>KvDMR</i>	<i>KvDMR</i> Sequencing	GTAGATTTTAAAGTTAGAAGTAGA	Pyrosequencing Sequencing Primer	
<i>Peg1/Mest</i> ICR	<i>Peg1/Mest</i> ICR F	GGAGGTTTTATATAGTATTTGTTTT	Pyrosequencing PCR	
<i>Peg1/Mest</i> ICR	<i>Peg1/Mest</i> ICR R-biotinylated	ACCACCACTAACACTAAA	Pyrosequencing PCR	
<i>Peg1/Mest</i> ICR	<i>Peg1/Mest</i> Sequencing	GGTTTTATATAGTATTTGTTTT	Pyrosequencing Sequencing Primer	
<i>Peg3</i> ICR	<i>Peg3A-BL</i> (1st round)	TTTTGATAAGGAGGTTT	Bisulfite Sequencing PCR	(Mann et al., 2004)
<i>Peg3</i> ICR	<i>Peg3D-BL</i> (1st round)	ACTCTAATATCCACTATAATA	Bisulfite Sequencing PCR	
<i>Peg3</i> ICR	<i>Peg3B-BL</i> (2nd round)	AGTGTGGGTATATGAT	Bisulfite Sequencing PCR	(Market-Velker et al., 2010)
<i>Peg3</i> ICR	<i>Peg3C-BL</i> (2nd round)	TAACAAAACCTCTATCATCAT	Bisulfite Sequencing PCR	
<i>H19/Igf2</i> ICR	BMsp2t1 (H19 A) (1st round)	GAGTATTTAGGAGGATAAGAAAT	Bisulfite Sequencing PCR	(Tremblay et al., 1997)
<i>H19/Igf2</i> ICR	BHha1t3 (H19 D) (1st round)	ATCAAAAACTAACATAAACCCCT	Bisulfite Sequencing PCR	
<i>H19/Igf2</i> ICR	Bmsp2t2c (H19 B) (2nd round)	GTAAGGAGATTAATGTTTTATTTTGG	Bisulfite Sequencing PCR	(Ideraabduallah et al., 2014)
<i>H19/Igf2</i> ICR	BHha1t4ct (H19 C) (second round)	CTAACTCATAAAACCACTAATAT	Bisulfite Sequencing PCR	

Table 4.2: List of PCR cycling conditions for each PCR used in this study.

Assay	Thermal Cycler	PCR conditions	Annealing Temperature (TA), °C	No. of cycles
Tet1	Thermo Electron Hybaid PCR Express Thermal Cycler	2 min denaturation at 94°C; number of cycles of [15 s at 94°C, 15 s at TA, and 40 s at 72°C]	60	35
Smc	BioRad C1000 Touch Thermal Cycler	5 min denaturation at 95°C; number of cycles of [15 s at 95°C, 1 min at TA, and 1 min at 72°C]; 7 min extension at 72°C	55	40
qPCR: All genes	7900HT Fast Real-Time PCR System	2 min hold at 50°C; 10 min hold at 95°C; number of cycles of [15 s at 95°C, 1 min at 60°C]; Melting Curve: 95°C for 15 s, 60°C for 15 s, 95°C for 15 s.	-	40
Allele-Specific <i>H19</i>	BioRad C1000 Touch Thermal Cycler	2 min denaturation at 95°C; number of cycles of [15 s at 95°C, 20 s at TA, and 20 s at 72°C]; 5 min extension at 72°C	58	21-31
Allele-Specific <i>Igf2</i>	BioRad C1000 Touch Thermal Cycler	2 min denaturation at 94°C; number of cycles of [20 s at 94°C, 20 s at TA, and 20 s at 72°C]; 5 min extension at 72°C	60	24-32
Allele-Specific <i>Cdkn1c</i>	BioRad C1000 Touch Thermal Cycler	2 min denaturation at 95°C; number of cycles of [15 s at 95°C, 20 s at TA, and 20 s at 72°C]; 5 min extension at 72°C	60	25-30
Allele-Specific <i>Peg3</i>	BioRad C1000 Touch Thermal Cycler	2 min denaturation at 94°C; number of cycles of [20 s at 95°C, 20 s at TA, and 20 s at 72°C]; 5 min extension at 72°C	60	29-34
Allele-Specific <i>Lit1/Kcnq1ot1</i>	BioRad C1000 Touch Thermal Cycler	2 min denaturation at 95°C; number of cycles of [20 s at 95°C, 20 s at TA, and 50 s at 72°C]; 5 min extension at 72°C	64	32-34
Allele-Specific <i>Snrpn</i>	Roche LightCycler 1.5	Amplification: 95°C 1 s (20°C/s), 50°C, 15 s (20°C/s), 72°C, 6 s (20°C/s); Melt: 95°C, 4 min (20°C/s), 35°C, 3 min (20°C/s), 40°C, 1 min (20°C/s), 45°C, 1 min (20°C/s), 85°C, 0 s, (0.5°C/s); Cooling: 40°C 30 s, (20°C/s)	-	Amplification: 45; Melt: 3; Cooling: 1
Pyrosequencing	BioRad C1000 Touch Thermal Cycler	(Hur et al., 2016)		
<i>Peg3</i> Bisulfite	BioRad C1000 Touch Thermal Cycler	First Round: 5 min denaturation at 94°C; number of cycles of [94°C for 30 s, TA for 30 s, 72°C for 1 min]; 10 min extension at 72°C	50	25
		Second Round: 5 min denaturation at 94°C; number of cycles of [94°C for 30 s, TA for 30 s, 72°C for 1 min]; 10 min extension at 72°C	53	35
<i>H19</i> Bisulfite	BioRad C1000 Touch Thermal Cycler	First Round: 5 min denaturation at 94°C; number of cycles of [94°C for 30 s, TA for 30 s, 72°C for 1 min]; 10 min extension at 72°C	50	25
		Second Round: 5 min denaturation at 94°C; number of cycles of [94°C for 30 s, TA for 30 s, 72°C for 1 min]; 10 min extension at 72°C	58	35

Table 4.3 Complete PCR protocols with linear range information for imprinted genes

<i>Cdkn1c</i>		Thermal cycler (Deg C, time (min))		Cycle #		Reference	Enzyme
MM	/rxn	95	2:00	E10.5			Taq ^q I
dH2O	9.5	95	0:15	E12.5	30X	4- pg 30	65° C
57-4 (10 uM)	1	60	0:20	P0 Brain	30X	8 -pg 30	1 hour
57-L (10 uM)	1	72	0:20	P0 Tongue	25X	8 -pg 30	heat inact
GoTaq	12.5	72	5:00	P0 Liver	30X	8 -pg 30	20 min, 80° C
cDNA	1 each	12	∞				
<i>Lit1/Kcnq1ot1</i>		Thermal cycler		Cycle #		Reference	Enzyme
MM	/rxn	95	2:00	E10.5			StuI
dH2O	8.84	95	0:20	E12.5			37° C
Lit1-F (15 uM)	0.83	64	0:20	P0 Brain	33X	BC rotation pg 21	3 hours
Lit1-R (15 uM)	0.83	72	0:50	P0 Tongue	32X	BC rotation pg 21	heat inact
GoTaq	12.5	72	5:00	P0 Liver	32X	BC rotation pg 21	None
cDNA	1 each	12	∞				
<i>H19</i>		Thermal cycler		Cycle #		Reference	Enzyme
MM	/rxn	95	2:00	EM E10.5	26X	6- pg 32	Cac8I
dH2O	10.5	95	0:15	PL E10.5	24X	6- pg 32	37° C
HE2 (25 uM)	0.5	58	0:20	E12.5	31X	4- pg 30	3 hours
HE4 (25 uM)	0.5	72	0:20	P0 Brain	28X	8 -pg 30	heat inact
GoTaq	12.5	72	5:00	P0 Tongue	21-22X	8 -pg 30	20 min, 65° C
cDNA	1 each	12	∞	P0 Liver	22X	8 -pg 30	
<i>Igf2</i>		Thermal cycler		Cycle #		Reference	Enzyme
MM	/rxn	94	2:00	(EM & PL) E10.5	32X	6- pg 35	MluCI
dH2O	10.9	94	0:20	E12.5	25X	4- pg 121	37° C
Igf2-18 (25 uM)	0.3	60	0:20	P0 Brain	26X	8 -pg 30	3 hours
Igf2-20 (25 uM)	0.3	72	0:20	P0 Tongue	24X	8 -pg 30	heat inact
GoTaq	12.5	72	5:00	P0 Liver	24X	8 -pg 30	None
cDNA	1 each	12	∞				
<i>Peg3</i>		Thermal cycler		Cycle #		Reference	Enzyme
MM	/rxn	94	2:00	E10.5			
dH2O	10.5	94	0:20	E12.5			
PG4	0.5	60	0:20	P0 Brain	32X	BC rotation pg 21	
PG7	0.5	72	0:20	P0 Tongue	29-30X	3- pg126	
GoTaq	12.5	72	5:00	P0 Liver	32X	BC rotation pg 21	
cDNA	1 each	12	∞				

BIBLIOGRAPHY

- Alexander, K. A., Wang, X., Shibata, M., Clark, A. G. and García-García, M. J.** (2015). TRIM28 Controls Genomic Imprinting through Distinct Mechanisms during and after Early Genome-wide Reprogramming. *Cell Rep.* **13**, 1194–1205.
- Amouroux, R., Nashun, B., Shirane, K., Nakagawa, S., Hill, P. W. S., D'Souza, Z., Nakayama, M., Matsuda, M., Turp, A., Ndjetehe, E., et al.** (2016). De novo DNA methylation drives 5hmC accumulation in mouse zygotes. *Nat. Cell Biol.* **18**, 225–233.
- Ancelin, K., Lange, U. C., Hajkova, P., Schneider, R., Bannister, A. J., Kouzarides, T. and Surani, M. A.** (2006). Blimp1 associates with Prmt5 and directs histone arginine methylation in mouse germ cells. *Nat. Cell Biol.* **8**, 623–630.
- Anderson, R., Copeland, T. K., Schöler, H., Heasman, J. and Wylie, C.** (2000). The onset of germ cell migration in the mouse embryo. *Mech. Dev.* **91**, 61–68.
- Anvar, Z., Cammisa, M., Riso, V., Baglivo, I., Kukreja, H., Sparago, A., Girardot, M., Lad, S., De Feis, I., Cerrato, F., et al.** (2015). ZFP57 recognizes multiple and closely spaced sequence motif variants to maintain repressive epigenetic marks in mouse embryonic stem cells. *Nucleic Acids Res.* **44**, 1118–1132.
- Aten, E., Fountain, M. D., Van Haeringen, A., Schaaf, C. P. and Santen, G. W. E.** (2016). Imprinting: The Achilles heel of trio-based exome sequencing. *Genet. Med.* **18**, 1163–1164.
- Bannister, A. J., Zegerman, P., Partridge, J. F., Miska, E. a, Thomas, J. O., Allshire, R. C. and Kouzarides, T.** (2001). Selective recognition of methylated lysine 9 on histone H3 by the HP1 chromo domain. *Nature* **410**, 120–124.

- Barau, J., Teissandier, A., Zamudio, N., Roy, S., Nalesso, V., Hérault, Y., Guillou, F. and Bourc'his, D.** (2016). The DNA methyltransferase DNMT3C protects male germ cells from transposon activity. *Science* **354**, 909–912.
- Barlow, D. P. and Bartolomei, M. S.** (2014). Genomic Imprinting in Mammals. *Cold Spring Harb. Perspect. Biol.* **37**, 1–12.
- Barlow, D. P., Stöger, R., Herrmann, B. G., Saito, K. and Schweifer, N.** (1991). The mouse insulin-like growth factor type-2 receptor is imprinted and closely linked to the Tme locus. *Nature* **349**, 84–87.
- Bartolomei, M. S., Zemel, S. and Tilghman, S. M.** (1991). Parental imprinting of the mouse H19 gene. *Nature* **351**, 153–155.
- Bartolomei, M. S., Webber, A. L. and Brunkow, M. E.** (1993). Epigenetic mechanisms underlying the imprinting of the mouse H19 gene. *Genes Dev.* **7**, 1663–1673.
- Bhatnagar, S., Zhu, X., Ou, J., Lin, L., Chamberlain, L., Zhu, L. J., Wajapeyee, N. and Green, M. R.** (2014). Genetic and pharmacological reactivation of the mammalian inactive X chromosome. *Proc. Natl. Acad. Sci.* **111**, 12591–12598.
- Bhogal, B., Arnaudo, A., Dymkowski, A., Best, A. and Davis, T. L.** (2004). Methylation at mouse Cdkn1c is acquired during postimplantation development and functions to maintain imprinted expression. *Genomics* **84**, 961–970.
- Bian, C. and Yu, X.** (2014). PGC7 suppresses TET3 for protecting DNA methylation. *Nucleic Acids Res.* **42**, 2893–2905.
- Bisht, K., Grill, S., Graniel, J. and Nandakumar, J.** (2017). A lentivirus-free inducible CRISPR-Cas9 system for efficient targeting of human genes. *Anal. Biochem.* **530**, 40–49.

- Bliek, J., Maas, S. M., Ruijter, J. M., Hennekam, R. C., Alders, M., Westerveld, a and Mannens, M. M.** (2001). Increased tumour risk for BWS patients correlates with aberrant H19 and not KCNQ1OT1 methylation: occurrence of KCNQ1OT1 hypomethylation in familial cases of BWS. *Hum. Mol. Genet.* **10**, 467–476.
- Bochtler, M., Kolano, A. and Xu, G. L.** (2017). DNA demethylation pathways: Additional players and regulators. *BioEssays* **39**, 1–13.
- Bodian, D. L., Solomon, B. D., Khromykh, A., Thach, D. C., Iyer, R. K., Link, K., Baker, R. L., Baveja, R., Vockley, J. G. and Niederhuber, J. E.** (2014). Diagnosis of an imprinted-gene syndrome by a novel bioinformatics analysis of whole-genome sequences from a family trio. *Mol. Genet. genomic Med.* **2**, 530–8.
- Bostick, M., Kim, J. K., Esteve, P.-O., Clark, A., Pradhan, S. and Jacobsen, S. E.** (2007). UHRF1 plays a role in maintaining DNA methylation in mammalian cells. *Science* **317**, 1760–1764.
- Bourc'his, D., Xu, G.-L., Lin, C.-S., Bollman, B. and Bestor, T. H.** (2001). Dnmt3L and the Establishment of Maternal Genomic Imprints. *Science* **294**, 2536–2539.
- Brioude, F., Kalish, J. M., Mussa, A., Foster, A. C., Bliek, J., Ferrero, G. B., Boonen, S. E., Cole, T., Baker, R., Bertoletti, M., et al.** (2018). Clinical and molecular diagnosis, screening and management of Beckwith–Wiedemann syndrome: an international consensus statement. *Nat. Publ. Gr.* **14**, 229–249.
- Buiting, K., Groß, S., Lich, C., Gillessen-Kaesbach, G., El-Maarri, O. and Horsthemke, B.** (2003). Epimutations in Prader-Willi and Angelman Syndromes: A Molecular Study of 136 Patients with an Imprinting Defect. *Am. J. Hum. Genet.* **72**, 571–577.

- Calvopina, J. H., Cook, H., Vincent, J. J., Nee, K. and Clark, A. T.** (2015). The Aorta-Gonad-Mesonephros Organ Culture Recapitulates 5hmC Reorganization and Replication-Dependent and Independent Loss of DNA Methylation in the Germline. *Stem Cells Dev.* **24**, 1536–1545.
- Caspary, T., Cleary, M. A., Baker, C. C., Guan, X. J. and Tilghman, S. M.** (1998). Multiple mechanisms regulate imprinting chromosome 7 gene cluster. *Dev. Biol.* **198**, 61.
- Cattanach, B. M. and Kirk, M.** (1985). Differential activity of maternally and paternally derived chromosome regions in mice. *Nature* **315**, 496–498.
- Ciccarone, F., Klinger, F. G., Catizone, A., Calabrese, R., Zampieri, M., Bacalini, M. G., de Felici, M. and Caiafa, P.** (2012). Poly(ADP-ribosyl)ation Acts in the DNA Demethylation of Mouse Primordial Germ Cells Also with DNA Damage-Independent Roles. *PLoS One* **7**,.
- Cooper, W. N., Luharia, A., Evans, G. A., Raza, H., Haire, A. C., Grundy, R., Bowdin, S. C., Riccio, A., Sebastio, G., Bliet, J., et al.** (2005). Molecular subtypes and phenotypic expression of Beckwith–Wiedemann syndrome. *Eur. J. Hum. Genet.* **13**, 1025–1032.
- Cortázar, D., Kunz, C., Selfridge, J., Lettieri, T., Saito, Y., MacDougall, E., Wirz, A., Schuermann, D., Jacobs, A. L., Siegrist, F., et al.** (2011). Embryonic lethal phenotype reveals a function of TDG in maintaining epigenetic stability. *Nature* **470**, 419–423.
- Cortellino, S., Xu, J., Sannai, M., Moore, R., Caretti, E., Cigliano, A., Le Coz, M., Devarajan, K., Wessels, A., Soprano, D., et al.** (2011). Thymine DNA glycosylase is essential for active DNA demethylation by linked deamination-base excision repair. *Cell* **146**, 67–79.

- Costa, Y., Ding, J., Theunissen, T. W., Faiola, F., Hore, T. A., Shliaha, P. V., Fidalgo, M., Saunders, A., Lawrence, M., Dietmann, S., et al.** (2013). NANOG-dependent function of TET1 and TET2 in establishment of pluripotency. *Nature* **495**, 370–374.
- Court, F., Martin-Trujillo, A., Romanelli, V., Garin, I., Iglesias-Platas, I., Salafsky, I., Guitart, M., Perez de Nanclares, G., Lapunzina, P. and Monk, D.** (2013). Genome-Wide Allelic Methylation Analysis Reveals Disease-Specific Susceptibility to Multiple Methylation Defects in Imprinting Syndromes. *Hum. Mutat.* **34**, 595–602.
- Couture, J.-F., Collazo, E., Ortiz-Tello, P. A., Brunzelle, J. S., Trievel, R. C., Couture, J.-F., Collazo, E., Ortiz-Tello, P. A., Brunzelle, J. S. and Trievel, R. C.** (2007). Specificity and mechanism of JMJD2A, a trimethyllysine-specific histone demethylase. *Nat. Struct. Mol. Biol.* **14**, 689–95.
- Crichton, J. H., Dunican, D. S., MacLennan, M., Meehan, R. R. and Adams, I. R.** (2014). Defending the genome from the enemy within: Mechanisms of retrotransposon suppression in the mouse germline. *Cell. Mol. Life Sci.* **71**, 1581–1605.
- Dan, J. and Chen, T.** (2016). Genetic Studies on Mammalian DNA Methyltransferases. In *DNA Methyltransferases - Role and Function*, pp. 123–150. Springer International Publishing Switzerland.
- Davis, T. L., Yang, G. J., McCarrey, J. R. and Bartolomei, M. S.** (2000). The H19 methylation imprint is erased and re-established differentially on the parental alleles during male germ cell development. *Hum. Mol. Genet.* **9**, 2885–2894.
- Dawlaty, M. M., Ganz, K., Powell, B. E., Hu, Y. C., Markoulaki, S., Cheng, A. W., Gao, Q., Kim, J., Choi, S. W., Page, D. C., et al.** (2011). Tet1 is

dispensable for maintaining pluripotency and its loss is compatible with embryonic and postnatal development. *Cell Stem Cell* **9**, 166–175.

Dawlaty, M. M., Breiling, A., Le, T., Raddatz, G., Barrasa, M. I., Cheng, A.

W., Gao, Q., Powell, B. E., Li, Z., Xu, M., et al. (2013). Combined Deficiency of Tet1 and Tet2 Causes Epigenetic Abnormalities but Is Compatible with Postnatal Development. *Dev. Cell* **24**, 310–323.

Dean, W. (2016). Pathways of DNA demethylation. In *DNA Methyltransferases - Role and Function*, pp. 247–274. Springer International Publishing Switzerland.

de Waal, E., Mak, W., Calhoun, S., Stein, P., Ord, T., Krapp, C., Coutifaris,

C., Schultz, R. M. and Bartolomei, M. S. (2014). In Vitro Culture Increases the Frequency of Stochastic Epigenetic Errors at Imprinted Genes in Placental Tissues from Mouse Concepti Produced Through Assisted Reproductive Technologies¹. *Biol. Reprod.* **90**, 22–22.

DeChiara, T. M., Robertson, E. J. and Efstratiadis, A. (1991). Parental imprinting of the mouse insulin-like growth factor II gene. *Cell* **64**, 849–859.

Delaval, K., Govin, J., Cerqueira, F., Rousseaux, S., Khochbin, S., Feil, R., Rô

Me Govin, J., Dé Rique Cerqueira, F., Rousseaux, S., Khochbin, S., et al. (2007). Differential histone modifications mark mouse imprinting control regions during spermatogenesis. *EMBO J.* **26**, 720–9.

Dong, K. B., Maksakova, I. a, Mohn, F., Leung, D., Appanah, R., Lee, S.,

Yang, H. W., Lam, L. L., Mager, D. L., Schübeler, D., et al. (2008). DNA methylation in ES cells requires the lysine methyltransferase G9a but not its catalytic activity. *EMBO J.* **27**, 2691–2701.

Eckersley-Maslin, M. A. and Spector, D. L. (2014). Random monoallelic

expression: Regulating gene expression one allele at a time. *Trends Genet.* **30**, 237–

- Elhamamsy, A. R.** (2017). Role of DNA methylation in imprinting disorders: an updated review. *J. Assist. Reprod. Genet.* **34**, 549–562.
- Engemann, S., Strödicke, M., Paulsen, M., Franck, O., Reinhardt, R., Lane, N., Reik, W. and Walter, J.** (2000). Sequence and functional comparison in the Beckwith-Wiedemann region: implications for a novel imprinting centre and extended imprinting. *Hum. Mol. Genet.* **9**, 2691–2706.
- Faisal, M., Kim, H. and Kim, J.** (2014). Sexual differences of imprinted genes' expression levels. *Gene* **533**, 434–438.
- Fatemi, M., Hermann, A., Pradhan, S. and Jeltsch, A.** (2001). The activity of the murine DNA methyltransferase Dnmt1 is controlled by interaction of the catalytic domain with the N-terminal part of the enzyme leading to an allosteric activation of the enzyme after binding to methylated DNA. *J. Mol. Biol.* **309**, 1189–1199.
- Ferry, L., Fournier, A., Tsusaka, T., Arita, K., Ferry, L., Fournier, A., Tsusaka, T., Adelmant, G., Shimazu, T. and Matano, S.** (2017). Methylation of DNA Ligase 1 by G9a/GLP Recruits UHRF1 to Replicating DNA and Regulated DNA Methylation. *Mol. Cell* **67**, 1–16.
- Fortier, A. L., Lopes, F. L., Darricarrere, N., Martel, J. and Trasler, J. M.** (2008). Superovulation alters the expression of imprinted genes in the midgestation mouse placenta. *Hum. Mol. Genet.* **17**, 1653–1665.
- Fournier, C., Goto, Y., Ballestar, E., Delaval, K., Hever, A. M., Esteller, M. and Feil, R.** (2002). Allele-specific histone lysine methylation marks regulatory regions at imprinted mouse genes. *EMBO J.* **21**, 6560–6570.
- Frauer, C., Rottach, A., Meilinger, D., Bultmann, S., Fellingner, K., Hasenöder, S., Wang, M., Qin, W., Söding, J., Spada, F., et al.** (2011).

Different binding properties and function of CXXC zinc finger domains in Dnmt1 and Tet1. *PLoS One* **6**,.

Gahurova, L., Tomizawa, S. S., Smallwood, S. A., Stewart-Morgan, K. R., Saadeh, H., Kim, J., Andrews, S. R., Chen, T. and Kelsey, G. (2017).

Transcription and chromatin determinants of de novo DNA methylation timing in oocytes. *Epigenetics Chromatin* **10**, 25.

Ginsburg, M., Snow, M. H. and McLaren, A. (1990). Primordial germ cells in the mouse embryo during gastrulation. *Development* **110**, 521–528.

Gjerset, R. A. and Martin, D. W. (1982). Presence of a DNA demethylating activity in the nucleus of murine erythroleukemic cells. *J. Biol. Chem.* **257**, 8581–8583.

Globisch, D., Münzel, M., Müller, M., Michalakis, S., Wagner, M., Koch, S., Brückl, T., Biel, M. and Carell, T. (2010). Tissue distribution of 5-hydroxymethylcytosine and search for active demethylation intermediates. *PLoS One* **5**, 1–9.

Grafodatskaya, D., Choufani, S., Basran, R. and Weksberg, R. (2017). An update on molecular diagnostic testing of human imprinting disorders. *J. Pediatr. Genet. Mar*(**6**), 3–17.

Grosser, C., Wagner, N., Grothaus, K. and Horsthemke, B. (2015). Altering TET dioxygenase levels within physiological range affects DNA methylation dynamics of HEK293 cells. *Epigenetics* **10**, 819–833.

Gu, T. P., Guo, F., Yang, H., Wu, H. P., Xu, G. F., Liu, W., Xie, Z. G., Shi, L., He, X., Jin, S. G., et al. (2011). The role of Tet3 DNA dioxygenase in epigenetic reprogramming by oocytes. *Nature* **477**, 606–610.

Guibert, S., Forné, T. and Weber, M. (2012). Global profiling of DNA methylation erasure in mouse primordial germ cells. *Genome Res.* **22**, 633–641.

- Guo, J. U., Su, Y., Shin, J. H., Shin, J., Li, H., Xie, B., Zhong, C., Hu, S., Le, T., Fan, G., et al.** (2014a). Distribution, recognition and regulation of non-CpG methylation in the adult mammalian brain. *Nat. Neurosci.* **17**, 215–222.
- Guo, F., Li, X., Liang, D., Li, T., Zhu, P., Guo, H., Wu, X., Wen, L., Gu, T. P., Hu, B., et al.** (2014b). Active and passive demethylation of male and female pronuclear DNA in the mammalian zygote. *Cell Stem Cell* **15**, 447–458.
- Guo, H., Hu, B., Yan, L., Yong, J., Wu, Y., Gao, Y., Guo, F., Hou, Y., Fan, X., Dong, J., et al.** (2017). DNA methylation and chromatin accessibility profiling of mouse and human fetal germ cells. *Cell Res.* **27**, 165–183.
- Gyory, I., Wu, J., Fejér, G., Seto, E. and Wright, K. L.** (2004). PRDI-BF1 recruits the histone H3 methyltransferase G9a in transcriptional silencing. *Nat. Immunol.* **5**, 299–308.
- Hackett, J. A., Sengupta, R., Zyllicz, J. J., Murakami, K., Lee, C., Down, T. A. and Surani, M. A.** (2013). Germline DNA Demethylation Dynamics and Imprint Erasure Through 5-Hydroxymethylcytosine. *Science* **339**, 448–452.
- Hahn, M. A., Qiu, R., Wu, X., Li, A. X., Zhang, H., Wang, J., Jui, J., Jin, S. G., Jiang, Y., Pfeifer, G. P., et al.** (2013). Dynamics of 5-Hydroxymethylcytosine and Chromatin Marks in Mammalian Neurogenesis. *Cell Rep.* **3**, 291–300.
- Hahn, M. A., Szabó, P. E. and Pfeifer, G. P.** (2014). 5-Hydroxymethylcytosine: A stable or transient DNA modification? *Genomics* **104**, 314–323.
- Hajkova, P., Erhardt, S., Lane, N., Haaf, T., El-Maarri, O., Reik, W., Walter, J. and Surani, M. A.** (2002). Epigenetic reprogramming in mouse primordial germ cells. *Mech. Dev.* **117**, 15–23.
- Hajkova, P., Ancelin, K., Waldmann, T., Lacoste, N., Lange, U. C., Cesari, F., Lee, C., Almouzni, G., Schneider, R. and Surani, M. A.** (2008). Chromatin

- dynamics during epigenetic reprogramming in the mouse germ line. *Nature* **452**, 877–81.
- Hajkova, P., Jeffries, S. J., Lee, C., Miller, N., Jackson, S. P. and Surani, M. A.** (2010). Genome-Wide Reprogramming in the Mouse Germ Line Entails the Base Excision Repair Pathway. *Science* **329**, 78–82.
- Hargan-Calvopina, J., Taylor, S., Cook, H., Chiang, Y.-S. S., Chen, P.-Y. Y., Correspondence, A. T. C., Hu, Z., Lee, S. A., Yen, M.-R. R., Clark, A. T., et al.** (2016). Stage-Specific Demethylation in Primordial Germ Cells Safeguards against Precocious Differentiation. *Dev. Cell* **39**, 75–86.
- Haston, K. M., Tung, J. Y. and Reijo Pera, R. A.** (2009). Dazl functions in maintenance of pluripotency and genetic and epigenetic programs of differentiation in mouse primordial germ cells in vivo and in vitro. *PLoS One* **4**, e5654.
- Hata, K., Okano, M., Lei, H. and Li, E.** (2002). Dnmt3L cooperates with the Dnmt3 family of de novo DNA methyltransferases to establish maternal imprints in mice. *Development* **129**, 1983–1993.
- Hayashi, K. and Saitou, M.** (2013). Generation of eggs from mouse embryonic stem cells and induced pluripotent stem cells. *Nat. Protoc.* **8**, 1513–24.
- Hayashi, K., Ohta, H., Kurimoto, K., Aramaki, S. and Saitou, M.** (2011). Reconstitution of the mouse germ cell specification pathway in culture by pluripotent stem cells. *Cell* **146**, 519–532.
- He, Y.-F., Li, B.-Z., Li, Z., Liu, P., Wang, Y., Tang, Q., Ding, J., Jia, Y., Chen, Z., Li, L., et al.** (2011). Tet-mediated formation of 5-carboxylcytosine and its excision by TDG in mammalian DNA. *Science* **333**, 1303–1307.
- Heard, E. and Martienssen, R. A.** (2014). Transgenerational Epigenetic Inheritance: Myths and Mechanisms. *Cell* **157**, 95–109.

- Henckel, A., Nakabayashi, K., Sanz, L. A., Feil, R., Hata, K. and Arnaud, P.** (2009). Histone methylation is mechanistically linked to DNA methylation at imprinting control regions in mammals. *Hum. Mol. Genet.* **18**, 3375–3383.
- Henckel, A., Chebli, K., Kota, S. K., Arnaud, P., Feil, R. and Henckel** (2011). Transcription and histone methylation changes correlate with imprint acquisition in male germ cells. *EMBO J.* **31**, 606–615.
- Hill, P. W. S., Amouroux, R. and Hajkova, P.** (2014). DNA demethylation, Tet proteins and 5-hydroxymethylcytosine in epigenetic reprogramming: An emerging complex story. *Genomics* **104**, 324–333.
- Hirasawa, R., Chiba, H., Kaneda, M., Tajima, S., Li, E., Jaenisch, R. and Sasaki, H.** (2008). Maternal and zygotic Dnmt1 are necessary and sufficient for the maintenance of DNA methylation imprints during preimplantation development. *Genes Dev.* **22**, 1607–1616.
- Hjelm, L. N., Chin, E. L. H., Hegde, M. R., Coffee, B. W. and Bean, L. J. H.** (2010). A Simple Method to Confirm and Size Deletion , Duplication , and Insertion Mutations Detected by Sequence Analysis. *J. Mol. Diagnostics* **12**, 607–610.
- Hsu, P. D., Scott, D. A., Weinstein, J. a, Ran, F. A., Konermann, S., Agarwala, V., Li, Y., Fine, E. J., Wu, X., Shalem, O., et al.** (2013). DNA targeting specificity of RNA-guided Cas9 nucleases. *Nat. Biotechnol.* **31**, 827–32.
- Hu, L., Li, Z., Cheng, J., Rao, Q., Gong, W., Liu, M., Shi, Y. G., Zhu, J., Wang, P. and Xu, Y.** (2013). Crystal Structure of TET2-DNA Complex: Insight into TET-Mediated 5mC Oxidation. *Cell* **155**, 1545–1555.
- Hu, L., Lu, J., Cheng, J., Rao, Q., Li, Z., Hou, H., Lou, Z., Zhang, L., Li, W., Gong, W., et al.** (2015). Structural insight into substrate preference for TET-mediated oxidation. *Nature* **527**, 118–22.

- Huang, Y., Chavez, L., Chang, X., Wang, X., Pastor, W. A., Kang, J., Zepeda-Martínez, J. A., Pape, U. J., Jacobsen, S. E., Peters, B., et al.** (2014). Distinct roles of the methylcytosine oxidases Tet1 and Tet2 in mouse embryonic stem cells. *Proc. Natl. Acad. Sci. U. S. A.* **111**, 1361–6.
- Huq, A. H. M. M., Sutcliffe, J. S., Nakao, M., Shen, Y., Gibbs, R. A. and Beaudet, A. L.** (1997). Sequencing and functional analysis of the SNRPN promoter: In vitro methylation abolishes promoter activity. *Genome Res.* **7**, 642–648.
- Hur, S. K., Freschi, A., Ideraabdullah, F., Thorvaldsen, J. L., Luense, L. J., Weller, A. H., Berger, S. L., Cerrato, F., Riccio, A. and Bartolomei, M. S.** (2016). Humanized *H19/Igf2* locus reveals diverged imprinting mechanism between mouse and human and reflects Silver–Russell syndrome phenotypes. *Proc. Natl. Acad. Sci.* **113**, 10938–10943.
- Ideraabdullah, F. Y., Thorvaldsen, J. L., Myers, J. A. and Bartolomei, M. S.** (2014). Tissue-specific insulator function at *H19/Igf2* revealed by deletions at the imprinting control region. *Hum. Mol. Genet.* **23**, 6246–6259.
- Inoue, A. and Zhang, Y.** (2011). Replication-Dependent Loss of 5-Hydroxymethylcytosine in Mouse Preimplantation Embryos. *Science* **334**, 194–194.
- Inoue, A., Shen, L., Dai, Q., He, C. and Zhang, Y.** (2011). Generation and replication-dependent dilution of 5fC and 5caC during mouse preimplantation development. *Cell Res.* **21**, 1670–1676.
- Ito, S., D’Alessio, A. C., Taranova, O. V, Hong, K., Sowers, L. C. and Zhang, Y.** (2010). Role of Tet proteins in 5mC to 5hmC conversion, ES-cell self-renewal and inner cell mass specification. *Nature* **466**, 1129–1133.
- Ito, S., Shen, L., Dai, Q., Wu, S. C., Collins, L. B., Swenberg, J. A., He, C. and**

- Zhang, Y.** (2011). Tet Proteins Can Convert 5-Methylcytosine to 5-Formylcytosine and 5-Carboxylcytosine. *Science* **333**, 1300–1303.
- Jähner, D. and Jaenisch, R.** (1984). DNA Methylation in Early Mammalian Development. In *DNA methylation, biochemistry, and biological significance* (ed. Howard Cedar, Aharon Razin, A. D. R.), pp. 189–219. New York, New York: Springer.
- Jay, F. and Ciaudo, C.** (2013). An RNA tool kit to study the status of mouse ES cells: Sex determination and stemness. *Methods* **63**, 85–92.
- Jin, C., Lu, Y., Jelinek, J., Liang, S., Estecio, M. R. H., Barton, M. C. and Issa, J. P. J.** (2014). TET1 is a maintenance DNA demethylase that prevents methylation spreading in differentiated cells. *Nucleic Acids Res.* **42**, 6956–6971.
- Jost, J. P., Oakeley, E. J., Zhu, B., Benjamin, D., Thiry, S., Siegmann, M. and Jost, Y. C.** (2001). 5-Methylcytosine DNA glycosylase participates in the genome-wide loss of DNA methylation occurring during mouse myoblast differentiation. *Nucleic Acids Res.* **29**, 4452–4461.
- Jurkowska, R. Z. and Jeltsch, A.** (2016). Mechanisms and Biological Roles of DNA Methyltransferases and DNA Methylation: From Past Achievements to Future Challenges. In *DNA Methyltransferases - Role and Function*, pp. 1–17. Springer International Publishing Switzerland.
- Kagiwada, S., Kurimoto, K., Hirota, T., Yamaji, M. and Saitou, M.** (2013). Replication-coupled passive DNA demethylation for the erasure of genome imprints in mice. *EMBO J.* **32**, 340–353.
- Kalish, J. M., Jiang, C. and Bartolomei, M. S.** (2014). Epigenetics and imprinting in human disease. *Int. J. Dev. Biol.* **58**, 291–298.
- Kaneda, M., Okano, M., Hata, K., Sado, T., Tsujimoto, H., Li, E., Sasaki, H.,**

- Tsujimoto, N., Li, E. and Sasaki, H.** (2004). Essential role for de novo DNA methyltransferase Dnmt3a in paternal and maternal imprinting. *Nature* **429**, 900–903.
- Kang, J., Lienhard, M., Pastor, W. A., Chawla, A., Novotny, M., Tsagaratou, A., Lasken, R. S., Thompson, E. C., Surani, M. A., Koralov, S. B., et al.** (2015). Simultaneous deletion of the methylcytosine oxidases Tet1 and Tet3 increases transcriptome variability in early embryogenesis. *Proc. Natl. Acad. Sci.* **112**, E4236–E4245.
- Kawahara, M., Wu, Q., Takahashi, N., Morita, S., Yamada, K., Ito, M., Ferguson-Smith, A. C. and Kono, T.** (2007). High-frequency generation of viable mice from engineered bi-maternal embryos. *Nat. Biotechnol.* **25**, 1045–1050.
- Kawasaki, Y., Lee, J., Matsuzawa, A., Kohda, T., Kaneko-Ishino, T. and Ishino, F.** (2014). Active DNA demethylation is required for complete imprint erasure in primordial germ cells. *Sci. Rep.* **4**, 3658.
- Kearns, N. a, Genga, R. M. J., Enuameh, M. S., Garber, M., Wolfe, S. a and Maehr, R.** (2013). Cas9 effector-mediated regulation of transcription and differentiation in human pluripotent stem cells. *Development* **141**, 219–223.
- Kim, S.-H., Kang, Y.-K., Koo, D.-B., Kang, M.-J., Moon, S.-J., Lee, K.-K. and Han, Y.-M.** (2004). Differential DNA methylation reprogramming of various repetitive sequences in mouse preimplantation embryos. *Biochem. Biophys. Res. Commun.* **324**, 58–63.
- Ko, M., An, J., Bandukwala, H. S., Chavez, L., Aijö, T., Pastor, W. a, Segal, M. F., Li, H., Koh, K. P., Lähdesmäki, H., et al.** (2013). Modulation of TET2 expression and 5-methylcytosine oxidation by the CXXC domain protein IDAX. *Nature* **497**, 122–6.

- Kobayashi, H., Sakurai, T., Miura, F., Imai, M., Mochiduki, K., Yanagisawa, E., Sakashita, A., Wakai, T., Suzuki, Y., Ito, T., et al.** (2013). High-resolution DNA methylome analysis of primordial germ cells identifies gender-specific reprogramming in mice. *Genome Res.* **23**, 616–627.
- Koehler, K. E., Cherry, J. P., Lynn, A., Hunt, P. A. and Hassold, T. J.** (2002). Genetic control of mammalian meiotic recombination. I. Variation in exchange frequencies among males from inbred mouse strains. *Genetics* **162**, 297–306.
- Kohli, R. M. and Zhang, Y.** (2013). TET enzymes, TDG and the dynamics of DNA demethylation. *Nature* **502**, 472–479.
- Korostowski, L., Sedlak, N. and Engel, N.** (2012). The Kcnq1ot1 Long Non-Coding RNA Affects Chromatin Conformation and Expression of Kcnq1, but Does Not Regulate Its Imprinting in the Developing Heart. *PLoS Genet.* **8**,.
- Kriaucionis, S. and Heintz, N.** (2009). The Nuclear DNA Base 5-Hydroxymethylcytosine Is Present in Purkinje Neurons and the Brain. *Science* **324**, 929–930.
- Kumaki, Y., Oda, M. and Okano, M.** (2008). QUMA: quantification tool for methylation analysis. *Nucleic Acids Res.* **36**,.
- Kurimoto, K., Yabuta, Y., Ohinata, Y., Shigeta, M., Yamanaka, K. and Saitou, M.** (2008). Complex genome-wide transcription dynamics orchestrated by Blimp1 for the specification of the germ cell lineage in mice. *Genes Dev.* **22**, 1617–1635.
- Lachner, M., O’Carroll, D., Rea, S., Mechtler, K. and Jenuwein, T.** (2001). Methylation of histone H3 lysine 9 creates a binding site for HP1 proteins. *Nature* **410**, 116–20.
- Latos, P. A., Pauler, F. M., Koerner, M. V, Senergin, H. B., Hudson, Q. J., Stocsits, R. R., Allhoff, W., Stricker, S. H., Klement, R. M., Warczok, K.**

- E., et al.** (2012). Airn transcriptional overlap, but not its lncRNA products, induces imprinted Igf2r silencing. *Science* **338**, 1469–1472.
- Lee, J., Inoue, K., Ono, R., Ogonuki, N., Kohda, T., Kaneko-Ishino, T., Ogura, A. and Ishino, F.** (2002). Erasing genomic imprinting memory in mouse clone embryos produced from day 11.5 primordial germ cells. *Development* **129**, 1807–1817.
- Lengner, C. J., Camargo, F. D., Hochedlinger, K., Welstead, G. G., Zaidi, S., Gokhale, S., Scholer, H. R., Tomilin, A. and Jaenisch, R.** (2007). Oct4 Expression Is Not Required for Mouse Somatic Stem Cell Self-Renewal. *Cell Stem Cell* **1**, 403–415.
- Leung, D., Du, T., Wagner, U., Xie, W., Lee, A. Y., Goyal, P., Li, Y., Szulwach, K. E., Jin, P., Lorincz, M. C., et al.** (2014). Regulation of DNA methylation turnover at LTR retrotransposons and imprinted loci by the histone methyltransferase Setdb1. *Proc. Natl. Acad. Sci. U. S. A.* **111**, 6690–5.
- Li, E., Bestor, T. H. and Jaenisch, R.** (1992). Targeted mutation of the DNA methyltransferase gene results in embryonic lethality. *Cell* **69**, 915–926.
- Li, E., Beard, C., Forster, A. C. C., Bestor, T. H. and Jaenisch, R.** (1993a). DNA methylation, genomic imprinting, and mammalian development. *Cold Spring Harb Symp Quant Biol* **58**, 297–305.
- Li, E., Beard, C. and Jaenisch, R.** (1993b). Role for DNA methylation in genomic imprinting. *Nature* **366**, 362–365.
- Li, X., Ito, M., Zhou, F., Youngson, N., Zuo, X., Leder, P. and Ferguson-Smith, A. C.** (2008). A Maternal-Zygotic Effect Gene, Zfp57, Maintains Both Maternal and Paternal Imprints. *Dev. Cell* **15**, 547–557.
- Li, Z., Cai, X., Cai, C. L., Wang, J., Zhang, W., Petersen, B. E., Yang, F. C. and**

- Xu, M.** (2011). Deletion of Tet2 in mice leads to dysregulated hematopoietic stem cells and subsequent development of myeloid malignancies. *Blood* **118**, 4509–4518.
- Li, L., Li, C., Mao, H., Zhenfang, D., Chan, W. Y., Murray, P., Luo, B., Chan, A. T. C., Mok, T. S. K., Chan, F. K. L., et al.** (2016). Epigenetic inactivation of the CpG demethylase TET1 as a DNA methylation feedback loop in human cancers. *Sci. Rep.* **6**,.
- Lin, Y. and Page, D. C.** (2005). Dazl deficiency leads to embryonic arrest of germ cell development in XY C57BL/6 mice. *Dev. Biol.* **288**, 309–316.
- Lin, S.-P., Youngson, N., Takada, S., Seitz, H., Reik, W., Paulsen, M., Cavaille, J. and Ferguson-Smith, A. C.** (2003). Asymmetric regulation of imprinting on the maternal and paternal chromosomes at the Dlk1-Gtl2 imprinted cluster on mouse chromosome 12. *Nat. Genet.* **35**, 97–102.
- Lin, S., Ferguson-Smith, A. C., Schultz, R. M. and Bartolomei, M. S.** (2011). Nonallelic Transcriptional Roles of CTCF and Cohesins at Imprinted Loci. *Mol. Cell. Biol.* **31**, 3094–3104.
- Long, H. K., Blackledge, N. P. and Klose, R. J.** (2013). ZF-CxxC domain-containing proteins, CpG islands and the chromatin connection. *Biochem. Soc. Trans.* **41**, 727–740.
- Lorthongpanich, C., Cheow, L. F., Balu, S., Quake, S. R., Knowles, B. B., Burkholder, W. F., Solter, D. and Messerschmidt, D. M.** (2013). Single-Cell DNA-Methylation Analysis Reveals Epigenetic Chimerism in Preimplantation Embryos. *Science* **341**, 1110–1112.
- Lu, F., Liu, Y., Jiang, L., Yamaguchi, S. and Zhang, Y.** (2014). Role of Tet proteins in enhancer activity and telomere elongation. *Genes Dev.* **28**, 2103–2119.
- Lucifero, D., Mann, M. R. W., Bartolomei, M. S. and Trasler, J. M.** (2004).

- Gene-specific timing and epigenetic memory in oocyte imprinting. *Hum. Mol. Genet.* **13**, 839–849.
- Lyko, F.** (2018). The DNA methyltransferase family: A versatile toolkit for epigenetic regulation. *Nat. Rev. Genet.* **19**, 81–92.
- Macdonald, W. A. and Mann, M. R. W.** (2014). Epigenetic regulation of genomic imprinting from germ line to preimplantation. *Mol. Reprod. Dev.* **81**, 126–140.
- Mackay, D. J. G. and Temple, I. K.** (2017). Human imprinting disorders: Principles, practice, problems and progress. *Eur. J. Med. Genet.* **60**, 618–626.
- Mancini-DiNardo, D., Steele, S. J. S., Levorsse, J. M., Ingram, R. S. and Tilghman, S. M.** (2006). Elongation of the *Kcnq10t1* transcript is required for genomic imprinting of neighboring genes. *Genes Dev.* **20**, 1268–1282.
- Mann, M. R. W.** (2004). Selective loss of imprinting in the placenta following preimplantation development in culture. *Development* **131**, 3727–3735.
- Mann, M. R. W., Lee, S. S., Doherty, A. S., Verona, R. I., Nolen, L. D., Schultz, R. M. and Bartolomei, M. S.** (2004). Selective loss of imprinting in the placenta following preimplantation development in culture. *Development* **131**, 3727–3735.
- Market-Velker, B. A., Fernandes, A. D. and Mann, M. R. W.** (2010). Side-by-Side Comparison of Five Commercial Media Systems in a Mouse Model: Suboptimal In Vitro Culture Interferes with Imprint Maintenance. *Biol. Reprod.* **83**, 938–950.
- McGrath, J. and Solter, D.** (1984). Completion of mouse embryogenesis requires both the maternal and paternal genomes. *Cell* **37**, 179–183.
- Messerschmidt, D. M.** (2012). Should I stay or should I go, protection and maintenance of DNA methylation at imprinted genes. *Epigenetics* **7**, 969–975.
- Messerschmidt, D. M., de Vries, W., Ito, M., Solter, D., Ferguson-Smith, A.,**

- Knowles, B. B. and Messerschmidt** (2012). Trim28 Is Required for Epigenetic Stability During Mouse Oocyte to Embryo Transition. *Science* **335**, 1499 LP-1502.
- Monk, M., Boubelik, M. and Lehnert, S.** (1987). Temporal and regional changes in DNA methylation in the embryonic, extraembryonic and germ cell lineages during mouse embryo development. *Development* **99**, 371–82.
- Nakamura, T., Arai, Y., Umehara, H., Masuhara, M., Kimura, T., Taniguchi, H., Sekimoto, T., Ikawa, M., Yoneda, Y., Okabe, M., et al.** (2007). PGC7/Stella protects against DNA demethylation in early embryogenesis. *Nat Cell Biol* **9**, 64–71.
- Nakamura, T., Liu, Y.-J., Nakashima, H., Umehara, H., Inoue, K., Matoba, S., Tachibana, M., Ogura, A., Shinkai, Y. and Nakano, T.** (2012). PGC7 binds histone H3K9me2 to protect against conversion of 5mC to 5hmC in early embryos. *Nature* **486**, 415–419.
- Nakashima, H., Kimura, T., Kaga, Y., Nakatani, T., Seki, Y., Nakamura, T. and Nakano, T.** (2013). Effects of dppa3 on DNA methylation dynamics during primordial germ cell development in mice. *Biol. Reprod.* **88**, 125.
- Nestor, C. E., Ottaviano, R., Reddington, J., Sproul, D., Reinhardt, D., Dunican, D., Katz, E., Dixon, J. M., Harrison, D. J. and Meehan, R. R.** (2012). Tissue type is a major modifier of the 5-hydroxymethylcytosine content of human genes. *Genome Res.* **22**, 467–477.
- Ochiai, H., Sugawara, T. and Yamamoto, T.** (2015). Simultaneous live imaging of the transcription and nuclear position of specific genes. *Nucleic Acids Res.* **43**, e127.
- Ohno, R., Nakayama, M., Naruse, C., Okashita, N., Takano, O., Tachibana, M., Asano, M., Saitou, M. and Seki, Y.** (2013). A replication-dependent passive mechanism modulates DNA demethylation in mouse primordial germ cells.

Development **140**, 2892–2903.

- Ohta, T., Gray, T. A., Rogan, P. K., Buiting, K., Gabriel, J. M., Saitoh, S., Muralidhar, B., Bilienska, B., Krajewska-Walasek, M., Driscoll, D. J., et al.** (1999). Imprinting-Mutation Mechanisms in Prader-Willi Syndrome. *Am. J. Hum. Genet.* **64**, 397–413.
- Okano, M., Xie, S. and Li, E.** (1998). Cloning and characterization of a family of novel mammalian DNA (cytosine-5) methyltransferases. *Nat. Am. Inc.* **19**, 219–220.
- Okano, M., Bell, D. W., Haber, D. A. and Li, E.** (1999). DNA methyltransferases Dnmt3a and Dnmt3b are essential for de novo methylation and mammalian development. *Cell* **99**, 247–257.
- Ono, R., Taki, T., Taketani, T., Taniwaki, M., Kobayashi, H. and Hayashi, Y.** (2002). LCX, leukemia-associated protein with a CXXC domain, is fused to MLL in acute myeloid leukemia with trilineage dysplasia having t(10;11)(q22;q23). *Cancer Res.* **62**, 4075–4080.
- Ooi, S. K. T. and Bestor, T. H.** (2008). The Colorful History of Active DNA Demethylation. *Cell* **133**, 1145–1148.
- Palomares-Bralo, M., Vallespín, E., Del Pozo, Á., Ibañez, K., Silla, J. C., Galán, E., Gordo, G., Martínez-Glez, V., Alba-Valdivia, L. I., Heath, K. E., et al.** (2017). Pitfalls of trio-based exome sequencing: Imprinted genes and parental mosaicism - MAGEL2 as an example. *Genet. Med.* **19**, 1283–1285.
- Pastor, W. A., Pape, U. J., Huang, Y., Henderson, H. R., Lister, R., Ko, M., McLoughlin, E. M., Brudno, Y., Mahapatra, S., Kapranov, P., et al.** (2011). Genome-wide mapping of 5-hydroxymethylcytosine in embryonic stem cells. *Nature* **473**, 394–7.

- Pfaffeneder, T., Hackner, B., Truß, M., Münzel, M., Müller, M., Deiml, C. A., Hagemeyer, C. and Carell, T.** (2011). The discovery of 5-formylcytosine in embryonic stem cell DNA. *Angew. Chemie - Int. Ed.* **50**, 7008–7012.
- Piccolo, F. M., Bagci, H., Brown, K. E., Landeira, D., Soza-Ried, J., Feytout, A., Mooijman, D., Hajkova, P., Leitch, H. G., Tada, T., et al.** (2013). Different Roles for Tet1 and Tet2 Proteins in Reprogramming-Mediated Erasure of Imprints Induced by EGC Fusion. *Mol. Cell* **49**, 1023–1033.
- Plasschaert, R. N. and Bartolomei, M. S.** (2014). Genomic imprinting in development, growth, behavior and stem cells. *Development* **141**, 1805–1813.
- Plasschaert, R. N. and Bartolomei, M. S.** (2015). Tissue-specific regulation and function of Grb10 during growth and neuronal commitment. *Proc. Natl. Acad. Sci.* **112**, 6841–6847.
- Popp, C., Dean, W., Feng, S., Cokus, S. J., Andrews, S., Pellegrini, M., Jacobsen, S. E. and Reik, W.** (2010). Genome-wide erasure of DNA methylation in mouse primordial germ cells is affected by AID deficiency. *Nature* **463**, 1101–5.
- Quenneville, S., Verde, G., Corsinotti, A., Kapopoulou, A., Jakobsson, J., Offner, S., Baglivo, I., Pedone, P. V., Grimaldi, G., Riccio, A., et al.** (2011). In embryonic stem cells, ZFP57/KAP1 recognize a methylated hexanucleotide to affect chromatin and DNA methylation of imprinting control regions. *Mol. Cell* **44**, 361–372.
- Razin, A., Szyf, M., Kafri, T., Roll, M., Giloh, H., Scarpa, S., Carotti, D. and Cantoni, G. L.** (1986). Replacement of 5-methylcytosine by cytosine: A possible mechanism for transient DNA demethylation during differentiation. *Proc. Natl. Acad. Sci. U. S. A.* **83**, 2827–2831.
- Razin, A., Levine, A., Kafri, T. A. L., Agostinit, S., Gomi, T. and Cantoni, G. L.**

- (1988). Relationship between transient DNA hypomethylation and erythroid differentiation of murine erythroleukemia cells. *Proc Natl Acad Sci U S A* **85**, 9003–9006.
- Rhee, I., Jair, K.-W., Yen, R.-W. C., Lengauer, C., Herman, J. G., Kinzler, K. W., Vogelstein, B., Baylin, S. B. and Schuebel, K.** (2000). CpG methylation is maintained in human cancer cells lacking DNMT1. *Nature* **404**, 1003–1007.
- Riggs, A. D.** (1975). X inactivation, differentiation, and DNA methylation. *Cytogenet. Cell Genet.* **14**, 9–25.
- Rivera, R. M., Stein, P., Weaver, J. R., Mager, J., Schultz, R. M. and Bartolomei, M. S.** (2008). Manipulations of mouse embryos prior to implantation result in aberrant expression of imprinted genes on day 9.5 of development. *Hum. Mol. Genet.* **17**, 1–14.
- Ruggiu, M., Speed, R., Taggart, M., McKay, S. J., Kilanowski, F., Saunders, P., Dorin, J. and Cooke, H. J.** (1997). The mouse Dazla gene encodes a cytoplasmic protein essential for gametogenesis. *Nature* **389**, 73–77.
- Sachs, M., Onodera, C., Blaschke, K., Ebata, K., Song, J. and Ramalho-Santos, M.** (2013). Bivalent Chromatin Marks Developmental Regulatory Genes in the Mouse Embryonic Germline InVivo. *Cell Rep.* **3**, 1777–1784.
- Saitou, M. and Yamaji, M.** (2012). Primordial germ cells in mice. *Cold Spring Harb. Perspect. Biol.* **4**, a008375.
- Saitou, M., Kagiwada, S. and Kurimoto, K.** (2012). Epigenetic reprogramming in mouse pre-implantation development and primordial germ cells. *Development* **139**, 15–31.
- SanMiguel, J. M. and Bartolomei, M. S.** (2018). DNA methylation dynamics of genomic imprinting in mouse development. *Biol. Reprod.* 1–11.

- SanMiguel, J. M., Abramowitz, L. K. and Bartolomei, M. S.** (2018). Imprinted gene dysregulation in a Tet1 null mouse model is stochastic and variable in the germline and offspring. *Development* dev.160622.
- Santos, F., Hendrich, B., Reik, W. and Dean, W.** (2002). Dynamic Reprogramming of DNA Methylation in the Early Mouse Embryo. *Dev. Biol.* **241**, 172–182.
- Sato, M., Kimura, T., Kurokawa, K., Fujita, Y., Abe, K., Masuhara, M., Yasunaga, T., Ryo, A., Yamamoto, M. and Nakano, T.** (2002). Identification of PGC7, a new gene expressed specifically in preimplantation embryos and germ cells. *Mech. Dev.* **113**, 91–94.
- Sato, S., Yoshimizu, T., Sato, E. and Matsui, Y.** (2003). Erasure of methylation imprinting of Igf2r during mouse primordial germ-cell development. *Mol. Reprod. Dev.* **65**, 41–50.
- Schrans-Stassen, B. H., Saunders, P. T., Cooke, H. J. and de Rooij, D. G.** (2001). Nature of the spermatogenic arrest in Dazl $-/-$ mice. *Biol. Reprod.* **65**, 771–776.
- Seah, M. K. Y. and Messerschmidt, D. M.** (2017). From Germline to Soma: Epigenetic Dynamics in the Mouse Preimplantation Embryo. In *Current Topics in Developmental Biology* (ed. Plusa, B.) and Hadjantonakis, A.-K. B. T.-C. T. in D. B.), pp. 203–235. Academic Press.
- Searle, A. G. and Beechey, C. V** (1978). Complementation studies with mouse translocations. *Cytogenet. Cell Genet.* **20**, 282–303.
- Seisenberger, S., Andrews, S., Krueger, F., Arand, J., Walter, J., Santos, F., Popp, C., Thienpont, B., Dean, W. and Reik, W.** (2012a). The Dynamics of Genome-wide DNA Methylation Reprogramming in Mouse Primordial Germ Cells.

Mol. Cell **48**, 849–862.

Seisenberger, S., Peat, J. R., Hore, T. A., Santos, F., Dean, W. and Reik, W.

(2012b). Reprogramming DNA methylation in the mammalian life cycle: building and breaking epigenetic barriers. *Philos. Trans. R. Soc. B Biol. Sci.* **368**, 20110330–20110330.

Seki, Y., Hayashi, K., Itoh, K., Mizugaki, M., Saitou, M. and Matsui, Y. (2005).

Extensive and orderly reprogramming of genome-wide chromatin modifications associated with specification and early development of germ cells in mice. *Dev. Biol.* **278**, 440–458.

Sharif, J., Muto, M., Takebayashi, S.-I., Suetake, I., Iwamatsu, A., Endo, T.

A., Shinga, J., Mizutani-Koseki, Y., Toyoda, T., Okamura, K., et al.

(2007). The SRA protein Np95 mediates epigenetic inheritance by recruiting Dnmt1 to methylated DNA. *Nature* **450**, 908–912.

Shen, L., Inoue, A., Lu, F., Zhang Correspondence, Y., He, J., Liu, Y., Zhang,

Y., Lu, F. and Zhang, Y. (2014). Tet3 and DNA replication mediate

demethylation of both the maternal and paternal genomes in mouse zygotes. *Cell Stem Cell* **15**, 459–470.

Singh, P., Cho, J., Tsai, S. Y., Rivas, G. E., Larson, G. P. and Szabó, P. E.

(2010). Coordinated allele-specific histone acetylation at the differentially methylated regions of imprinted genes. *Nucleic Acids Res.* **38**, 7974–7990.

Singh, P., Lee, D. H. and Szabó, P. E. (2012). More than insulator: Multiple roles of

CTCF at the H19-Igf2 imprinted domain. *Front. Genet.* **3**, 1–9.

Sleutels, F., Tjon, G., Ludwig, T. and Barlow, D. P. (2003). Imprinted silencing of

Slc22a2 and Slc22a3 does not need transcriptional overlap between Igf2r and Air.

EMBO J. **22**, 3696–3704.

- Smilinich, N. J., Day, C. D., Fitzpatrick, G. V, Caldwell, G. M., Lossie, A. C., Cooper, P. R., Smallwood, A. C., Joyce, J. A., Schofield, P. N., Reik, W., et al.** (1999). A maternally methylated CpG island in KvLQT1 is associated with an antisense paternal transcript and loss of imprinting in Beckwith–Wiedemann syndrome. *Genetics* **96**, 8064–8069.
- Smith, A. and Hung, D.** (2017). The dilemma of diagnostic testing for Prader-Willi syndrome. *Transl. Pediatr.* **5**, 46–56.
- Smith, Z. D., Chan, M. M., Mikkelsen, T. S., Gu, H., Gnirke, A., Regev, A. and Meissner, A.** (2012). A unique regulatory phase of DNA methylation in the early mammalian embryo. *Nature* **484**, 339–344.
- Snowden, A. W., Gregory, P. D., Case, C. C. and Pabo, C. O.** (2002). Gene-specific targeting of H3K9 methylation is sufficient for initiating repression in vivo. *Curr. Biol.* **12**, 2159–2166.
- Stewart, K. R., Veselovska, L., Kim, J., Huang, J., Saadeh, H., Tomizawa, S. I., Smallwood, S. a., Chen, T. and Kelsey, G.** (2015). Dynamic changes in histone modifications precede de novo DNA methylation in oocytes. *Genes Dev.* **29**, 2449–2462.
- Stewart, K. R., Veselovska, L. and Kelsey, G.** (2016). Establishment and functions of DNA methylation in the germline. *Epigenomics* **8**, 1399–1413.
- Stöger, R., Kubička, P., Liu, C. G., Kafri, T., Razin, A., Cedar, H. and Barlow, D. P.** (1993). Maternal-specific methylation of the imprinted mouse Igf2r locus identifies the expressed locus as carrying the imprinting signal. *Cell* **73**, 61–71.
- Strogantsev, R., Krueger, F., Yamazawa, K., Shi, H., Gould, P., Goldman-Roberts, M., McEwen, K., Sun, B., Pedersen, R. and Ferguson-Smith, A. C.** (2015). Allele-specific binding of ZFP57 in the epigenetic regulation of imprinted

- and non-imprinted monoallelic expression. *Genome Biol.* **16**, 112.
- Surani, M. A.** (1999). Reprogramming a somatic nucleus by trans-modification activity in germ cells. *Semin Cell Dev Biol* **10**, 273–277.
- Surani, M. A. H., Barton, S. C., Norris, M. L., Surani, L.-L., Barton, S. C. and Norris, M. L.** (1986). Nuclear transplantation in the mouse: Heritable differences between parental genomes after activation of the embryonic genome. *Cell* **45**, 127–136.
- Swain, J. L., Stewart, T. A. and Leder, P.** (1987). Parental legacy determines methylation and expression of an autosomal transgene: A molecular mechanism for parental imprinting. *Cell* **50**, 719–727.
- Szabo, P. E. and Mann, J. R.** (1995). Allele-specific expression and total expression levels of imprinted genes during early mouse development: implications for imprinting mechanism. *Genes Dev.* **9**, 3097–3108.
- Tachibana, M., Matsumura, Y., Fukuda, M., Kimura, H. and Shinkai, Y.** (2008). G9a/GLP complexes independently mediate H3K9 and DNA methylation to silence transcription. *EMBO J.* **27**, 2681–90.
- Tada, S., Tada, T., Lefebvre, L., Barton, S. C. and Surani, M. A.** (1997). Embryonic germ cells induce epigenetic reprogramming of somatic nucleus in hybrid cells. *EMBO J.* **16**, 6510–6520.
- Tahiliani, M., Koh, K. P., Shen, Y., Pastor, W. A., Bandukwala, H., Brudno, Y., Agarwal, S., Iyer, L. M., Liu, D. R., Aravind, L., et al.** (2009). Conversion of 5-Methylcytosine to 5-Hydroxymethylcytosine in Mammalian DNA by MLL Partner TET1. *Science* **324**, 930–935.
- Thorvaldsen, J. L., Duran, K. L. and Bartolomei, M. S.** (1998). Deletion of the *H19* differentially methylated domain results in loss of imprinted expression of *H19*

and *Igf2*. *Genes Dev.* **12**, 3693–3702.

Thorvaldsen, J. L., Fedoriw, A. M., Nguyen, S. and Bartolomei, M. S. (2006).

Developmental Profile of H19 Differentially Methylated Domain (DMD) Deletion Alleles Reveals Multiple Roles of the DMD in Regulating Allelic Expression and DNA Methylation at the Imprinted H19/*Igf2* Locus. *Mol. Cell. Biol.* **26**, 1245–1258.

Tremblay, K. D., Saam, J. R., Ingram, R. S., Tilghman, S. M. and Bartolomei,

M. S. (1995). A paternal-specific methylation imprint marks the alleles of the mouse H19 gene. *Nat. Genet.* **9**, 407–413.

Tremblay, K. D., Duran, K. L. and Bartolomei, M. S. (1997). A 5' 2-kilobase-pair

region of the imprinted mouse H19 gene exhibits exclusive paternal methylation throughout development. *Mol. Cell. Biol.* **17**, 4322–4329.

Tsukada, Y.-I., Akiyama, T. and Nakayama, K. I. (2015). Maternal TET3 is

dispensable for embryonic development but is required for neonatal growth. *Sci. Rep.* **5**, 15876.

Tsumura, A., Hayakawa, T., Kumaki, Y., Takebayashi, S. I., Sakaue, M.,

Matsuoka, C., Shimotohno, K., Ishikawa, F., Li, E., Ueda, H. R., et al.

(2006). Maintenance of self-renewal ability of mouse embryonic stem cells in the absence of DNA methyltransferases Dnmt1, Dnmt3a and Dnmt3b. *Genes to Cells* **11**, 805–814.

Turner, C. L. S., MacKay, D. M., Callaway, J. L. A., Docherty, L. E., Poole, R.

L., Bullman, H., Lever, M., Castle, B. M., Kivuva, E. C., Turnpenny, P. D.,

et al. (2010). Methylation analysis of 79 patients with growth restriction reveals novel patterns of methylation change at imprinted loci. *Eur. J. Hum. Genet.* **18**, 648–655.

Uemura, T., Kubo, E., Kanari, Y., Ikemura, T., Tatsumi, K. and Muto, M.

- (2000). Temporal and spatial localization of novel nuclear protein NP95 in mitotic and meiotic cells. *Cell Struct. Funct.* **25**, 149–159.
- Vairapandi, M. and Duker, N. J.** (1993). Enzymic removal of 5-methylcytosine from DNA by a human DNA-glycosylase. *Nucleic Acids Res.* **21**, 5323–5327.
- van Zelst-Stams, W. A., Scheffer, H. and Veltman, J. A.** (2014). Clinical exome sequencing in daily practice: 1,000 patients and beyond. *Genome Med.* **6**, 2–4.
- Vella, P., Scelfo, A., Jammula, S., Chiacchiera, F., Williams, K., Cuomo, A., Roberto, A., Christensen, J., Bonaldi, T., Helin, K., et al.** (2013). Tet Proteins Connect the O-Linked N-acetylglucosamine Transferase Ogt to Chromatin in Embryonic Stem Cells. *Mol. Cell* **49**, 645–656.
- Verona, R. I., Thorvaldsen, J. L., Reese, K. J. and Bartolomei, M. S.** (2008). The transcriptional status but not the imprinting control region determines allele-specific histone modifications at the imprinted H19 locus. *Mol. Cell. Biol.* **28**, 71–82.
- Vertino, P. M., Chiu Yen, R.-W., Gao, J. and Baylin, S. B.** (1996). De Novo Methylation of CpG Island Sequences in Human Fibroblasts Overexpressing DNA (Cytosine-5)-Methyltransferase. *Mol. Cell. Biol.* **16**, 4555–4565.
- Wakeling, E. L., Brioude, F., Lokulo-sodipe, O., Connell, S. M. O., Salem, J., Bliet, J., Canton, A. P. M., Chrzanowska, K. H., Davies, J. H., Dias, R. P., et al.** (2016). Diagnosis and management of Silver–Russell syndrome: first international consensus statement. *Nat. Publ. Gr.* **13**, 105–124.
- Watanabe, T., Tomizawa, S., Mitsuya, K., Totoki, Y., Yamamoto, Y., Kuramochi-Miyagawa, S., Iida, N., Hoki, Y., Murphy, P. J., Toyoda, A., et al.** (2011). Role for piRNAs and Noncoding RNA in de Novo DNA Methylation of the Imprinted Mouse *Rasgrf1* Locus. *Science* **332**, 848–852.

- Weaver, J. R., Sarkisian, G., Krapp, C., Mager, J., Mann, M. R. W. and Bartolomei, M. S.** (2010). Domain-Specific Response of Imprinted Genes to Reduced DNMT1. *Mol. Cell. Biol.* **30**, 3916–3928.
- Williams, K., Christensen, J., Pedersen, M. T., Johansen, J. V., Cloos, P. A. C., Rappsilber, J. and Helin, K.** (2011). TET1 and hydroxymethylcytosine in transcription and DNA methylation fidelity. *Nature* **473**, 343–348.
- Williams, K., Christensen, J. and Helin, K.** (2012). DNA methylation: TET proteins—guardians of CpG islands? *EMBO Rep.* **13**, 28–35.
- Wossidlo, M., Nakamura, T., Lepikhov, K., Marques, C. J., Zakhartchenko, V., Boiani, M., Arand, J., Nakano, T., Reik, W. and Walter, J.** (2011). 5-Hydroxymethylcytosine in the mammalian zygote is linked with epigenetic reprogramming. *Nat. Commun.* **2**, 241.
- Wu, H. and Zhang, Y.** (2011). Mechanisms and functions of Tet protein-mediated 5-methylcytosine oxidation. *Genes Dev.* **25**, 2436–2452.
- Wu, H., D'Alessio, A. C., Ito, S., Xia, K., Wang, Z., Cui, K., Zhao, K., Eve Sun, Y. and Zhang, Y.** (2011a). Dual functions of Tet1 in transcriptional regulation in mouse embryonic stem cells. *Nature* **473**, 389–393.
- Wu, H., D'Alessio, A. C., Ito, S., Wang, Z., Cui, K., Zhao, K., Sun, Y. E. and Zhang, Y.** (2011b). Genome-wide analysis of 5-hydroxymethylcytosine distribution reveals its dual function in transcriptional regulation in mouse embryonic stem cells. *Genes Dev.* **25**, 679–84.
- Xie, W., Barr, C. L., Kim, A., Yue, F., Lee, A. Y., Eubanks, J., Dempster, E. L. and Ren, B.** (2012). Base-Resolution Analyses of Sequence and Parent-of-Origin Dependent DNA Methylation in the Mouse Genome.
- Xin, Z., Tachibana, M., Guggiari, M., Heard, E., Shinkai, Y. and Wagstaff, J.**

- (2003). Role of histone methyltransferase G9a in CpG methylation of the Prader-Willi syndrome imprinting center. *J. Biol. Chem.* **278**, 14996–15000.
- Xu, Y., Wu, F., Tan, L., Kong, L., Xiong, L., Deng, J., Barbera, A. J., Zheng, L., Zhang, H., Huang, S., et al.** (2011). Genome-wide Regulation of 5hmC, 5mC, and Gene Expression by Tet1 Hydroxylase in Mouse Embryonic Stem Cells. *Mol. Cell* **42**, 451–464.
- Xu, C., Liu, K., Lei, M., Yang, A., Li, Y., Hughes, T. R. and Min, J.** (2018). DNA Sequence Recognition of Human CXXC Domains and Their Structural Determinants. *Structure* **26**, 85–95.e3.
- Yamaguchi, S., Hong, K., Liu, R., Shen, L., Inoue, A., Diep, D., Zhang, K. and Zhang, Y.** (2012). Tet1 controls meiosis by regulating meiotic gene expression. *Nature* **492**, 443–447.
- Yamaguchi, S., Shen, L., Liu, Y., Sandler, D. and Zhang, Y.** (2013). Role of Tet1 in erasure of genomic imprinting. *Nature* **504**, 460–464.
- Yamane, K., Toumazou, C., Tsukada, Y. I., Erdjument-Bromage, H., Tempst, P., Wong, J. and Zhang, Y.** (2006). JHDM2A, a JmjC-Containing H3K9 Demethylase, Facilitates Transcription Activation by Androgen Receptor. *Cell* **125**, 483–495.
- Yotova, I. Y., Vlatkovic, I. M., Pauler, F. M., Warczok, K. E., Ambros, P. F., Oshimura, M., Theussl, H. C., Gessler, M., Wagner, E. F. and Barlow, D. P.** (2008). Identification of the human homolog of the imprinted mouse Air non-coding RNA. *Genomics* **92**, 464–473.
- Zemel, S., Bartolomei, M. S. and Tilghman, S. M.** (1992). Physical linkage of two mammalian imprinted genes, H19 and insulin-like growth factor 2. *Nat. Genet.* **2**, 61–65.

- Zhang, H., Zhang, X., Clark, E., Mulcahey, M., Huang, S. and Shi, Y. G.** (2010). TET1 is a DNA-binding protein that modulates DNA methylation and gene transcription via hydroxylation of 5-methylcytosine. *Cell Res.* **20**, 1390–1393.
- Zhang, T., Termanis, A., Özkan, B., Bao, X. X., Culley, J., de Lima Alves, F., Rappsilber, J., Ramsahoye, B. and Stancheva, I.** (2016a). G9a/GLP Complex Maintains Imprinted DNA Methylation in Embryonic Stem Cells. *Cell Rep.* **15**, 77–85.
- Zhang, W., Xia, W., Wang, Q., Towers, A. J., Chen, J., Gao, R., Zhang, Y., Yen, C. an, Lee, A. Y., Li, Y., et al.** (2016b). Isoform Switch of TET1 Regulates DNA Demethylation and Mouse Development. *Mol. Cell* **64**, 1062–1073.
- Zhang, P., Hastert, F. D., Ludwig, A. K., Breitwieser, K., Hofstätter, M. and Cardoso, M. C.** (2017). DNA base flipping analytical pipeline. *Biol. Methods Protoc.* **2**, 1–12.
- Zhu, B., Zheng, Y., Hess, D., Angliker, H., Schwarz, S., Siegmann, M., Thiry, S. and Jost, J. P.** (2000). 5-methylcytosine-DNA glycosylase activity is present in a cloned G/T mismatch DNA glycosylase associated with the chicken embryo DNA demethylation complex. *Proc. Natl. Acad. Sci. U. S. A.* **97**, 5135–5139.